WAVE PROPAGATION THROUGH FLOWING GAS-LIQUID MIXTURES IN LONG PIPELINES

A THESIS

Presented to

The Faculty of the Division of Graduate Studies

By

Mahadevan Padmanabhan

In Partial Fulfillment

of the Requirements for the Degree

Doctor of Philosophy in the School of Civil Engineering

Georgia Institute of Technology

August, 1976

WAVE PROPAGATION THROUGH

FLOWING GAS-LIQUID MIXTURES IN LONG PIPELINES

Approved:

Charles S. Martin, Chairman

William F. Ames

George M. Rentzepis

Date of Approval by Chairman July 12, 1976

DEDICATION

This thesis is dedicated to my father late Mr. P. Mahadevan who was the Chief Civil Engineer of the Kerala State Electricity Board, India, Unfortunately he did not live to see the successful completion of my doctoral program.

ACKNOWLEDGMENTS

The author wishes to express his sincere appreciation to Dr. Charles S. Martin, his thesis advisor, without whose encouragement, generous contribution of time, and competent advice this thesis would not have been possible. Thanks are due to Dr. William F. Ames and Dr. George M. Rentzepis who served as members of the reading committee for their valuable suggestions. Thanks are also due to Dr. D. C. Wiggert of Michigan State University for his valuable suggestions during the development of the theoretical models.

The help given by Mr. Homer Bates, Laboratory Technician, in carrying out the experimental program is invaluable. Thanks are due to Mrs. Elaine Dampier and Ms. Annette Plunkett for typing this thesis.

The author is grateful to the Director, School of Civil Engineering, in providing the financial assistance through the National Science Foundation Grant, GK-38570, while conducting this study.

Finally the author wishes to thank his wife Ranjana for her patience and encouragement during his long period of graduate study. He is also grateful for the interest and encouragement of his parents. He only regrets that his father did not live to see the completion of this thesis --- which, in effect, is dedicated to him.

Special permission was received from the Division of Graduate Studies to deviate from the requirements of its thesis manual so that a part of this dissertation could be published as a report.

TABLE OF CONTENTS

LIST OF TABLES

LIST OF ILLUSTRATIONS

NOMENCLATURE

A	=	Pipe cross-sectional area
C	=	Universal gas constant
C_d	=	Coefficient of discharge
C_o	=	Distribution factor
C_1	=	Drift-velocity coefficient
C'	=	Bubble-shape constant used in Levich's Model of bubble motion
C_M	=	Added-mass coefficient
C^+, C^-	=	Characteristics lines
D	=	Diameter of pipe
D_o	=	Diameter of orifice
D_g	=	Thermal diffusivity of gas
E	=	Young's Modulus of elasticity of pipe wall
F	=	A function of Mach number
F_f	=	Force due to frictional resistance
F_v	=	Viscous force acting on a bubble
K	=	Bulk modulus of elasticity
L	=	Length of pipe
M	=	Mach number
M_a	=	Mass rate of flow of air
P_1, P_2	=	Piezometers
Q	=	Volume rate of flow

Q_{ij}; i,j = 1,2,3	=	Functions in conservation equations
Q'_{il}; i = 1,2,3	=	Smoothed variables of Q_{il}
ΔQ_{ir}; i = 1,2,3	=	Reference variables used in smoothing technique
R	=	Bubble radius
Re	=	Reynolds number
T	=	Temperature
ΔT	=	Change in temperature across a shock wave
U	=	Speed of propogation of a shock wave
V_{kj}, k = g, ℓ	=	Drift velocity of component k relative to the volumetric average flux of the mixture
V_{km}, k = g, ℓ	=	Diffusion velocity of component k relative to the mass average velocity of the mixture
W	=	Weight of mixture in a control volume
X	=	Coordinate along pipe axis at a particular location
Z	=	A Constant
a	=	Speed of sound, celerity of a dynamic wave
b_1, b_2, b_3, b_4	=	Functions used in the derivation of characteristic equations
c_ℓ	=	Specific heat of liquid
d_A	=	Thickness of A-type shock waves
d_B	=	Thickness of the steep front of a B-type shock wave
d'_B	=	Thickness of gradually-rising portion of a B-type shock wave
d_C	=	Thickness of a C-type shock wave

d_{50}	=	Average bubble diameter
e	=	Pipe-wall thickness
f	=	Darcy-Weisbach resistance coefficient
g	=	Acceleration due to gravity
j	=	Volumetric flux
k	=	Ratio of gas velocity to liquid velocity
m	=	Polytropic exponent
n	=	Number density of bubbles
p	=	Cross-sectional average pressure
Δp	=	Pressure drop
p^*	=	Pressure at the end of the steep front of a B-type shock wave
q	=	Vector in the linearized version of a hyperbolic system of equations.
t	=	Time
t_c	=	Time of closure of a valve
Δt	=	Incremental time in a finite-difference grid
u	=	Liquid velocity in bubble-dynamics model
v	=	Bubble velocity in the bubble-dynamics model; time and space averaged weighted velocity in the drift-flux model
v_b	=	Bubble rise velocity
v_r	=	Relative velocity of the gas phase with respect to the liquid phase
w	=	Mean molecular weight of gas
x	=	Distance along the pipe from the reservoir end
Δx	=	Incremental distance; Mesh length in a finite-difference grid

y	=	Function of shock strength
z	=	Vector in the linearized version of a hyperbolic system of equations
Γ	=	Gas production rate per unit volume
Λ	=	Wave length of oscillations behind a shock wave
Φ	=	A function of void fraction and pressure
Ψ	=	A function of Mach number
α	=	Average cross-sectional void fraction
β	=	Average cross-sectional volumetric quality
γ	=	Isentropic exponent
δ	=	Damping factor used in shock-wave theory
δ'	=	A function of δ
ε	=	Pipe constraint factor
η	=	Average cross-sectional mass quality
θ	=	Angle to horizontal
θ_i	=	Smoothing Parameter
θ	=	Reference parameter in smoothing procedure
λ	=	Maximum modulus eigenvalue of the coefficient matrix in a hyperbolic system
λ_g	=	Acoustic wave length in gas phase
μ	=	Dynamic viscosity
ν	=	Kinematic viscosity
ξ	=	Mass fraction of gas to mass fraction of liquid in a given volume of mixture
ρ	=	Mass density

$\Delta\rho$	=	Difference in densities between liquid and gas
σ	=	Surface tension
τ	=	A relaxation time associated with viscous dissipation
τ'	=	A relaxation time associated with thermal dissipation
τ_o	=	Boundary shear stress
ϕ, ϕ', ϕ''	=	Multipliers used in the derivation of characteristic equations
ϕ_1, ϕ_2, ϕ_3	=	Characteristic roots
ω	=	Frequency of bubble oscillations

Subscripts

o	=	Before the passage of a shock wave; Value at initial steady flow
oo	=	Value at x = o
1	=	Behind a shock wave
g	=	Gas phase
h	=	Based on homogeneous theory
ℓ	=	Liquid phase
m	=	Mixture
p	=	Effect of pipe-wall elasticity and end supports included
tp	=	Two-phase flow

SUMMARY

The propagation of finite pressure waves through air-water mixtures has been investigated both experimentally and analytically. Two different experimental apparatuses were used, one consisting of a 61.5 ft long lucite pipe of 1 inch diameter and the other a 334 ft long coiled copper tubing of 0.5 inch diameter. Transient pressure records were obtained for a simple case of rapid closure of a valve at the downstream end of the pipe. Experiments covering bubbly-flow and slug-flow regimes were conducted for air-water mixtures for which the volumetric quality β varied from 0.005 to 0.18. The steepening phenomenon of compression waves, shock wave formation, and speed of propagation and structure of shock waves have been studied in detail.

One-dimensional conservation equations for unsteady two-phase flow are derived using both homogeneous and separated flow concepts. Two analytical models are proposed for transient analysis in bubbly flows: the bubble-dynamics model and the drift-flux model. A numerical computational procedure using the Lax-Wendroff scheme is developed and used for the numerical integration of conservation equations in both of the proposed models. Using the homogeneous model characteristic equations are derived and have been used to simulate the boundary conditions. Comparisons between the experimental and computed transient pressure records have been done to establish the suitability of the proposed models. The drift-flux model has been used for analysis of transients in slug flow and comparisons with experimental records of pressure transients have been

incorporated.

For the condition of strong shocks caused by the rapid closure of the downstream valve, adiabatic theory gives an adequate prediction of the shock speed for bubble diameters between 0.5 and 4 mm. Based upon the shock-wave classification of Noordzij and van Wijngaarden, only B and C-type shocks were observed in this study. The C-type shocks existed only for very weak shocks, however. The application of the shock-tube theory of Noordzij and van Wijngaarden to shock waves in flowing mixtures in long conduits is questionable as the structure of the shock waves formed by steepening of compression waves is influenced by the structure of the compression waves themselves. The thickness of the steep portion behind the shock and the period of oscillation are much higher than values predicted from theory.

Both the bubble-dynamics model and the drift-flux model solutions compare reasonably well with experimental results of transient pressures caused by the closure of the downstream valve. Although the bubble-dynamics is, strickly speaking, only valid for uniformly distributed and uniformly sized spherical bubbles, the use of a representative average bubble size has produced satisfactory results. Furthermore, the bubble-dynamics model is capable of simulating transient bubble motion relative to the liquid motion.

An advantage of the drift-flux model is its capability of incorporating velocity and concentration profiles into the analysis. The model is also relatively simple and possesses the facility to simulate transients in other two-phase flow regimes.

With the bubble-dynamics model the effect of pipe-wall elasticity

and water compressibility can be included. The model is also well suited for very low void fractions if the bubbles are very small and uniformly sized.

Because of the relatively small difference in the relative velocity between the gas and liquid phases, theoretical results based upon the homogeneous model, the bubble-dyanmics model, and the drift-flux model, do not differ very much. For other two-phase flows, for example choked flow, the agreement would not be expected to be as good.

CHAPTER I

INTRODUCTION

The presence of free gases in liquids can markedly alter the results as well as complicate analyses regarding the prediction of water-hammer pressures. Gases may be present either in the dissolved or the entrained state, or both, in cooling-water systems of fossil-fuel and nuclear power stations, in sewage pumping lines, or in crude oil lines. The effect of the compressibility of any free gas on the wave-propagation speed, and on the resulting pressure changes, must be considered in any transient analysis for which even the smallest amount of gas may be present. If pressure changes during a transient lower the pressure to, or near to, the saturation vapor pressure of the liquid, large quantities of gas dissolved in the liquid may come out of solution and considerably alter the wave propagation speed. If, in the design of conduits and appurtenant structures, the acoustic velocity of the pure liquid is not reduced to account for the presence of the gas, the predicted pressure changes will be too great, possibly resulting in structures that are over-designed, and hence too costly. On the other hand, if the mixture is treated as a so-called pseudo-liquid, for which the sound velocity is reduced, the predicted pressure changes will be too low for rapid flow changes, leading to possible failures. More properly and correctly, such an analysis must proceed on the basis of shock-wave theory for the mixture, either considering only the gas compressible at relatively large void fraction, or accounting for both the gas and the liquid compressibilities at relatively

small void fractions. In other words the calculation of pressure changes in gas-liquid mixtures undergoing rapid changes in flow must involve the study of shock-wave propagation in a dispersive medium. Furthermore, the passage of pressure waves in a mixture will increase or decrease the percentage by volume of gas present, thereby altering the wave speed.

Practical Examples of Transient Two-Phase Flow in Conduits

The possible effect of any dissolved gas or free gas in a liquid is frequently ignored in the transient analysis of pressure drop in liquid pipelines subsequent to the loss of power to a pump. In practice free gas probably occurs frequently as a result of the evolution of dissolved gas (gas release) during a transient. In sewage, however, the free gas content is usually great enough to have a measurable effect on the acoustic velocity. Pearsall [1] has shown by actual tests in sewage pumping lines that the acoustic velocity can be reduced by as much as 86 per cent as a result of gas content. Although, as reported by Hulsemann [2], dissolved gas in a liquid can not effect the acoustic velocity provided it remains in solution, gas release during a pressure-reducing transient produces the same end result. As shown by Swaffield [3] and Driels [4] the cushioning effect of released gas during a severe pressure drop can significantly reduce the maximum pressure rise during resurge. Kranenburg [5] has demonstrated the importance of the consideration of dissolved gas and its evolution on the simulation of liquid-column separation and gaseous cavitation in liquid pipelines.

In large circulating-water systems of nuclear and fossil-fueled power plants the water is usually saturated with gas, especially if the

system contains cooling towers in the circuit. Due to the required height of the condenser to accomodate the high number of tubes, and the usual low pumping head the water pressure in the condenser box may even be negative during steady-flow operation, allowing for possible gas release and entrappment during normal operation. The calculation of the pressure transients subsequent to pump failure can be complicated by the initial two-phase regime in the condenser as well as further gas release as the pressure reduces toward vapor pressure. Sheer [6] has shown the wide discrepancy between actual experimental transient pressure data in a large cooling-water system and a single liquid-phase theory that completely ignores any presence of gas, dissolved or free. It is very apparent that there is a dire need for (1) good two-phase flow models for transient calculations and (2) a better understanding of the physical chemistry of gas evolution and gas absorption in liquids. The purpose of this study is to focus on the development of transient two-phase flow models for which no gas evolution or gas absorption occurs.

Another example of transient two-phase flow is the postulated loss-of-coolant accident (LOCA) in a nuclear reactor. The development of analytical models to simulate the resulting transient flow through a pipe break is complicated by nonequilibrium thermodynamics, critical flow, heat transfer, two-phase flow through the primary coolant pumps, two- and three-dimensional flow in the reactor plenum, etc. The blowdown problem in general has generated considerable interest in two-phase choking flow, however, as evidenced by papers by Moody [7], Henry and Fauske [8], Moody [9], and D'Arcy [10], to cite several sources.

Acoustic Velocity

It is well known that small amounts of free gas in a liquid can cause the acoustic velocity to be reduced considerably from that in the pure liquid itself. For a mixture flowing in the bubbly-flow regime the effect of the gas on the acoustic velocity has been well documented in the technical literature by numerous investigators. Some of the more significant work on the speed of sound in bubbly mixtures has been by Silberman [11], Hsieh and Plesset [12], Henry [13], and van Wijngaarden [14, 15]. Situations leading to the development of finite-amplitude (shock) waves in mixtures have been considered by Campbell and Pitcher [16], Crespo [17], and Noordzij and van Wijngaarden [18].

Knowledge of the acoustic velocity variation for other flow regimes--slug, annular, or plug--is not as complete. In the case of slug flow, the results of Henry, Grolmes and Fauske [19] indicate that the usual homogeneous bubbly model is completely inadequate for the prediction of the speed of sound.

Flow Regimes and Analytical Models

The fact that two-phase flow in conduits can occur in many different regimes--bubbly, churn, wispy-annular, and annular, to name a few--inhibits the development of accurate and definitive comprehensive one-dimensional models. For transient phenomena flow-regime transition may also play a role, but has hardly been considered to date.

As reported by Wallis [20] the most widely used analytical models are the homegeneous model, the separated-flow model, and the drift-flux model. Unless there exists a significant difference in the velocities of the respective phases the homogeneous model can be applied with mod-

erate success to dispersed flows, whether bubbly or droplet. Relative velocity effects can be incorporated into the separated-flow and drift-flux models. In the latter case, however, one must have knowledge of the drift-flux or the drift-velocity in the momentum equation. The first step in the analytical modeling of unsteady two-phase flow is deciding upon the proper constitutive equations; that is, whether they are to be homogeneous, separated-flow, or drift-flux representations. The obvious next step is the development and testing of various explicit or implicit numerical modeling techniques.

Objectives of Current Study

Except for the study of the acoustic velocity and the formation and propagation of shock waves in bubbly mixtures there have been relatively few investigations performed on the effect of the presence of gas bubbles on pressure surges. For longer conduits in which the pressure and gas concentration may vary along the pipe as a result of boundary friction and elevation change, a simple knowledge of the acoustic wave speed is inadequate for the prediction of peak pressures resulting from a transient condition, such as valve closure or power failure to a pump.

The purpose of this investigation is to demonstrate the effect of free gas on pressure wave propagation in pipelines that are long enough for the effect of boundary friction and elevation change to be important. Several numerical techniques are developed for testing the suitability of homogeneous, separated-flow, and drift-flux model representation of transient bubbly and slug flows. An extensive experimental investigation is conducted for the verification of the various numerical techniques and

two-phase flow constitutive equations. In addition, the propagation of a shock wave in a long conduit is investigated.

CHAPTER II

EXPERIMENTAL SETUP AND PROCEDURE

The overall experimental setup and the special instrumentation utilized will be described with reference to the measurement of wave propagation speed, shock-wave structure and pressure-time transients. Following the general description of the experimental setup and instrumentation will be a detailed explanation of the testing procedure employed in this investigation.

Experimental Setup

The experimental program has been conducted in two separate apparatuses, one of which was built specifically for this investigation. This newly built equipment will be hereafter referred to as the plexiglass piping apparatus. All the experimental studies on shock waves and transients in two-phase bubbly-flow regime have been performed in the plexiglass piping apparatus. The other experimental apparatus hereafter referred to as the copper tubing apparatus was mainly used for preliminary studies on wave propagation and for studies on transients in two-phase slug flows.

Plexiglass-Piping Apparatus

It was deemed necessary to construct a long pipe in order to facilitate the investigation of the effect of boundary friction and the resulting initial pressure gradient on transient response of long conduits carrying mixtures. The piping was constructed so that at least some portions of the flow would be vertical, which would help to limit the buoyant effect

of gravity on the movement of the air bubbles. Fig. 1 shows a schematic sketch of the experimental setup.

The Test Pipe. Clear lucite pipe having an internal diameter of 1 inch and thickness of about 0.25 inch has been used as the test pipe. Including the two long-radius bends, the total pipe length is 61.5 ft. Individual lengths of the pipe, nominally 4 ft, are bolted firmly together with 5/8 inch thick flanges. An 1/16 inch pressure tap with the appropriate fitting was installed in one of the flanges at each joint. Piezometers were connected to the fittings for steady-flow friction measurements. During the dynamic studies all piezometers not directly connected to the pressure transducers were completely plugged up at the pipe wall. The inverted U-shape of the pipe provides a vertical upward-flow portion 20 ft long, a horizontal portion of 16 ft, and a vertical downward flow portion of 22.5 ft. The two long-radius elbows are made of PVC and have a length of 18 inches and a radius of curvature of about 11 inches.

Water is supplied to the test pipe from a pressure tank 2.5 ft in diameter and 5 ft in height, as shown in Fig. 1. By means of an air pressure regulator the air pressure above the water surface can be varied from 20-80 psig. The tank is supplied with tap water from the laboratory water supply main by a copper pipe, in which is installed a valve for flow and air pressure regulation, and a calibrated bend meter for measurement of the flow. As shown in Fig. 1, the downstream end of the test pipe also has a valve which can be adjusted to regulate the discharge through the pipe. The discharge from the pipe is measured gravimetrically by means of a weighing tank. The outflow from the pressure tank into the pipe and the inflow into the tank from the water supply main are maintained equal

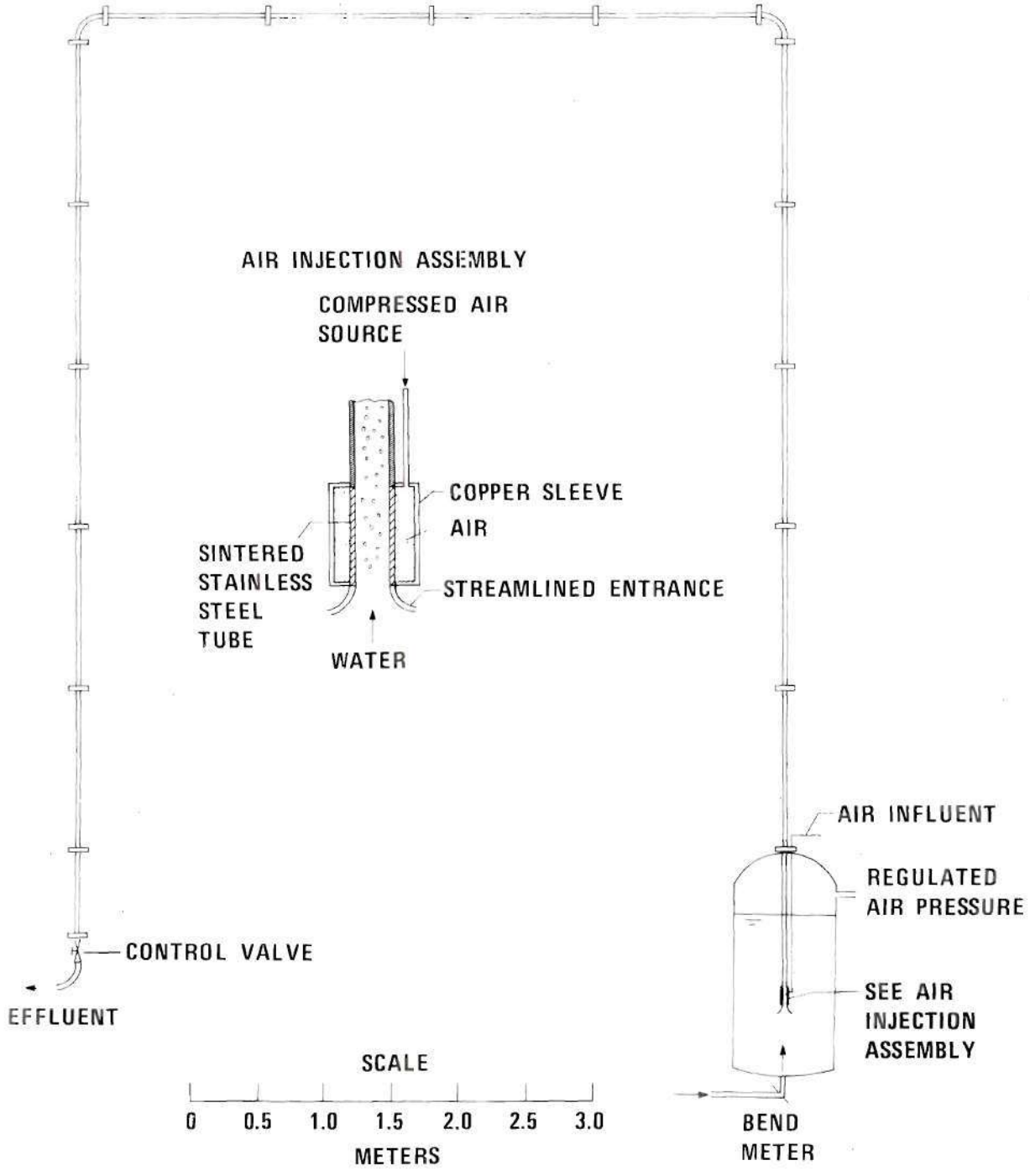

Figure 1. Schematic Layout of Plexiglass-Piping Apparatus.

by adjusting the corresponding valves. A sight glass on the outside of the pressure tank was used to observe the water level in the tank, and to confirm that the pipe inlet was well immersed in the water in the tank during the experiments. Small variations in pressure in the tank are taken care of by the pressure regulator.

Apart from the regulating valves mentioned earlier, the downstream end of the pipe has a quick-acting hand valve, which may also be actuated by a spring for a very rapid closure. A closure time of about 10 ms can be obtained using the spring closure, which was employed to generate rapid valve movement. A similar valve is provided at the upstream end of the system where the pressure tank is connected to the pipe. This valve is always open, except when it is desired to empty the test pipe completely.

Air Injection and Metering. Air can be injected into the pipe from an independent compressed air source. The air from the compressed air source passes through a pressure regulator, which controls the air pressure anywhere from 0 to 80 psig, and then on to the flow metering devices. The flow metering is done using a micrometering valve of Nupro S series, which has an orifice opening of 0.055 inch. Using a vernier handle, the metering valve can be set at any desired opening from 0 to 10 turns, the latter of which corresponds to fully open. The metering valve has been calibrated with water for three different settings: 2 turns, 5 turns and 10 turns open. The pressure drop across the meter is measured using a U-tube water manometer, from which the mass rate of air flow can be determined from the calibration curve for the particular air inlet pressure, which was measured by an accurate pressure guage in the supply

line upstream of the meter. Details on the calibration and a typical calibration curve are given in Appendix A. Initially the air flow measurement was determined by ball rotameters, but it was subsequently found that the micrometering valves were more accurate. All of the air flow measurements reported herein were obtained using the micrometering valve.

The metered air is directed to the test pipe through the porous wall of a sintered stainless steel tube, as shown in the inlet view on Fig. 1. As the sintered metal has an average pore opening of one micron, it was possible to obtain a fairly uniform distribution of bubbles.

Copper-Tubing Apparatus

The copper-tubing apparatus consists of a 0.528-inch ID copper tube 334 feet in length. This coil of tubing has been utilized in earlier investigations on pressure-transient phenomena, and its characterisitcs are reported in Carstens and Hagler [21]. A photograph of the experimental setup is shown on Fig. 2, and a schematic on Fig. 3. The same pressure tank employed in conjunction with the transparent tubing was also used to supply water under pressure to the copper tubing. Compressed air is forced into the copper tubing through a disc of porous plastic fitted into a tee section. Pressure regulators are used to maintain a constant pressure level. The mass flow rate of air has been metered with rotameters and micrometering valves, as described for the plexiglass apparatus. The water flow rate is measured gravimetrically by means of a weighing tank. For the determination of steady and transient pressures along the pipe, pressure taps and connections for transducer mountings were located at approximately the 1/8th points along the pipe length.

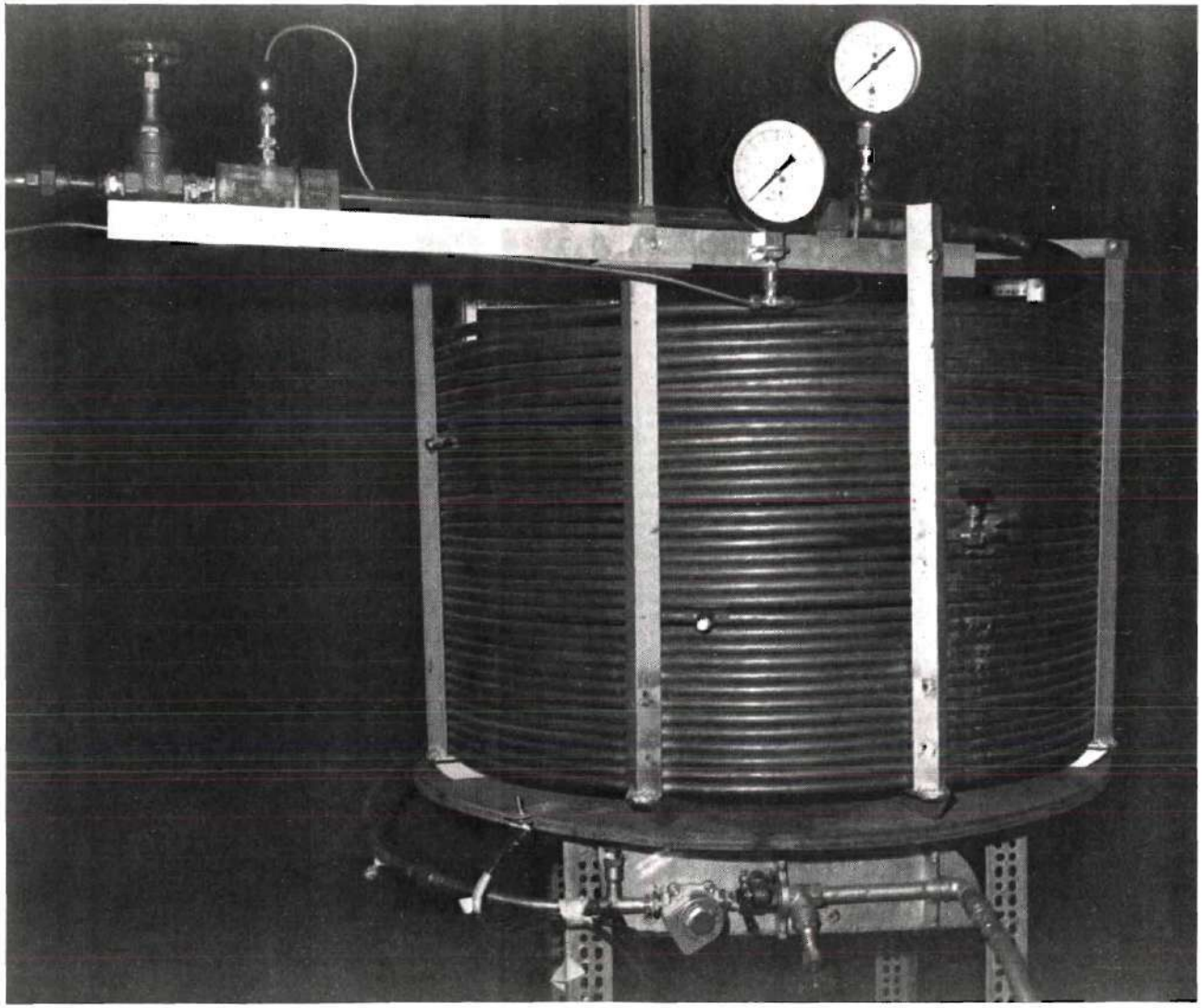

Figure 2. Photograph of Copper-Tubing Apparatus.

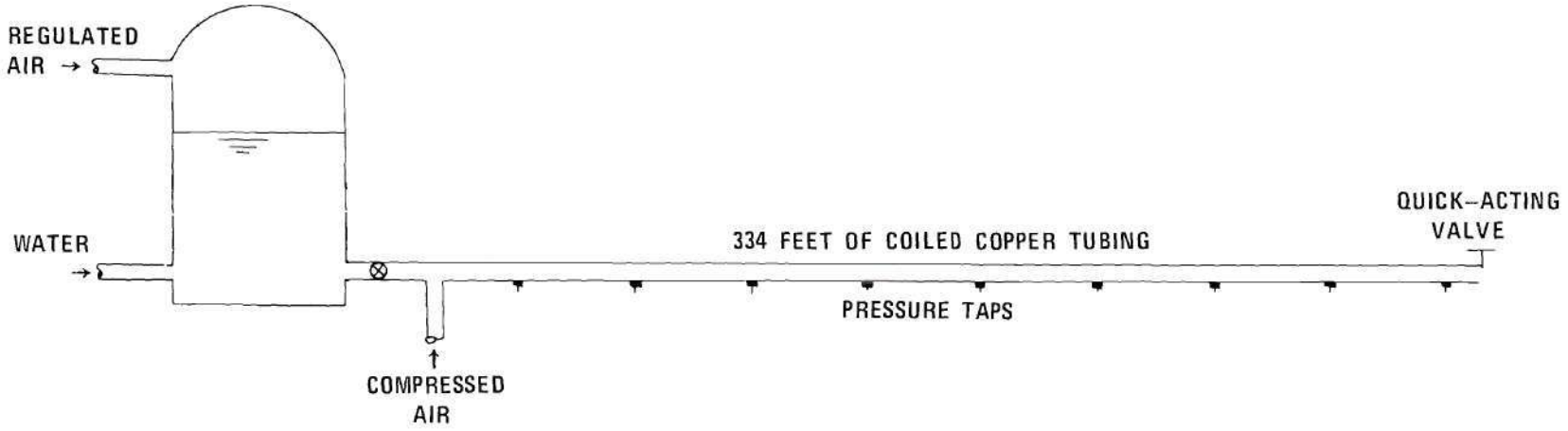

Figure 3. Schematic Layout of Copper-Tubing Apparatus.

Experimental Procedure

The copper-tubing apparatus was used for initial investigations on wave propagation and shock wave formation while the plexiglass-piping apparatus was under construction. Some useful qualitative information on the formation and velocity of propagation of shock waves was obtained. However, as the flow-regime identification and determination of bubble sizes were not possible with this equipment, further studies on propagation of shock waves and their structure and transients in bubbly mixtures were conducted in the plexiglass apparatus. Only a few experiments on transients in two-phase slug flow were conducted using the copper-tubing apparatus. Therefore, with the exception of the procedure for the measurement of transient pressures, the following discussion of flow regimes and bubble sizes, steady-state friction, measurement of wave celerity, and observations on shock structure is restricted to the plexiglass-piping apparatus alone.

The initial portion of the experimental work in the plexiglass piping-apparatus consisted of flow-regime identification, determination of the nature of the bubbly flow, and measurement of the bubble-size distribution in each portion of the test pipe for different water and air flows. This helped in fixing the desirable ranges of water flow, air flow, and the initial operating pressure in the tank. Then experiments were conducted to determine the frictional loss in the pipe for the steady flow of a bubbly air-water mixture. Once the flow-regime identification and the steady-flow data were obtained, the dynamic tests were conducted for the determination of wave celerity, shock structure, and pressure-transient records.

Flow Regimes and Bubble Sizes

It was observed that by maintaining the water velocity between approximately 3-5ft/sec, the complete range of bubbly flow could be covered with the available setup for air injection and metering. The transition to slug flow occurred first in the vertical downward flow portion, when the flowing volumetric concentration, or quality β, was about 0.10. Hence, this value of β was set as a desirable upper limit even though bubbly flow prevailed in the riser for higher air concentrations. Throughout the bubbly-flow regime the features of the bubbly mixture were noticed to be different for each leg of the U-tube. The vertical upward-flow portion or riser has an almost uniform distribution of bubbles, which usually varied in size from 0.5 to 2.0 mm. In the horizontal leg the bubbles occupied the upper portion of the pipe cross section, finally resulting in coalesence, especially for lower water velocities and higher air concentrations. In the downward-flow portion or downcomer, the bubbles were quite large, 2 mm to 4 mm, mostly nonspherical and deformed, and occupied the central portion of the pipe cross section. The individual bubbles were spaced well apart for air concentrations corresponding to $\beta < 0.01$. For concentrations $\beta > 0.05$ the bubbles formed clusters, which became intermittent in nature. The size of the bubbles in this portion of the pipe was observed to be fairly uniform (2 to 4 mm) for the whole range of bubbly flow.

Photographs were taken at each portion of the pipe for determining bubble size and distribution. To avoid the effect of refraction by the curved thick-walled plastic pipe a plexiglass box was installed around the pipe so that the inner portion between the outside of the pipe wall

and the wall of the box could be filled with water.

Steady-Flow Friction

To determine the steady-flow frictional loss in the plexiglass test pipe a manometer board was connected to the 16 piezometers, each of which was connected to the pressure tap in the respective flange. Initially, the frictional loss for pure water flow was determined. In all instances care was taken to insure that all of the piezometer tubes were free of any air bubbles. For pure water flow the Darcy-Weisbach resistances coefficient f was found to follow the smooth pipe friction data for Reynolds numbers ranging from 15,000 to 70,000. The friction loss for the bubbly flow was then determined for air flows corresponding to the transport concentration or volumetric quality β ranging from 0.004 to 0.018. During all of the steady-flow friction experiments, the manometer tubes were kept free of air, so that the head loss was measured in terms of head of water column. The friction factor for the bubbly flow was calculated based on the volumetric liquid flux and mixture density. The friction factor for vertically-upward flow was found to be slightly higher than that for horizontal and vertically-downward flow. An average friction factor has been worked out for the whole pipe, and is found to be about 9 per cent greater than that for pure water flow. Details regarding these results are provided in Appendix B. However, it may be noted that during transients the Reynolds number is a variable and as such a time dependent friction factor may be required. Furthermore, during transient conditions, the mixture density also varies and an exact value of a friction factor is difficult to ascertain. Notwithstanding all of the uncertainties associated with resistance in transient two-

phase flow, it was decided to use a constant value of the two-phase flow resistance coefficient for the range of air concentrations encountered. For all of the transient flow experiments, the initial steady-flow Reynolds number ranged from 2.5 (10^4) to 4.5 (10^4), clearly within the turbulent-flow regime. For the calculation of the boundary-drag term in the momentum equation the mixture density and liquid velocity are used.

Measurement of Transient Pressures

Transducers could be mounted on any of the sixteen flanges of the plexiglass piping, which are 4 ft apart. Two types of transducers were used for this study; namely diaphragm transducers (Whittaker Model KP15), and semiconductor transducers (Kulite XTM-1-190). The diaphragm transducers were connected as close as possible to the outer edge of the pipe flange, which is about 1.5 inches from the inside wall of the pipe. The semiconductor transducers have a 0.1 inch diameter sensing area and were screwed in to remain flush with the inside of the pipe wall. As only two of the high-frequency response semi-conductor transducers were available, they were used mainly for the investigation of shock structure, for which the oscillations behind the shocks were desired. The diaphragm transducers were not used for this purpose because of the possibility of an air bubble entering the connecting portion between the inside of the pipe and transducer diaphragm itself, thereby possibly affecting its response. Both types of transducers were used for obtaining the pressure-time history of the transients. The $\pm$ 500 psi diaphragm had a natural frequency of 40 KHz, while the natural frequency of the 250 psi semiconductor transducers was 125 KHz.

For the recording of transient pressures a four channel Hewlett-

Packard Sanborn recorder with carrier-preamplifier units was used, allowing for the simultaneous recording of the pressure history at 4 points along the pipe. The output from the recorder could also be fed into a dual-trace RM35A Tektronix oscilloscope, to which a Polaroid camera unit could be also attached for photographing the pressure traces. The quicker response of the oscilloscope allowed for the detailed study of the shock structure.

Transient pressure records were obtained for a wide range of air concentrations, corresponding to the volumetric quality $0.005 < \beta < 0.10$. For the higher air concentrations slug flow occurred in the vertical downcomer. The lower limit of $\beta = 0.005$ was set so as to limit the maximum pressure rise to less than 150 psig. The liquid velocity was kept in the range of 4 fps to 5 fps, depending upon the desired air concentration.

Calibration of the pressure records corresponding to the desired amplifier setting was accomplished by keeping the water in the pipe stationary and adjusting the air pressure in the pressure tank. Both types of transducers used yielded nearly a linear response over the calibrated range. The positions of the oscilloscope beams were also calibrated in the same way, by taking a photograph of the beam position for each pressure setting. In the case of the copper-tubing apparatus the same four-channel Hewlett-Packard recorder with carrier amplifiers was used in conjunction with diaphragm pressure transducers to record the transient pressure at nine locations. For each set of conditions three tests were conducted in order to obtain data for all nine pressure taps. The pressure transducers for the respective tests were repositioned so that all nine

locations were eventually monitored, with overlapping to verify the reproducibility.

Measurement of Wave Celerity

The wave celerity was measured by noting on the photographs of the oscilloscope traces the time taken for the wave to pass two cross sections 4 ft apart. By means of a microswitch mounted in the arc of its path, the quick-acting gate valve at the downstream end of the pipe was employed to trigger the oscilloscope. By positioning the microswitch, the triggering time could be adjusted by trial. The microswitch provided a triggering signal to the oscilloscope from a 6 volt battery power supply. As explained in the previous section, the oscilloscope has input signals from the desired two channels of the recorder which in turn are connected to the pressure transducers through their carrier-preamplifier units. The sweeptime and voltage in the oscilloscope unit are adjusted suitably to obtain records as accurate as possible. In the case of shock waves with well-defined steep fronts, the celerity of the waves passing through the two-phase mixture could be accurately measured.

However, for determining the wave speed with only water in the test pipe, the above mentioned procedure is not as accurate as the beginning of the wave fronts could not be exactly located due to a precursor wave. For the case of pure water the wave speed was calculated from the initial pressure rise resulting from the sudden closure of the downstream valve. By also observing the period of oscillation, $T = 4L/a_{\ell p}$, subsequent to sudden closure the wave speed $a_{\ell p}$ was verified for pure water to be 2033 ft/sec.

Observation on Shock Structure

The shock structure was studied at two locations, 8 ft apart, on each leg of the test-pipe; namely, vertically-upward flow in the riser, horizontal flow, and vertically-downward flow in the downcomer. Photographs were obtained using the oscilloscope-triggering technique. The shock speed determined from these photographs were used in calculating shock thickness and period of oscillations behind the shock. Most of the photographs have a time scale of 5 ms/cm. The approximate range of volumetric quality in this investigation was $0.005 < \beta < 0.05$. For values of β above 0.05 the bubbles in the downcomer frequently have a tendency to form clusters and coalesce. Hence, the upper limit for the study of shock structure was limited to $\beta = 0.05$. The lower value of $\beta = 0.005$ is to limit the maximum pressures to about 150 psi, so as not to damage the pipe. Photographs were taken at one cross section of each leg of the pipe to determine the bubble-size distribution for each air concentration. From a statistical analysis, an average bubble size d_{50} was obtained from each photograph, from which a representative bubble size for other sections of the pipe was determined using the adiabatic law of expansion.

In order to observe the radial and translational oscillations of the bubble during the passage of the pressure wave, high-speed motion pictures were taken of the bubble motion 5 ft from the downstream valve subsequent to its sudden closure.

CHAPTER III

VELOCITY OF SOUND IN BUBBLY MIXTURE

The acoustic velocity or speed of sound in a bubbly mixture can be less than that for either phase as the effect of compressibility is governed by the gas while the effect of density is influenced by the liquid. For mixtures flowing in long conduits boundary resistance and elevation change influence the pressure gradient, which in turn affect the void fraction and finally the acoustic velocity. Furthermore, in the case of bubbly mixtures any relative velocity between the bubbles and the liquid can also affect the wave propagation velocity. In transient analyses of two-phase flow problems the space and time variation of the wave speed makes the problem even more complex if the possibility of the formation of shock waves from the steepening of compression waves is considered. In the following, various aspects of the velocity of sound, or the propagation velocity of small amplitude pressure pulses, are considered.

Wave celerity in two-phase media has been the subject of extensive study because of its vast applicability in transient problems, especially critical and choking-flow problems associated with the safety of nuclear reactors. Henry [13] gives a detailed derivation of an expression for a two-phase wave propagation velocity, defined by

$$a_{tp}^2 = \frac{dp}{d\rho_m} \tag{3.1}$$

in which p is the average cross-sectional pressure and ρ_m the mixture density. In terms of the average void fraction α and the densities of the gas phase ρ_g and the liquid phase ρ_ℓ, the mixture density ρ_m is defined as

$$\rho_m = \alpha\ \rho_g + (1-\alpha)\ \rho_\ell \tag{3.2}$$

As shown by Wallis [20] the void fraction α and the mass quality η can be expressed

$$\alpha = \frac{\eta\rho_\ell}{[(1-\eta)\ k\rho_g + \eta\rho_\ell]} \tag{3.3}$$

in which k is the ratio of gas velocity to liquid velocity. Combining Eqs. (3.2) and (3.3) and substituting in Eq. (3.1)

$$\begin{aligned} a_{tp}^2 = \{ & [\alpha^2 + \alpha(1-\alpha)\ \rho_\ell/\rho_g]\ \frac{d\rho_g}{dp} + [(1-\alpha)^2 \\ & + \alpha(1-\alpha)\ \rho_g/\rho_\ell]\ \frac{d\rho_\ell}{dp} + (\rho_g - \rho_\ell)\ \frac{\alpha(1-\alpha)}{\eta(1-\eta)}\ \frac{d\eta}{dp} \\ & - \alpha(1-\alpha)\ (\rho_g - \rho_\ell)\ \frac{dk}{dp}\ \}^{-1} \end{aligned} \tag{3.4}$$

For bubbly air-water mixtures it is reasonable to assume that no mass transfer occurs, or $d\eta/dp = 0$. The speed of sound in the liquid alone is defined by

$$a_\ell^2 = \frac{dp}{d\rho_\ell} \tag{3.5}$$

For gas-liquid mixtures at moderate pressures $\rho_g << \rho_\ell$. If a polytropic gas law

$$\frac{p}{\rho_g^m} = \text{constant} \tag{3.6}$$

is employed, Eq. (3.4) becomes

$$a_{tp}^2 = \{ [\alpha^2 + \alpha(1-\alpha)\ \rho_\ell/\rho_g]\ \frac{\rho_g}{mp} + [(1-\alpha)^2 + \alpha(1-\alpha)\ \rho_g/\rho_\ell]\ \frac{1}{a_\ell^2} + \alpha(1-\alpha)\ \rho_\ell\ \frac{dk}{dp} \}^{-1} \tag{3.7}$$

If a homogeneous model is considered in which the gas bubbles are assumed to move with the liquid velocity dk/dp is equal to zero. Eq. (3.7) then reduces to a form which is well documented in most of the literature, namely

$$a_h^2 = \{\frac{\rho_g}{mp}\ [\alpha^2 + \alpha(1-\alpha)\ \rho_\ell/\rho_g] + [(1-\alpha)^2 + \alpha(1-\alpha)\ \rho_g/\rho_\ell]\ \frac{1}{a_\ell^2}\ \}^{-1} \tag{3.8}$$

For $p/\rho_\ell a_\ell^2 << 1$ and $\alpha << 1$, Eq. (3.8) may be simplified by neglecting small-order terms

$$a_h^2 = \frac{mp}{\rho_\ell\ \alpha(1-\alpha)} \tag{3.9}$$

The polytropic exponent m will have a value of 1 for isothermal process and 1.4 for adiabatic process.

When the relative motion between the phases is to be considered dk/dp will not be zero. Henry [13] includes a virtual-mass term in the momentum equation for a discrete volume of gas and defines a coefficient of virtual mass C_M as a function of α. The value of dk/dp is approximated to $(-1/C_M a_{tp}^2 \rho_\ell)$ under certain assumptions and an expression for a_{tp} is obtained by substitution in Eq. (3.7)

$$a_{tp}^2 = [1 + \alpha(1-\alpha)/C_M]\, a_h^2 \tag{3.10}$$

in which a_h is given by Eq. (3.8). The added-mass coefficient C_M is shown to depend on the void fraction α and the bubble size distribution. For spherical bubbles Prosperetti and van Wijngaarden [22] suggest the following empirical relation between C_M and α

$$C_M = 0.5(1 + 2.76\ \alpha) \tag{3.11}$$

It appears that a value of 0.5 for C_M is reasonable for spherical bubbles for which $\alpha << 1$.

Crespo [17] considered the relative motion of gas bubbles in deriving expressions for the acoustical velocity. For low frequencies the gas bubbles have been shown to behave isothermally because of the negligible effect of relative motion. At high frequencies the viscous forces are negligible, causing the relative motion to have an influence on the acoustic velocity. The bubbles in this case are shown to behave adiabat-

ically. The low frequency speed of sound is given by Eq. (3.9) with $m = 1$

$$a_{tp}^2 = \frac{p}{\rho_\ell \alpha(1-\alpha)} \tag{3.12}$$

The high frequency speed is higher than that predicted by Eq. (3.9) with $m = \gamma = 1.4$ by a factor $(1 + 2\alpha)$ and hence,

$$a_{tp}^2 = \frac{\gamma\, p(1+2\alpha)}{\rho_\ell \alpha(1-\alpha)} \tag{3.13}$$

in which γ is the isentropic exponent. The frequencies are defined as being high when $\omega R^2 >> \nu_\ell$, in which ω is the frequency, R the bubble radius and ν_ℓ the kinematic viscosity of the liquid. These definitions of low and high frequencies are the limiting cases.

Mori et al. [23] have demonstrated the effect of pipe elasticity on the wave-propagation velocity, showing that the pipe elasticity has any appreciable effect only for void fractions $\alpha < 0.01$. Fanelli and Reali [24] have proposed an analytical method for predicting the speed of sound in a two-phase gas-liquid mxiture, including surface-tension effects. The actual numerical calculation is elaborate and requires the numerical solution of a system of equations, however.

The size and distribution of the bubbles can have an appreciable influence on the propagation of disturbances through a mixture. The size of bubbles is an important factor in deciding upon the proper law of expansion for the bubbles. Plessent [25] has investigated the radial oscillations of bubbles at arbitrary frequencies, concluding that the oscil-

lations are isothermal at both low and high frequencies and adiabatic in an intermediate range. If the acoustical wave length λ_g in gas is much greater than the bubble radius R and if the thermal penetration depth defined as $(D_g/\omega)^{1/2}$, in which D_g is the thermal diffusivity for gas and ω the angular frequency of bubble oscillations, is much less than R, the frequencies are defined as intermediate, Plesset [25]. Van Wijngaarden [26] has shown, based on Plesset's theory, that for shock velocities of order 10^2 m/sec and thicknesses of order 10^{-2} m the frequencies of oscillations of bubbles of radii of the order of 10^{-3} m fall in the intermediate range, and therefore the velocity of propagation is governed by the adiabatic theory. In fact, this is the case with the present investigation, and hence Eq. (3.8), or Eq. (3.9) with m = 1.4, will be a better representation for the calculation of the acoustic velocity. To take into account the effect of relative motion Eq. (3.10) may be used. Use of Eq. (3.13), which was formulated by Crespo [17], is probably less desirable because the viscous resistance due to relative bubble motion has been neglected in the analytical development. For very low values of void fraction, for example $0.005 < \alpha < 0.08$ for this study, the correction for relative motion does not produce any large changes in the wave celerity from that predicted from homogeneous theory.

Gregor and Rumpf [27] have developed a theory for calculating the velocity of sound using mass and momentum balances. The velocity of sound has been shown to depend on the relative velocity between phases, the ratio of mass densities, porosity, particle diameter and the drag coefficient. However, the theory is applicable only to evenly distributed bubbles of uniform spherical shape, a condition which limits its usefulness.

CHAPTER IV

SHOCK-WAVE THEORY

Waves involving a step change or a finite discontinuity in pressure, density, temperature and velocity are referred to as shock waves. As discussed earlier, a compression wave propagating in a long pipe carrying a gas-liquid mixture undergoes a continuous change in its form because of the varying pressure, void fraction, and consequently wave celerity along the conduit. The velocity of propagation is higher near the wave crest and lower towards the wave trough, resulting in a steepening of the front of the wave, ultimately leading to shock-wave formation.

Noordzij and van Wijngaarden [28] have described in detail the formation of shock waves in mixtures of liquid and air bubbles, based on the similar processes in gas dynamics, as explained by Lighthill [29]. In gas dynamics it is well established that a compression wave steepens due to convection, ultimately resulting in a steady shock wave if wave steepening is balanced by viscous diffusion. In the case of bubbly mixtures the steepening, also referred to as amplitude dispersion, is mainly caused by wave compression. For the compressed part of the wave the pressure is higher and the void fraction is lower than the expanding part. As can be demonstrated upon inspection of Eq. (3.9) the velocity of propagation in the compressed region is higher than that in the expanding portion, resulting in an unbalance known as nonlinear steepening by compression. This steepening process is resisted by two other phenomena, frequency dispersion and dissipation. The frequency dispersion is due to the existence of a

pressure difference across the gas bubble, and the associated radial oscillations. The relative translational and radial motions of bubbles are resisted by the viscosity of the liquid, which constitutes the viscous dissipation effect. Other dissipation mechanisms due to thermal conduction and acoustic radiation may exist. Van Wijngaarden [30] has shown that steady shock-wave solutions of the hydrodynamic equation for wave propagation in bubbly mixtures are not possible without the inclusion of the dissipation term.

Noordzij and van Wijngaarden [28] have described in detail the relaxation effects caused by the radial and translational motion of the bubbles. The radial motion is described by an equation similar to the form used by Plesset [25]

$$p_g - p = \rho_\ell [R \frac{d^2R}{dt^2} + \frac{3}{2}(\frac{dR}{dt})^2 + R\ \delta\omega_B \frac{dR}{dt}] \qquad (4.1)$$

in which p_g is the pressure inside the bubble and p is the pressure of the liquid outside the bubble. R is the radius of the bubble and ω_B its resonance frequency given by $(3\gamma p/\rho_\ell R^2)^{1/2}$. δ is a damping factor which embodies the sum effect of viscous dissipation, heat conduction and acoustic radiation.

The translational motion can be expressed by using the theory of bubble dynamics originated by Levich [31]. The frictional resistance offered by the liquid is related to the relative velocity of bubble and liquid. By neglecting the mass of the gas an equation of motion of a single bubble can be written

$$\frac{1}{2}\rho_{\ell}\forall\frac{d}{dt}(v-u)+12\pi R\mu_{\ell}(v-u)=-\forall\frac{dp}{dx} \qquad (4.2)$$

in which v and u represent the velocities of the bubble and the liquid, respectively, $\forall$ is the volume of a bubble, and μ_{ℓ} is the dynamic viscosity of the liquid. Noordzij and van Wijngaarden [28] use Eq. (4.1) and (4.2) together with the conservation of mass and momentum to describe the problem of wave propagation in bubbly mixtures. They also employ the concept of conservation of number density n, defined as the number of bubbles per unit volume, and an adiabatic law for the bubble behavior. It may be noted that the conservation of number density is based on the assumption that all bubbles are of uniform size and no coalescence or breakup occurs. Furthermore, in the use of Eq. (4.2) the interbubble influence, or in other words the bubble distribution pattern, is ignored.

By neglecting the relative translational effect and using Eq. (4.1) together with the conservation equations of mass, momentum and number density, Noordzij and van Wijngaarden [28] obtained a single hydrodynamic equation of the Korteweg-de Vries type with an additional dissipation term in it. Solutions of the shock-wave type are shown to exist for this equation. More details on this are not included here as the derivation of the equation is too involved.

Hugoniot Relations

Consider a shock wave moving with a constant speed U in the negative x-direction as illustrated in Fig. 4. Let the upstream quantities be expressed with a suffix o and the downstream quantities with a suffix 1.

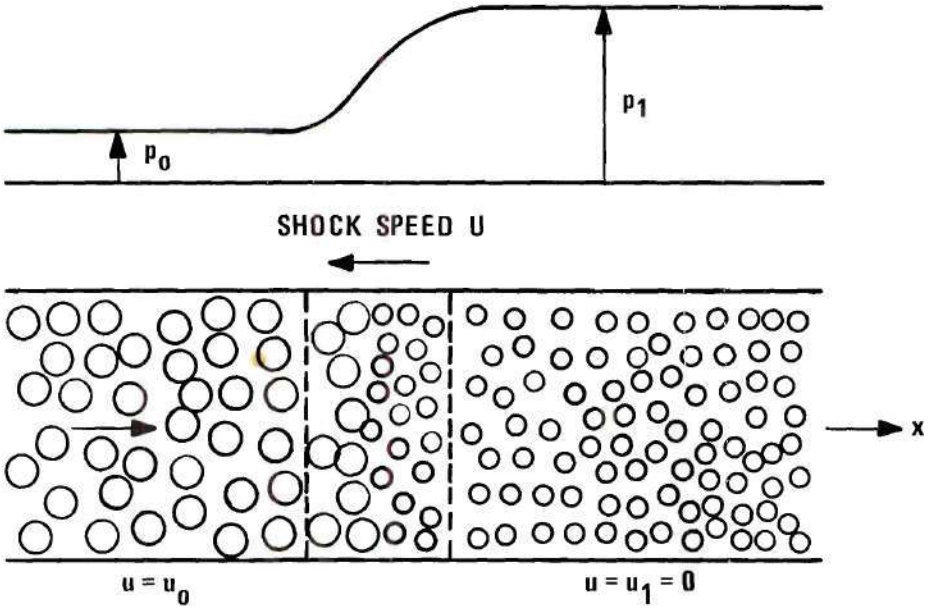

Figure 4. Shock Wave Propagating in the Negative x-Direction.

The velocity of the liquid u behind the shock is equal to zero, corresponding to the typical case of a wave resulting from the closure of a downstream valve in a pipeline. The shock can be considered stationary by superposing a velocity U in the direction opposite to that of the shock. The conservation of mass of the mixture gives

$$\rho_{m_o} (U + u_o) = \rho_{m_1} U \tag{4.3}$$

The conservation of momentum of the mixture yields

$$\rho_{m_o} (U + u_o)^2 - \rho_{m_1} U^2 = p_1 - p_o \tag{4.4}$$

Combining Eqs. (4.3) and (4.4)

$$\frac{\rho_{m_o}(U + u_o)^2}{p_o} \left(1 - \frac{\rho_{m_o}}{\rho_{m_1}}\right) = \frac{p_1}{p_o} - 1 \tag{4.5}$$

Campbell and Pitcher [16] have shown that the temperature rise ΔT across the shock is extremely small for moderate shocks. Using the unsteady energy equation for a perfect gas, they obtained this expression for ΔT

$$\Delta T = \frac{[(p_1/p_o)^2 - 1]\, \xi C T_o}{2 p_1/p_o \quad \rho c_\ell} \tag{4.6}$$

in which ξ is the mass of gas to mass of liquid in a given volume of mixture, C the universal gas constant, w the mean molecular weight of gas, and c_ℓ the specific heat of the liquid. Using Eq. (4.6) they showed that the temperature rise ΔT for $p_1/p_o = 10$, for $\epsilon = 0.5$, and for S.T.P., is only 0.1^oC for a mixture of air and water.

If the bubbles are assumed to move with the liquid the mass of air in a unit of mass of mixture is a constant, yielding

$$\frac{\rho_{g_o}\ \alpha_o}{\rho_{m_o}} = \frac{\rho_{g_1}\ \alpha_1}{\rho_{m_1}} \tag{4.7}$$

For the adiabatic gas behavior

$$\frac{p_o^{1/\gamma}}{\rho_{g_o}} = \frac{p_1^{1/\gamma}}{\rho_{g_1}} \tag{4.8}$$

By approximating $\rho_m = \rho_\ell(1-\alpha)$ in Eq. (4.7) and using Eq. (4.8)

$$\frac{1-\alpha_o}{1-\alpha_1} = \left(\frac{p_o}{p_1}\right)^{1/\gamma} \frac{\alpha_o}{\alpha_1} \tag{4.9}$$

The adiabatic speed of sound from Eq. (3.9) can be used assuming $\alpha_o << 1$ to obtain a relation

$$\frac{a_{h_o}^2\ \alpha_o}{\gamma} = \frac{p_o}{\rho_\ell(1-\alpha_o)} = \frac{p_o}{\rho_{m_o}} \tag{4.10}$$

Combining Eqs. (4.10) and (4.5)

$$\frac{(U + u_o)^2}{a_{h_o}^2} \gamma \left[\frac{\alpha_o - \alpha_1}{1-\alpha_1}\right] = \frac{p_1}{p_o} - 1 \tag{4.11}$$

If $1-\alpha \simeq 1$, Eqs. (4.9) and (4.11) can be combined to

$$\frac{(U + u_o)^2}{a_{h_o}^2} \gamma \left(1 - \frac{p_o}{p_1}\right)^{1/\gamma} = \frac{p_1}{p_o} - 1 \tag{4.12}$$

By defining a Mach number $M_o = U/a_{ho}$, and imposing the condition $U >> u_o$, Eq. (4.12) becomes

$$M_o^2 = \frac{p_1/p_o - 1}{\gamma[1 - (\frac{p_o}{p_1})^{1/\gamma}]} \tag{4.13}$$

For the isothermal case for which $\gamma = 1$, Eq. (4.13) reduces to

$$M_o^2 = \frac{p_1}{p_o} \tag{4.14}$$

which agrees with the expression derived by Campbell and Pitcher [16] for isothermal bubble behavior.

Shock-Wave Propagation through a Nonuniform Medium

In the case of a long pipe line the existence of a pressure gradient causes the average void fraction to vary along the pipe. For a vertical pipe gravity plays a very important role in addition to the

friction offered by the pipe wall. Noordzij [32] has discussed the effect of nonuniformity caused by elevation change, proving that the propagating pressure pulse is the difference between the actual and the undisturbed pressures. Whitham [33] has described in detail a theory to estimate the effects of the gravity-caused nonuniformity in the x direction on the Mach number and on the pressure ratio. Neglecting the relative-motion effects, pipe-wall friction, pipe-wall elasticity, and water compressibility for a vertical pipe in which the mixture flows upwards with a velocity u, the conservation of mass and the conservation of momentum can be stated respectively

$$\frac{\partial \rho_m}{\partial t} + \frac{\partial}{\partial x}(\rho_m u) = 0 \tag{4.15}$$

$$\rho_m \frac{\partial u}{\partial t} + \rho_m u \frac{\partial u}{\partial x} = -\frac{\partial p}{\partial x} - \rho_m g \tag{4.16}$$

By defining the material derivative

$$\frac{d}{dt} = \frac{\partial}{\partial t} + u \frac{\partial}{\partial x} \tag{4.17}$$

Eq. (4.15) can be written

$$\frac{d\rho_m}{dt} + \rho_m \frac{\partial u}{\partial x} = 0 \tag{4.18}$$

Defining

$$\frac{d\rho_m}{dt} = \frac{dp/dt}{dp/d\rho_m} = \frac{1}{a_m^2}\frac{dp}{dt} \tag{4.19}$$

in which a_m is the speed of sound in the mixture

$$\frac{\partial p}{\partial t} + u\frac{\partial p}{\partial x} + a_m^2 \rho_m \frac{\partial u}{\partial x} = 0 \tag{4.20}$$

Equations (4.16) and (4.20) can be used to derive the characteristic equation

$$\frac{dp}{dt} + \rho_m a_m \frac{du}{dt} + \rho_m a_m g = 0 \tag{4.21}$$

which is valid along the characteristic C^+

$$\frac{dx}{dt} = u + a_m \tag{4.22}$$

and

$$\frac{dp}{dt} - \rho_m a_m \frac{du}{dt} - \rho_m a_m g = 0 \tag{4.23}$$

valid along the characteristic C^-

$$\frac{dx}{dt} = u - a_m \tag{4.24}$$

For a shock wave moving in the negative x direction, Eqs. (4.23) and (4.24) can be applied just behind the shock with $p = p_1$, $\rho_m = \rho_{m_1}$, $u = u_1$, and $a = a_1$

$$dp_1 - \rho_{m_1} a_{m_1} du_1 = \frac{\rho_{m_1} a_{m_1} g}{u_1 - a_{m_1}} dx \tag{4.25}$$

Using the Hugoniot shock relationship Eq. (4.13), after some rearrangement and mathematical simplification of Eq. (4.25) a differential equation can be obtained having the form

$$\Psi(M_o) \frac{dM_o}{dx} - \Phi(\alpha_o, p_o) \rho_\ell g = 0 \tag{4.26}$$

in which $\Psi(M_o)$ is a function of M_o, and $\Phi(\alpha_o, p_o)$ is a function of α_o and p_o. Both functions Ψ and Φ depend upon the thermodynamic gas behavior, whether isothermal or adiabatic. The solution to Eq. (4.26) has been reported by Noordzij [32] in the form

$$\frac{M_o^2}{\gamma} - 1 = Z \left(\frac{1}{p_o}\right)^{1/2} \tag{4.27}$$

in which Z is a constant.

If M_{oo} defines the Mach number at x = 0 and M_o the corresponding one at x = X, from Eq. (4.27) it follows that

$$\frac{M_o^2 - \gamma}{M_{oo}^2 - \gamma} = \left\{\frac{p_{oo}}{p_o}\right\}^{1/2} \tag{4.28}$$

in which

$$p_o = p_{oo} - \rho_\ell g X \tag{4.29}$$

neglecting the weight of the gas phase. For a step-by-step derivation of the differential equation and the above relationships Noordzij [32] and Whitham [33] may be referred to.

Structure of Shock Waves

The shock waves formed in a bubbly gas-liquid mixture have a structure different from that of shocks in gas dynamics. The main difference is due to the frequency dispersion phenomenon peculiar to bubbly mixtures. This phenomenon has already been explained earlier as being caused by the inertia of the radial flow associated with an oscillating bubble. Crespo [17] defines two Mach numbers, one based on the low-frequency speed of sound and the other based on the high frequency. The condition for a shock to exist is that the former Mach number be greater than unity. Whenever both Mach numbers are greater than unity, the shock wave starts with an exponential rise in pressure, followed by a relaxation region in which the pressure oscillates around its final equilibrium value. The oscillations are damped by viscous and thermal dissipation. When the low frequency

Mach number is less than unity, the oscillations behind the shock disappear and a uniform and conventional shape occurs. Crespo's definition of the speed of sound for low and high frequencies are given by Eqs. (3.12) and (3.13). For low frequencies the bubbles are assumed to move with the same velocity of the liquid, whereas for high frequencies an unresisted relative motion is assumed.

The structure of a shock wave in a bubbly gas-liquid mixture is characterized by the steep-rising front region, the pressure oscillations at the back, and a smooth region in which pressure gradually attains its final value. The radial and translational relative motion of the bubble affect the shock structure considerably. Noordzij and van Winjaarden [28] have explained the nature of shocks based on the phenomena of compression, frequency dispersion, and dissipation, all of which are associated with the radial and translational relative motion of the bubbles. The resulting shock waves may be classified as A, B, and C types. An A-type shock has a steep front rising above the equilibrium pressure, followed by damped oscillations about the final equilibrium level. In this case the shock is governed by the balance between the nonlinear compression, dispersion and dissipation due to radial motion. It may be noted that the dissipation due to translational relative motion is negligibly small here. A B-type shock has a very narrow steep front, which does not reach the equilibrium pressure level, followed by an oscillating but gradually rising part, which ultimately does reach the equilibrium level. In this case the shock is governed by all of the above effects, including the dissipation due to relative translational motion. A C-type shock exists when the dissipation due to relative translational motion is larger than that

due to radial motion. Here the frequency dispersion effects are not pronounced and the oscillations do not appear. Hence, a C-type shock is mainly a weak shock resulting from a balance between nonlinear compression and dissipation due to translational relative motion. The pressure profile is smooth and covers a region at least an order of magnitude thicker than that of an A-type shock. Fig. 5 shows the typical profiles of the three types of shocks.

Noordzij and van Wijngaarden [28] have reported a gradual change of a shock's structure from type A to C during its passage through a shock tube of about 15 ft length and about 2 inches internal diameter. They attribute the changing shock structure to the effect of the relative translational motion, and compare the phenomenon with thermal relaxation in gas dynamics by defining a relaxation time τ as the time required for the bubbles to adjust to the liquid velocity by viscous drag. The time τ is given by

$$\tau = R^2/18\,\nu_\ell \tag{4.30}$$

in which R is the bubble radius and ν_ℓ the kinematic viscosity of the liquid. For a time less than the relaxation time, the translational motion does not affect the shock, resulting in the formation of an A-type shock. Noordzij [32] and Noordzij and van Wijngaarden [28] report that experimental results showed the relaxation times to be as much as 50 per cent less than that calculated from Eq. (4.30). This discrepancy is partly attributed to the increased drag due to the nonspherical shapes a bubble assumes on the passage of a shock wave. The experimental errors

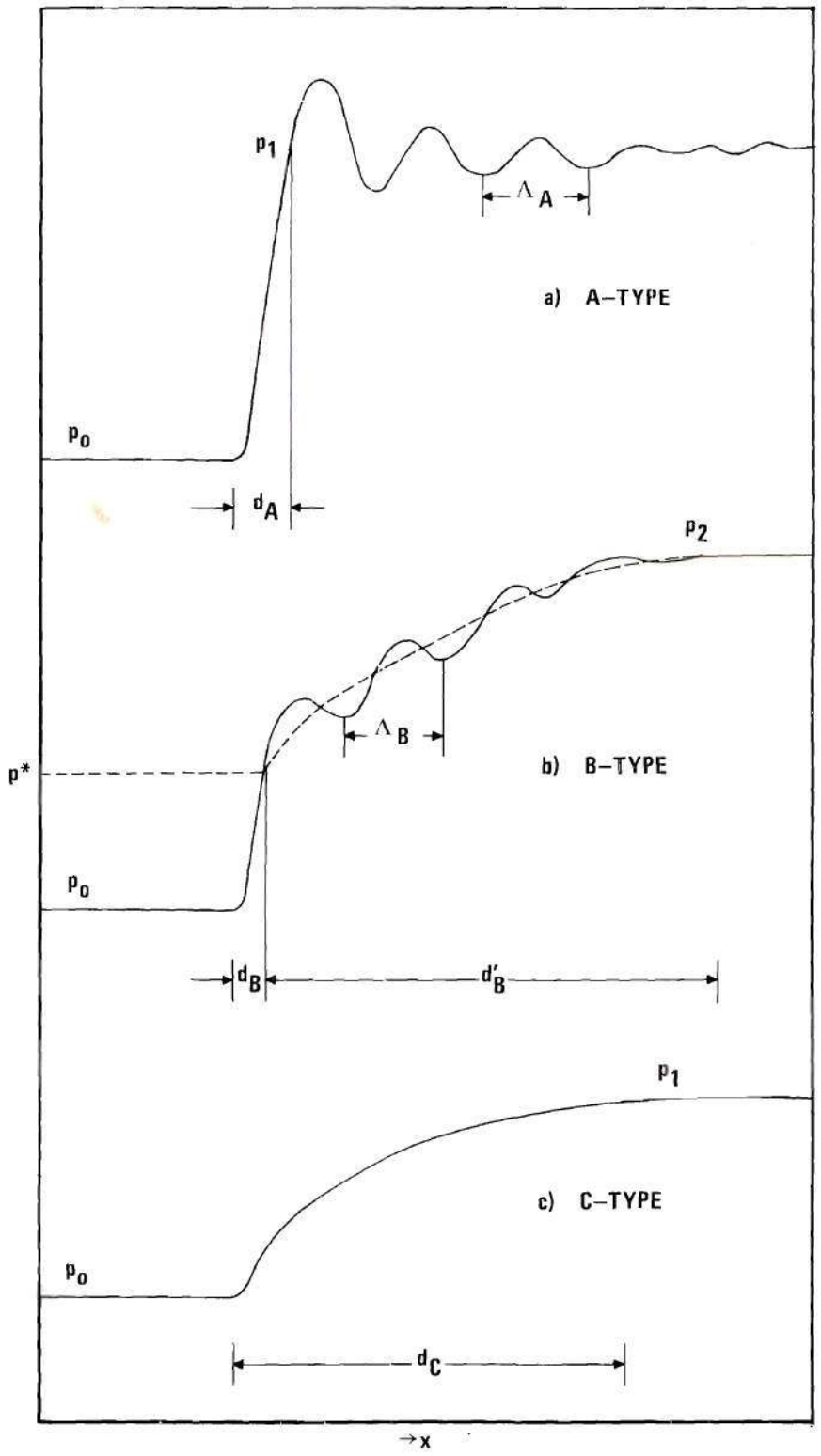

Figure 5. Definition of Types of Shock Waves.

involved in the determination of bubble radius, shock thickness and shock speed probably also contributed to inaccuracies in their experimental data, which were estimated to be as much as 20 per cent by the authors.

Noordzij [32] has investigated the three type of shocks separately. By using the continuity and momentum equations for the shock wave, and Eqs. (4.1) and (4.2), which describe the frequency disperison and relative translational motion, they formulated a third-order differential equation to describe the actual profile for each type of shock. The derivations of these differential equations are quite involved and are based upon many assumptions. Following a linearization procedure which considers the outskirts of the shock, theoretical expressions for the thicknesses d_A, d_B, d_B' and d_C defined in Fig. 5 can be obtained. The C-type shocks are shown to occur when

$$\frac{p_1}{p_o} < 1 + \frac{4\gamma\alpha_o}{1 + \gamma} \tag{4.31}$$

which is a condition for the front portion of the wave to represent a balance between the nonlinear compression and the dissipation due to relative motion. A summary of the theoretical expressions for the shock parameters for the three types of shocks obtained by Noordzij [32] is as follows.

The thickness of the steep front of a A-type shock is expressed as

$$d_A = \frac{R_o \ell_n 20}{(3\alpha_o)^{1/2} [(1 - M_o^{-2})^{1/2} - 0.5 \delta']} \tag{4.32}$$

in which M_o is defined by Eq. (4.13) and δ' is a damping parameter given by

$$\delta' = \delta\omega R_o / U(3\alpha_o)^{1/2} \tag{4.33}$$

The value of δ will include the effect of viscous, thermal and acoustical damping. Expression for each of these damping terms are given by Noordzij [32]. The wave length of oscillations behind a A-type shock is

$$\Lambda_A = \frac{2\pi R_o y^{2/3}}{[3\alpha_o (M_o^{-2} y^{-\gamma} - y)]^{1/2}} \tag{4.34}$$

in which

$$y = (p_o/p_1)^{1/\gamma} \tag{4.35}$$

The thickness of a B-type shock may be divided into two parts, a steep front part d_B and a gradual-rising rear part d_B'. Dispersion dominates in the front part, for which d_B is given by

$$d_B = \frac{R_o \ \ell n\ (20F)}{(3\alpha_o)^{1/2} \{ [1-M_o^{-2}(1 + 2\alpha_o)]^{1/2} - 0.5\ \delta' \}} \tag{4.36}$$

in which

$$F = 1 - \gamma\alpha_o \frac{y^{-\gamma}\ (1+y)}{\gamma y^{-\gamma} - y\ M_o^{\ 2}/\gamma} \tag{4.37}$$

The thickness d_B' of the relaxation-dominated rear part is expressed by

$$d_B' = \{ \ell n[20(1-F)] \quad U\tau/y^{2/3} \tag{4.38}$$

in which τ is defined by Eq. (4.30). The wave length Λ_B of the oscillations behind the shock is

$$\Lambda_B = \frac{2 \pi R_o y^{2/3}}{\left[3 \alpha_o [M_o^{-2} y^{-\gamma} - y_1 + 2 \alpha_o y_1^{1-\gamma} M_o^{-2}]\right]^{1/2}} \tag{4.39}$$

The thickness d_C of a C-type shock is given by

$$d_C = \frac{4 \alpha_o U\tau \ell n (20)}{(\gamma M_o^2 - 1)} \tag{4.40}$$

Noordzij [32] provides a comparison of the shock thicknesses and wave lengths obtained from the above relations with experimental values. Experimental results have been reported for air-bubble-liquid mixtures having three different liquid viscosities, $\nu_\ell \simeq 10^{-5}$ ft^2/sec for tap water, $\nu_\ell \simeq 0.7(10^{-4})$ ft^2/sec, 3 (10^{-4}) ft^2/sec, and 1.1 (10^{-3}) ft^2/sec for aqueous solutions of glycerine of 50, 70, and 85 per cent, respectively. The shock was produced in a shock tube by puncturing a diaphragm, below which a pressure below atmospheric was maintained. The bubbles were of about 1.1 mm radius and of uniform size. The value of the average void fraction ranged from about 0.005 to 0.06. At x = 0.66 ft in the 14.8 ft long tube a A-type of shock was observed, which in many cases

transformed to a B-type at x = 8.2 ft, and then to a C-type at x= 13.1 ft. The characteristics of the shocks, namely the thickness and wave length, were obtained from photographs.

The experimental values of thicknesses and wave lengths showed a large scatter, but a statistical average value was used by Noordzij [32]. Even this value differed considerably from the theoretical values, especially for B- and C-type shocks. The large differences were attributed to the nonspherical nature of bubbles causing higher drag forces than could be predicted by theory. The experimental shock thicknesses were reported to be higher than those determined theoretically. Both experiment and theory showed, however, that the shock thickness and corresponding wave lengths of oscillations behind the A or B-type shocks are of the same order of magnitude.

The existence of C-type shocks can be related to the effect of the viscous forces on the relative motion, as shown by Crespo [17]. This effect is also explained by Noordzij and van Wijngaarden [28], who stated that, if viscous dissipation is balanced by nonlinear steepening, and if thermal relaxation is neglected, the condition for C-type shocks to exist is given by Eq. (4.31). The relaxation time τ associated with viscous relaxation is given by Eq. (4.30). For the thermal relaxation a corresponding relaxation time may be defined by

$$\tau' = R_o^2/D_g \tag{4.41}$$

in which D_g is the thermal diffusivity of the gas. If τ and τ' are of the same order of magnitude thermal relaxation is also important. Thermal

relaxation signifies a gradual transition from adiabatic to isothermal behavior within the shock. Whenever a steady state is reached, the weak sound wavelets in front of the shock travel with the same speed as the shock itself. The maximum speed of the wavelets based on the thermal relaxation theory is the adiabatic speed given by Eq. (3.9) with m = 1.4. The condition for the existence of C-type shocks may be that the shock speed is less than the adiabatic speed of sound, which is $\gamma^{1/2}$ times the isothermal speed of sound. Using the Hugoniot relation given by Eq. (4.14), the above condition may be written as

$$p_1/p_o < 1.4 \tag{4.42}$$

Hence, in the event of the thermal relaxation being of equal importance, Eq. (4.42) may be an approximate condition for existence of C-type shocks.

Noordzij [32] has reported that the influence of the gravitational pressure gradient on shock structure is negligible. A shock propagating vertically downward will experience an extremely small stretching, which may be neglected in studies on shock structure with practically no error. The use of local values of pressure and void fraction is usually adequate.

It may be noted that the theoretical expressions for shock structure proposed by Noordzij [32] are based on assumptions of uniform spherical bubbles, Levich's model for fluid drag, conservation of number density which allows for no coalescence, no breakup of bubbles, and neglect of initial buoyancy-induced relative motion. The friction offered by pipe walls and the pipe-wall elasticity are also not considered. Experi-

mental verification of the theory has normally been accomplished by using a shock tube, in which the initial wave form has a very steep front. However, in the case of the present study, the initial wave form depends on the time of closure of a valve, which could be varied from about 10 ms to 100 ms, as desired. A shock produced in a shock tube induces a motion to the mixture, which was initially stationary. To the contrary, in the present study the mixture is brought nearly to rest by action of the shock. In the present study these differences limit the use of the theoretical equations for the prediction of the shock structure. Because of the extreme analytical difficulties, no attempt has been made to modify the theories described in Noordzij [32] and Noordzij and van Wijngaarden [28] to suit the present problem. Hence, a qualitative study of the shock structure is presented herein rather than a quantitative one. It was noted, however, that the oscillations behind a shock wave are damped very quickly due to the dissipative mechanisms involved and the amplitudes of the resulting oscillations are very small compared to the initial pressure rise associated with a shock wave. The above points are evident from a comparison of shock trace photographs presented by Noordzij [32] and by Noordzij and van Wijngaarden [28] with ones of the present study, which are included in Chapter VIII. The oscillations have a high frequency compared to the characteristic frequency associated with water-hammer in pipes. Hence, it is reasonable to assume that the shock structure may have no significant influence on transient analyses for gas-liquid mixtures in long conduits.

CHAPTER V

ONE-DIMENSIONAL CONSERVATION EQUATIONS

The governing equations for unsteady two-phase flow are more complicated and numerous than their single-phase flow counterparts. Consequently, in an effort to simplify the equations for easier mathematical handling, many research workers in the area have adopted their own assumptions and have proposed different types of models, which mostly lack a general applicability over a wide range of conditions. In the present study, two-phase two-component flow is investigated in only the bubbly and slug-flow regimes. Even if the analysis is restricted to the bubbly-flow regimes the problem is quite complex, allowing for varying assumptions in the formulation of an analytical model.

Wallis [20] has described the various analytical one-dimensional approaches to the problem. Mainly there are three types of models: homogeneous, separated-flow and drift-flux. In the homogeneous model the components are treated together as a single pseudofluid with average properties. The slip between the gas and liquid is not considered in this, and consequently the gas and liquid velocities are assumed equal at every instant. In the case of vertical flow of bubbly mixtures, the buoyancy effects can play an important enough role that relative velocity between the air bubbles and the liquid can be considerable. Hence, apart from the simplicity involved, a homogeneous model may not be appropriate in many cases. In the separated-flow model the phases are considered to flow side-by-side, interacting with each other. Generally, a separated-

flow model will necessitate six equations to represent the conservation of mass, momentum and energy of each of the phases. Additional equations describing the interaction between the phases are also needed, severely complicating the problem. Often a simplified version of a separated-flow model is used in which one or more of the conservation equations are written for the mixture rather than for the individual phases. In this type of formulation only the velocity difference between the phases is included. In the drift-flux model the relative motion between the two phases is given attention rather than the motion of the two phases individually. This model is particularly remarkable in that it can include the effect of velocity and concentration profiles. However, since several empirical relationships are an essential part of the drift-flux model, it may not have a general applicability for a wide range of problems. The relative advantages and disadvantages of each of the above models are dependent upon the nature of the transient two-phase flow.

In this section, the one-dimensional conservation equations of the mass of the liquid phase, the mass of the gas phase, and the momentum of the mixture are developed for the unsteady flow of a gas-liquid mixture in a long pipe line. The elasticity of pipe walls and the compressibility of the liquid are included and the void fracton α is assumed to be much less than unity. As the temperature change across a pressure wave in a gas-liquid mixture is normally small, as reported by Campbell and Pitcher [16] for shock waves in a bubbly air-water mixture, it is not necessary to employ the energy equation.

The three conservation equations are expressed in different forms by combining and rearranging them for use in the bubble-dynamics model in

the next chapter. The relative motion between the gas and liquid phases is incorporated in the momentum equation as an added-mass, or Kelvin-impulse effect, based upon the approach used by Noordzij [32] and Prosperetti and van Wijngaarden [22]. Finally, the derived conservation equations are simplified for a homogeneous equilibrium case in order that they can be expressed in characteristic form. A separated-flow model that incorporates bubble dynamics into the one-dimensional conservation equations is presented in the next chapter. Finally, in Chapter VII a drift-flux model is developed for transient-flow analysis.

Assumptions

The following assumptions are made in developing the one-dimensional conservation of mass and momentum equations for unsteady two-phase flow through a pipeline:

a) Average values of the liquid velocity, u, and density, ρ_ℓ are used for the specified cross-section of the pipe.

b) The void fraction α is the cross-sectional average value.

c) The difference between the pressure inside and outside of a bubble is ignored by using a constant value p for the cross section.

d) Contribution of the gas phase to the momentum of the mixture is neglected. This is a reasonable assumption as $\rho_g << \rho_\ell$ and $\alpha << 1$.

Conservation of Mass of Liquid

Let A be the area of cross section of the pipe, u the liquid velocity, ρ_ℓ the liquid density and α the average void fraction. Consider two cross sections in the pipe at a distance Δx apart. The conservation of the mass of the liquid within the control volume bounded by

the cross-sections yields

$$\rho_\ell(1-\alpha)Au - \{\rho_\ell(1-\alpha)Au + \frac{\partial}{\partial x}[\rho_\ell(1-\alpha)Au]\,\Delta x\}$$

$$= \frac{\partial}{\partial t}[\rho_\ell(1-\alpha)A\ \ \Delta x] - \Gamma A\Delta x \qquad (5.1)$$

or $$\frac{\partial}{\partial t}[\rho_\ell(1-\alpha)A] + \frac{\partial}{\partial x}[\rho_\ell(1-\alpha)Au] = -\Gamma A \qquad (5.2)$$

in which Γ is the rate of gas production per unit volume.

Expanding Eq. (5.2) for $\Gamma = 0$ and employing the material derivative defined in Eq. (4.17)

$$\rho_\ell(1-\alpha)\frac{dA}{dt} + A(1-\alpha)\frac{d\rho_\ell}{dt} + \rho_\ell A\frac{d(1-\alpha)}{dt} + \rho_\ell(1-\alpha)A\ \ \frac{\partial u}{\partial x} = 0 \qquad (5.3)$$

As reported by Streeter and Wylie [34], the wall elasticity effect can be expressed

$$\frac{1}{A}\ \frac{dA}{dt} = \frac{D\varepsilon}{Ee}\frac{dp}{dt} \qquad (5.4)$$

and the liquid compressibility

$$\frac{1}{\rho_\ell}\frac{d\rho_\ell}{dt} = \frac{1}{K_\ell}\frac{dp}{dt} \qquad (5.5)$$

Defining

$$\frac{1}{\rho_\ell\ a_{\ell p}{}^2} = \frac{1}{K_\ell} + \frac{D\varepsilon}{Ee} \qquad (5.6)$$

where D is the diameter of the pipe, e is the pipe wall thickness, ε is a pipe constraint factor, K is the liquid bulk modulus, E is Young's modulus of elasticity of pipe wall, and $a_{\ell p}$ is the acoustic velocity for the liquid phase alone in the elastic pipe.

Using Eqs. (5.4), (5.5) and (5.6), Eq. (5.3) may be written as

$$\frac{(1-\alpha)}{\rho_\ell a_{\ell p}^2} \frac{dp}{dt} + \frac{d(1-\alpha)}{dt} + (1-\alpha) \frac{\partial u}{\partial x} = 0 \tag{5.7}$$

Upon expanding

$$\frac{(1-\alpha)}{\rho_\ell a_{\ell p}^2} \frac{\partial p}{\partial t} + \frac{\partial(1-\alpha)}{\partial t} + \frac{(1-\alpha)u}{\rho_\ell a_{\ell p}^2} \frac{\partial p}{\partial x} + u \frac{\partial(1-\alpha)}{\partial x} + (1-\alpha) \frac{\partial u}{\partial x} = 0 \tag{5.8}$$

Eq. (5.7) can also be written

$$\frac{dp}{dt} + \rho_\ell a_{\ell p}^2 \frac{\partial u}{\partial x} - \frac{\rho_\ell a_{\ell p}^2}{(1-\alpha)} \frac{d\alpha}{dt} = 0 \tag{5.9}$$

If the pipe-wall expansion and the liquid compressibility are neglected, A and ρ_ℓ are constants, Eq. (5.2) reduces to

$$\frac{\partial}{\partial t}(1-\alpha) + \frac{\partial}{\partial x}[(1-\alpha)u] = 0 \tag{5.10}$$

Conservation of Mass of Gas

Consider a control volume bounded by two cross-sections in the pipe, which are a distance Δx apart. Let ρ_g be the density of gas phase, and Γ be the gas production rate within the control volume, and v be the velocity of the gas phase.

The conservation of mass of gas phase requires

$$\frac{\partial}{\partial t}(\alpha\rho_g A) + \frac{\partial}{\partial x}(\alpha\rho_g Av) = \Gamma A \tag{5.11}$$

Differentiating and rearranging,

$$\frac{1}{\alpha}\frac{D\alpha}{Dt} + \frac{1}{\rho_g}\frac{D\rho_g}{Dt} + \frac{1}{A}\frac{DA}{Dt} + \frac{\partial v}{\partial x} = \frac{\Gamma}{\rho_g \alpha} \tag{5.12}$$

in which

$$\frac{D}{Dt} = \frac{\partial}{\partial t} + v\frac{\partial}{\partial x} \tag{5.13}$$

If the homogeneous equilibrium theory is assumed, $v = u$, and if further no gas production is allowed, Eq. (5.12) becomes

$$\frac{1}{\alpha}\frac{d\alpha}{dt} + \frac{1}{\rho_g}\frac{d\rho_g}{dt} + \frac{1}{A}\frac{dA}{dt} + \frac{\partial u}{\partial x} = 0 \tag{5.14}$$

If the pipe-wall expansion is neglected Eq. (5.11) can be reduced to

$$\frac{\partial}{\partial t}(\alpha\rho_g) + \frac{\partial}{\partial x}(\alpha\rho_g v) = \Gamma \tag{5.15}$$

Dividing the liquid continuity Eq. (5.3) by $\rho_\ell A(1-\alpha)$

$$\frac{1}{A}\frac{dA}{dt} + \frac{1}{\rho_\ell}\frac{d\rho_\ell}{dt} - \frac{1}{1-\alpha}\frac{d\alpha}{dt} + \frac{\partial u}{\partial x} = 0 \tag{5.16}$$

Subtracting Eq. (5.16) from Eq. (5.14)

$$\frac{1}{\alpha}\frac{d\alpha}{dt} + \frac{1}{\rho_g}\frac{d\rho_g}{dt} - \frac{1}{\rho_\ell}\frac{d\rho_\ell}{dt} + \frac{1}{1-\alpha}\frac{d\alpha}{dt} = 0 \tag{5.17}$$

It is also assumed that

$$\frac{1}{\rho_\ell}\frac{d\rho_\ell}{dt} << \frac{1}{\rho_g}\frac{d\rho_g}{dt} \tag{5.18}$$

If Eq. (5.17) is multiplied through by $\rho_g\,\alpha/(1-\alpha)$, the following expression is obtained

$$\left[\frac{\rho_g}{1-\alpha} + \frac{\rho_g\,\alpha}{(1-\alpha)^2}\right]\frac{d\alpha}{dt} + \frac{\alpha}{1-\alpha}\frac{d\rho_g}{dt} = 0 \tag{5.20}$$

If the gas bubbles behave adiabatically, for which $\rho_g \propto p^{1/\gamma}$, Eq. (5.20) becomes

$$\frac{d}{dt}\left[\frac{p^{1/\gamma}\alpha}{(1-\alpha)}\right] = 0 \tag{5.21}$$

Eq. (5.20) simply means that if $v = u$, the mass of air in a unit mass of mixture is constant.

Conservation of Momentum of Mixture

Let θ be the angle of inclination of the pipe with the horizontal, positive for a downward x- direction. Consider a control volume bounded by two cross-sections in the pipe at a distance Δx apart. The various forces acting on the control volume are the pressure forces, friction exerted by the pipe wall, and the component of the weight of the mixture in the direction of flow. In addition to these forces the effect of the relative bubble motion with the respect to the liquid can be included by incorporating a virtual-mass effect into the development. From potential-flow theory each bubble can be considered to produce an impulse, as defined by Kelvin (Lamb [35]), expressed as the product of the relative velocity and added mass. For a single bubble the added mass is obtained by multiplying the mass of the liquid displaced by the bubble by a coefficient of added mass C_M.

Let n be a number density defined as the number of bubbles per unit volume of the mixture. If $\forall$ is the volume of a single bubble, the number density n is defined as

$$n = \alpha/\forall \tag{5.22}$$

provided all bubbles are of the same size. It will be assumed that either the bubbles are of uniform size, or a representative average size can be used as an approximation. Thus, the number of bubbles moving per unit time along a cross section is nvA and the number of bubbles contained within the control volume is $nA\Delta x$. The rate of change of the Kelvin impulse can be written by using the above definition for n

$$\frac{\partial}{\partial t}\left[C_M \rho_\ell \alpha (v-u) A \Delta x\right] + \frac{\partial}{\partial x}\left[C_M \rho_\ell \alpha v (v-u) A\right] \Delta x \tag{5.23}$$

*Neglecting any contribution from the gas phase the conservation of momentum can be expressed

$$\frac{\partial}{\partial t}\left[\rho_\ell (1-\alpha)\, u A \Delta x\right] + \frac{\partial}{\partial t}\left[C_M \rho_\ell \alpha (v-u) A \Delta x\right]$$

$$+ \frac{\partial}{\partial x}\left[\rho_\ell (1-\alpha) u^2 A\right] \Delta x + \frac{\partial}{\partial x}\left[C_M \rho_\ell \alpha v (v-u) A\right] \Delta x$$

$$= -\frac{\partial}{\partial x}\left[pA\right] \Delta x + p \frac{\partial A}{\partial x} \Delta x + \frac{\partial p}{\partial x} \frac{(\Delta x)^2}{2} \frac{\partial A}{\partial x}$$

$$- F_f + W \tag{5.24}$$

in which F_f represents the frictional force exerted by the pipewall and W the component of the weight of the mixture. The frictional force F_f may be expressed by

$$F_f = \tau_o \pi D \Delta x \tag{5.25}$$

in which the boundary shear stress τ_o is defined by

$$\tau_o = \rho_\ell (1-\alpha) f \frac{u|u|}{8} \tag{5.26}$$

---

*Noordzij [32] uses the same form as Eq. (5.23) to include the Kelvin impulse term in the momentum equation.

If the weight of the gas phase is neglected relative to that of the liquid phase

$$W = \rho_\ell g\ (1-\alpha)\ A\ \Delta x \sin\theta \tag{5.27}$$

Using Eqs. (5.4 - 5.6, 5.25- 5.27) and neglecting the second-order pressure-gradient term, Eq. (5.24) may be expanded to yield

$$\frac{u(1-\alpha)}{\rho_\ell a_{\ell p}^2}\frac{\partial p}{\partial t} + \frac{u^2(1-\alpha)}{\rho_\ell a_{\ell p}^2}\frac{\partial p}{\partial x} + \frac{\partial}{\partial t}[u(1-\alpha)] + u\frac{\partial}{\partial x}[u(1-\alpha)]$$

$$+ u(1-\alpha)\frac{\partial u}{\partial x} + \frac{C_M\alpha(v-u)}{\rho_\ell a_{\ell p}^2}\frac{\partial p}{\partial t} + \frac{C_M\alpha v(v-u)}{\rho_\ell a_{\ell p}^2}\frac{\partial p}{\partial x}$$

$$+ \frac{\partial}{\partial t}[C_M\alpha(v-u)] + \frac{\partial}{\partial x}[C_M\alpha v(v-u)] + \frac{1}{\rho_\ell}\frac{\partial p}{\partial x}$$

$$= (1-\alpha)\left[g\sin\theta - \frac{f}{2D}u|u|\right] \tag{5.28}$$

In the case of a homogeneous model in which $v=u$, Eq. (5.28) can be simplified

$$\frac{u(1-\alpha)}{\rho_\ell a_{\ell p}^2}\frac{dp}{dt} + \frac{d}{dt}[u(1-\alpha)] + u(1-\alpha)\frac{\partial u}{\partial x} + \frac{1}{\rho_\ell}\frac{\partial p}{\partial x}$$

$$= (1-\alpha)\left[g\sin\theta - \frac{f}{2D}u|u|\right] \tag{5.29}$$

Combining Eq.(5.29) and the conservation of liquid mass from Eq. (5.9)

$$\frac{du}{dt} + \frac{1}{\rho_{\ell}(1-\alpha)} \frac{\partial p}{\partial x} + \frac{f}{2D} u|u| - g \sin \theta = 0 \qquad (5.30)$$

The Method of Characteristics

For analyses of waterhammer in pipelines and for the analyses of open-channel waves the method of characteristics has been established to be a powerful method. It can be used to handle a variety of boundary conditions, and is particularly easy for numerical analysis of a transient problem in a single-phase liquid. The method of characteristics is used to transform the linear or quasilinear partial differential equations into particular total differential equations, valid along particular characteristic lines in the x-t plane. However, for two-phase flow problems the derivation of characteristic equations is very complicated because of the large number of variables involved, increasing the number of characteristic roots correspondingly. If, however, the partial differential equations are expressed in a matrix form, the characteristic roots can be determined by setting the determinant equal to zero.

For two-phase flow models, especially for separated-flow representations, the existence of complex characteristics has been reported by Lyczokowski et al. [36]. Many research workers simplify their equations by various assumptions to enable the evaluation of the characteristics and the corresponding compatibility equations. However, this narrowly restricts the formulation for many transient problems. For example, Prosperetti and van Wijngaarden [22] have obtained four real characteristics by considerably simplifying the partial differential equations.

They have assumed isothermal bubble behavior, neglected the added-mass terms in the mixture momentum equation, neglected gravity and pipe-wall friction effects, used a conservation of number density equation, and precluded bubble coalesence, to cite the major assumptions.

Moreover, in the case of bubble air-liquid mixtures, the formation of shock waves as a consequence of the nonlinear compression phenomenon has to be accounted for. Shock formation can be clearly noticed in a grid of characteristics when the like characteristics intersect, indicating the point of inception. An example of shock inception is shown on Fig. 6 from a grid of characteristics applied to a homogeneous model. The use of the characteristic equations beyond the inception point requires the incorporation of shock equations as internal boundary conditions; for example, as explained by Dronkers [37] for open-channel bores. This inevitably requires interpolation techniques, which seriously complicate the problem, especially as the compatibility equations obtained from the method of characteristics themselves are complex enough for two-phase flow problems. Considering these complications it was decided to propose analytical models in which a different numerical technique could be used to integrate the partial differential equations. However, the handling of the boundary conditions still required the use of the method of characteristics, which was accomplished by using a homogeneous model. It should be noted that the homogeneous model was used only to prescribe the boundary conditions, and a simplified separated-flow model or a drift-flux model was used for the computation at all interior points.

Characteristic Equations for the Homogeneous Model

For the homogeneous model the three dependent variables involved

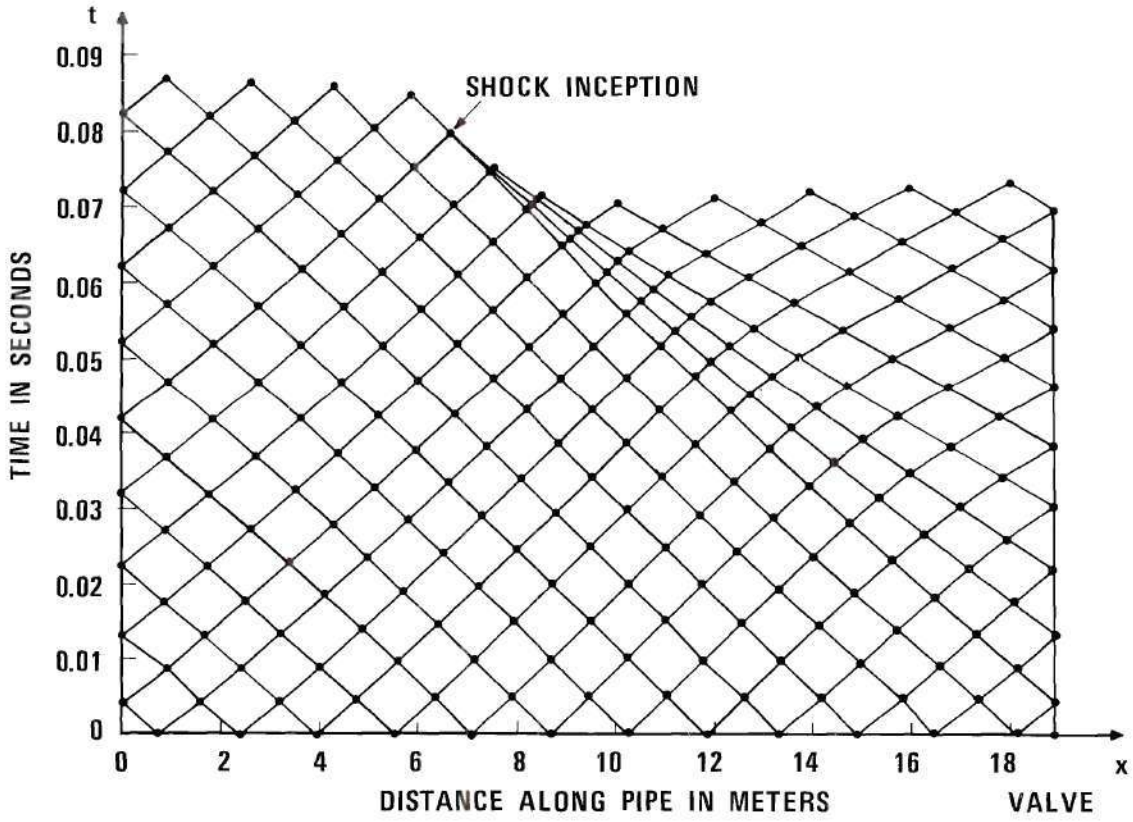

Figure 6. Grid of Characteristics and Location of Initial Shock for u_o = 5.0 ft/sec, p_o = 40 psig, and α_o = 0.0142 at x = 0.

are the pressure p, the void fraction α, and the liquid velocity u. The three available equations are: the conservation equations of liquid mass, of gas mass, and of mixture momentum. The two continuity equations are to be rearranged, however, by arithmetical manipulations and changed to a form adaptable to the determination of characteristic roots.

Similar to Eqs. (5.5) and (5.6) the gas-phase relationships are

$$\frac{1}{\rho_g}\frac{d\rho_g}{dt} = \frac{1}{K_g}\frac{dp}{dt} \tag{5.31}$$

and

$$\frac{1}{\rho_g a_{gp}^2} = \frac{1}{K_g} + \frac{D\varepsilon}{Ee} \tag{5.32}$$

in which K_g is the bulk modulus of the gas phase, being equal to p itself for isothermal behavior, or equal to γp for adiabatic behavior. The speed of sound for only gas ($\alpha = 1$) in the elastic pipe is defined by a_{gp}. Using Eq. (5.4), Eq. (5.14) can be rewritten

$$\frac{dp}{dt} + \rho_g a_{gp}^2 \frac{\partial u}{\partial x} + \frac{\rho_g a_{gp}^2}{\alpha}\frac{d\alpha}{dt} = 0 \tag{5.33}$$

Subtracting Eq. (5.33) from Eq. (5.9), the liquid continuity equation, yields

$$(\rho_\ell a_{\ell p}^2 - \rho_g a_{gp}^2)\frac{\partial u}{\partial x} - \left(\frac{\rho_\ell a_{\ell p}^2}{1-\alpha} + \frac{\rho_g a_{gp}^2}{\alpha}\right)\frac{d\alpha}{dt} = 0 \tag{5.34}$$

Multiplying Eq. (5.33) by $\rho_\ell a_{\ell p}^2$ and Eq. (5.9) by $\rho_g a_{gp}^2$ and then subtracting the resulting equations

$$\frac{dp}{dt} + \left[\frac{\rho_\ell \rho_g a_{\ell p}^2 a_{gp}^2}{\rho_\ell a_{\ell p}^2 - \rho_g a_{gp}^2}\right] \frac{1}{\alpha(1-\alpha)} \frac{d\alpha}{dt} = 0 \tag{5.35}$$

To derive the characteristic equations Eqs. (5.34) and (5.35) are used along with Eq. (5.30). These equations can be rewritten as

$$\frac{\partial \alpha}{\partial t} + u \frac{\partial \alpha}{\partial x} - b_1 \frac{\partial u}{\partial x} = 0 \tag{5.36}$$

$$\frac{\partial p}{\partial t} + u \frac{\partial p}{\partial x} + b_2 \left(\frac{\partial \alpha}{\partial t} + u \frac{\partial \alpha}{\partial x}\right) = 0 \tag{5.37}$$

$$\frac{\partial u}{\partial t} + u \frac{\partial u}{\partial x} + b_3 \frac{\partial p}{\partial x} = b_4 \tag{5.38}$$

in which

$$b_1 = \frac{(\rho_\ell a_{\ell p}^2 - \rho_g a_{gp}^2)\ \alpha\ (1-\alpha)}{(1-\alpha)\ \rho_g a_{gp}^2 + \alpha \rho_\ell\ a_{\ell p}^2} \tag{5.39}$$

$$b_2 = \frac{\rho_\ell \rho_g\ a_{\ell p}^2\ a_{gp}^2}{(\rho_\ell a_{\ell p}^2 - \rho_g a_{gp}^2)\ \alpha\ (1-\alpha)} \tag{5.40}$$

$$b_3 = \frac{1}{\rho_\ell (1-\alpha)} \tag{5.41}$$

$$b_4 = g \sin\theta - \frac{f}{2D} u|u| \tag{5.42}$$

Eqs. (5.36, 5.37 and 5.38) may be written in a matrix form

$$\begin{bmatrix} 1 & 0 & 0 \\ b_2 & 1 & 0 \\ 0 & 0 & 1 \end{bmatrix} \begin{bmatrix} \frac{\partial \alpha}{\partial t} \\ \frac{\partial p}{\partial t} \\ \frac{\partial u}{\partial t} \end{bmatrix} + \begin{bmatrix} u & 0 & -b_1 \\ ub_2 & u & 0 \\ 0 & b_3 & u \end{bmatrix} \begin{bmatrix} \frac{\partial \alpha}{\partial x} \\ \frac{\partial p}{\partial x} \\ \frac{\partial u}{\partial x} \end{bmatrix} = \begin{bmatrix} 0 \\ 0 \\ b_4 \end{bmatrix} \tag{5.43}$$

Following Ames [38], the characteristic roots are determined for the above system by equating the determinant $[A - \phi B]$ to zero, in which A and B are coefficient matrices and ϕ a multiplier. Hence

$$\det \begin{bmatrix} u-\phi & 0 & -b_1 \\ b_2(u-\phi) & u-\phi & 0 \\ 0 & b_3 & u-\phi \end{bmatrix} = 0 \tag{5.44}$$

or

$$(u-\phi)^3 - b_1 b_2 b_3 (u-\phi) = 0 \tag{5.45}$$

which has the roots

$$\phi_1 = u \tag{5.46}$$

$$\phi_{2,3} = u \pm (b_1 b_2 b_3)^{1/2} \tag{5.47}$$

Using Eqs. (5.39 - 5.41) yields

$$\frac{1}{b_1 b_2 b_3} = \rho_\ell (1-\alpha) \left[\frac{(1-\alpha)}{\rho_\ell a_{\ell p}^2} + \frac{\alpha}{\rho_g a_{gp}^2} \right] \tag{5.48}$$

Referring to Wallis [20], it can be seen that this expression is simply the inverse of the square of the speed of propagation of a disturbance in a pipe containing a bubbly mixture, provided that the mixture density can be expressed as $\rho_\ell(1-\alpha)$, in effect neglecting the gas phase. Hence, Eq. (5.47) may be written as

$$\phi_{2,3} = u \pm a_{mp} \tag{5.49}$$

in which a_{mp} is the wave propagation speed for a mixture in an elastic pipe. Eqs. (5.46) and (5.49) give the three characteristic roots ϕ_1, ϕ_2, and ϕ_3. To derive the compatibility conditions, Eqs. (5.36-5.38) are grouped together to yield

$$\phi' \left[\frac{\partial \alpha}{\partial t} + u \frac{\partial \alpha}{\partial x} - b_1 \frac{\partial u}{\partial x} \right] + \phi'' \left[\frac{\partial u}{\partial t} + u \frac{\partial u}{\partial x} + b_3 \frac{\partial p}{\partial x} - b_4 \right]$$

$$+ \frac{\partial p}{\partial t} + u \frac{\partial p}{\partial x} + a_2 \left(\frac{\partial \alpha}{\partial t} + u \frac{\partial \alpha}{\partial x} \right) = 0 \tag{5.50}$$

or

$$(\phi' + b_2) \frac{d\alpha}{dt} + \phi'' \left[\frac{\partial u}{\partial t} + \left(u - \frac{\phi' b_1}{\phi''} \right) \frac{\partial u}{\partial x} \right]$$

$$+ \left[\frac{\partial p}{\partial t} + (u + \phi'' b_3) \frac{\partial p}{\partial x}\right] - \phi'' b_4 = 0 \tag{5.51}$$

Case (a): $\phi_1 = u$

In this case ϕ' and ϕ'' are zero, and

$$b_2 \frac{d\alpha}{dt} + \frac{dp}{dt} = 0 \tag{5.52}$$

which is valid only along the characteristic

$$\frac{dx}{dt} = u \tag{5.53}$$

Case (b): $\phi_{2,3} = u \pm a_{mp}$

By comparing the coefficients in Eq. (5.51)

$$\phi'' b_3 = \pm a_{mp} \tag{5.54}$$

and

$$-\frac{\phi' b_1}{\phi''} = \pm a_{mp} \tag{5.55}$$

From Eq. (5.48) $b_1 b_2 b_3 = a_{mp}^2$ and hence, using Eqs. (5.54 and 5.55) $\phi' = - b_2$, and $\phi'' = \pm a_{mp}/b_3$. Substituting these values of ϕ' and ϕ'' in Eq. (5.51)

$$\pm \frac{a_{mp}}{b_3} \frac{du}{dt} + \frac{dp}{dt} \mp \frac{a_{mp}}{b_3} b_4 = 0 \qquad (5.56)$$

which is only valid along the characteristics lines

$$\frac{dx}{dt} = u \pm a_{mp} \qquad (5.57)$$

Equations (5.52, 5.53, 5.56, and 5.57) yield the required characteristic equations for a homogeneous model. It may be noted that if the mixture density ρ_m is approximated by $\rho_\ell(1-\alpha)$, b_3 has a value $1/\rho_m$. If the pipe wall expansion is neglected and it is assumed that $\rho_\ell a_{\ell p}^2 >> \rho_g a_{gp}^2$, the value of b_2 in Eq. (5.52) is simply $K_g/\alpha(1-\alpha)$. Using Eq. (5.31) the term dp/dt in Eq. (5.52) can be eliminated, resulting in

$$\frac{d}{dt}\left[\frac{\rho_g \alpha}{(1-\alpha)}\right] = 0 \qquad (5.58)$$

which has already been obtained earlier, Eq. (5.20). It may also be noted that the wave-propagation speed a_{mp} is a function of the pressure and void fraction, and hence of x. This means that the characteristic directions are not straight lines, but instead curved lines in the x-t plane.

CHAPTER VI

BUBBLE-DYNAMICS MODEL

In this chapter a one-dimensional separated-flow model for the transient analysis of gas-liquid mixtures in long pipelines is developed. The model is theoretically applicable to situations for which gas bubbles are well distributed and of uniform size at every cross section of the pipe. The model consists mainly of the one-dimensional equations of the conservation of the liquid mass, of the gas mass, and of the mixture momentum, together with an equation of relative motion of the bubbles with respect to the liquid. These four equations can be numerically solved to obtain the four dependent variables; namely, pressure p, void fraction α, liquid velocity u, and the bubble velocity v. In deriving the equation of relative translational bubble motion, the concepts used are similar to those employed by Noordzij [32], van Wijngaarden [26], and Prosperetti and van Wijngaarden [22] for the problem of wave propagation in air-water mixtures. Following the common gas-dynamics approach the conservation equations are expressed in the so-called conservation form

$$\frac{\partial Q_1}{\partial t} + \frac{\partial Q_2}{\partial x} = Q_3 \tag{6.1}$$

in which Q_1, Q_2, and Q_3 are functions of the dependent variables. In order to express the basic constitutive equations in conservation form certain terms were neglected by employing an order-of-magnitude analysis.

Kranenburg [5] utilized a homogeneous model for the analysis of waterhammer associated with cavitation, by expressing the conservation of mass and momentum equations in the conservation form. He neglected certain small-order terms and used the Lax-Wendroff two-step scheme for numerical integration. The procedure for numerical analysis used in the present study is similar to that employed by Kranenburg [5]. Richtmeyer and Morton [39] describe the advantage of expressing the conservation laws in the conservation form, and discuss in detail many of the available explicit, implicit, or combined numerical schemes for the integration of these nonlinear hyperbolic partial differential equations, for which finite discontinuities such as shock waves may occur. They have explained in detail the Lax-Wendroff explicit scheme and the stability conditions associated with it. A brief discussion of these aspects is given in this chapter, with more details in Appendix C.

Assumptions

The following assumptions are used in developing the bubble-dynamics model:

(a) The gas phase is present in the form of uniformly sized bubbles, well distributed at each cross-section.

(b) No mass transfer nor heat transfer occurs between phases.

(c) The bubbles expand or contract following a isentropic adiabatic law.

(d) The pressure difference between the inside and outside of bubbles is neglected; consequently, the oscillations of bubbles behind shocks are also neglected.

(e) Surface-tension effects are omitted.

(f) The temperature rise across the shock waves is negligibly small, as justified by Campbell and Pitcher [16].

(g) Average velocities, pressure, and void fraction over a cross section are used as constant values; hence, any effects of the velocity and concentration profiles are not considered.

(h) No transient cavitation is allowed for, meaning that the gas production term is zero.

(i) The contribution of the mass of the gas phase in the momentum equation is neglected.

(j) No coalescence or splitting up of bubbles is allowed.

(k) Very strong shocks of the order $p_1/p_o > 5$ are excluded as they are likely to produce severe bubble oscillations and breakup.

(l) An one-dimensional approach that neglects two- and three-dimensional effects is applicable.

(m) The void fraction $\alpha << 1$ and the mixture density can be approximated by $\rho_\ell(1-\alpha)$, neglecting the term $\rho_g\alpha$.

(n) The absolute pressures involved are relatively moderate, and $p/(\rho_\ell\, a_{\ell p}^2) << 1$. This assumption is necessary to justify the neglecting of small-order terms in the transformation of the governing partial differential equations to the conservation form.

(o) For $\alpha << 1$, and for moderate pressures with $\rho_g << 1$, the product $\alpha\rho_g$ is negligibly small, and under these circumstances the pipe-wall expansion may be neglected in the gas continuity equation.

(p) Levich's model [31] of frictional resistance imparted to the bubbles by the liquid is applicable.

Governing Equations

Conservation of Mass of the Liquid Phase

The equation of conservation of mass of the Eq. (5.8), may be expressed in conservation form, as follows

$$\frac{(1-\alpha)^2}{\rho_\ell a_{\ell p}^2}\frac{\partial p}{\partial t} = \frac{\partial}{\partial t}\left\{\frac{(1-\alpha)p}{\rho_\ell a_{\ell p}^2}\right\} - \frac{p^2}{\rho_\ell a_{\ell p}^2}\frac{\partial}{\partial t}(1-\alpha) \tag{6.2}$$

and

$$\frac{(1-\alpha)^2}{\rho_\ell a_{\ell p}^2} u \frac{\partial p}{\partial x} = \frac{\partial}{\partial x}\left\{\frac{(1-\alpha)up}{\rho_\ell a_{\ell p}^2}\right\} - \frac{p^2}{\rho_\ell a_{\ell p}^2}\frac{\partial}{\partial t}[u(1-\alpha)] \tag{6.3}$$

Substituting Eqs. (6.2) and (6.3) into Eq. (5.8) yields

$$\frac{\partial}{\partial t}\left[\frac{(1-\alpha)p}{\rho_\ell a_{\ell p}^2}\right] + \left(1-\frac{p^2}{\rho_\ell a_{\ell p}^2}\right)\frac{\partial(1-\alpha)}{\partial t} + \frac{\partial}{\partial x}\left[\frac{(1-\alpha)up}{\rho_\ell a_{\ell p}^2}\right]$$

$$+ \left(1-\frac{p^2}{\rho_\ell a_{\ell p}^2}\right)\frac{\partial[(1-\alpha)u]}{\partial t} = 0 \tag{6.4}$$

If

$$\frac{p^2}{\rho_\ell a_{\ell p}^2} \ll 1 \tag{6.5}$$

then

$$\left(1-\frac{p^2}{\rho_\ell a_{\ell p}^2}\right) \simeq 1 \tag{6.6}$$

Hence Eq. (6.4) assumes the following conservation form

$$\frac{\partial}{\partial t}\left[(1-\alpha)\left(1+\frac{p_2}{\rho_\ell a_{\ell p}}\right)\right]+\frac{\partial}{\partial x}\left[(1-\alpha)\,u\,\left(1+\frac{p_2}{\rho_\ell a_{\ell p}}\right)\right]=0 \tag{6.7}$$

Eq.(6.7) is used in the model to represent the conservation of mass of the liquid, and has the same form as the corresponding one used by Kranenburg [5]. If the pipe-wall expansion and water compressibility are neglected, Eq. (6.7) takes the form

$$\frac{\partial}{\partial t}(1-\alpha)+\frac{\partial}{\partial x}[(1-\alpha)u]=0 \tag{6.8}$$

or

$$\frac{d}{dt}(1-\alpha)+(1-\alpha)\frac{\partial u}{\partial x}=0 \tag{6.9}$$

in which $\frac{d}{dt}$ is defined by Eq. (4.17). This equation agrees with the corresponding expression used by Prosperetti and van Wijngaarden [22].

Conservation of Mass of the Gas Phase

For the case of zero gas production the conservation of the mass of the gas phase obtained in Chapter IV as Eq. (5.11) becomes

$$\frac{\partial}{\partial t}(\alpha\rho_g A)+\frac{\partial}{\partial x}(\alpha\rho_g Av)=0 \tag{6.10}$$

If $\alpha << 1$, and for moderate pressures $\rho_g << 1$, it is reasonable to neglect the term due to the area change, yielding

$$\frac{\partial}{\partial t}(\alpha\rho_g)+\frac{\partial}{\partial x}(\alpha\rho_g v)=0 \tag{6.11}$$

The gas phase is considered to be comprised of bubbles of uniform size. Therefore, if each bubble is assumed to behave according to an adiabatic process, ρ_g can be related to the pressure at a cross section by

$$\frac{p^{1/\gamma}}{\rho_g} = \text{constant} \tag{6.12}$$

where γ is the adiabatic constant.

Using Eq. (6.12), Eq. (6.11) yields

$$\frac{\partial}{\partial t}\left(p^{1/\gamma}\alpha\right) + \frac{\partial}{\partial x}\left(p^{1/\gamma}\alpha v\right) = 0 \tag{6.13}$$

It may be noted that in deriving Eq. (6.13) no gas production is allowed, and consequently the model does not consider a case of transient cavitation. From Eq.(6.13) a conservation of number density equation can be derived. The number density n is related to α by $n\forall = \alpha$, in which $\forall$ is the volume of a bubble. Substituting for α in Eq. (6.13)

$$\frac{\partial}{\partial t}\left(p^{1/\gamma}\, n\forall\right) + \frac{\partial}{\partial x}\left(p^{1/\gamma} n\forall v\right) = 0 \tag{6.14}$$

But if each bubble behaves adiabatically, for $p^{1/\gamma}\forall$ = a constant, Eq. (6.14) becomes

$$\frac{\partial n}{\partial t} + \frac{\partial}{\partial x}(nv) = 0 \tag{6.15}$$

Noordzij [32] and Prosperetti and van Wijngaarden [22] have used the concept of conservation of number density as given by Eq. (6.15). The velocity of the gas phase in Eqs. (6.13) and (6.15) is actually a representative constant velocity of all the gas bubbles at a given cross section. This assumption is unrealistic if coalascence or breakup of bubbles occurs, or if the bubbles at a cross section differ in sizes. If $v = u$, as in the homogeneous model, Eq. (6.13) gives

$$\frac{\partial}{\partial t}\left(p^{1/\gamma}\alpha\right) + \frac{\partial}{\partial x}\left(p^{1/\gamma}\alpha u\right) = 0 \tag{6.16}$$

Conservation of Momentum of the Mixture

The equation of the conservation of the momentum of the mixture has already been derived in Chapter V by neglecting the momentum of the gas phase. Following exactly the same approach adopted in deriving Eq. (6.7), and utilizing condition (6.5), Eq. (5.28) can be expressed as

$$\frac{\partial}{\partial t}\left\{\left[u(1-\alpha) + C_M\,\alpha(v-u)\right]\left[1 + \frac{p}{\rho_\ell a_{\ell p}^2}\right]\right\}$$

$$+ \frac{\partial}{\partial x}\left\{\left[u^2(1-\alpha) + C_M\,\alpha v(v-u)\right]\left[1 + \frac{p}{\rho_\ell a_{\ell p}^2}\right] + p/\rho_\ell\right\}$$

$$= (1-\alpha)\left[g\sin\theta - \frac{f}{2D}u|u|\right] \tag{6.17}$$

The term $\frac{1}{\rho_\ell}\frac{\partial p}{\partial x}$ in Eq. (5.28) can be written in Eq. (6.17) as $\frac{\partial(p/\rho_\ell)}{\partial x}$, since the $\frac{\partial(1/\rho_\ell)}{\partial x}$ term is indeed small and may be neglected.

The added-mass coefficient C_M in Eq. (6.17) is a function of α, but only an empirical relation can be prescribed for it, as C_M also depends upon the shape of the bubble. Prosperetti and van Wijngaarden [22] use the empirical relationship between C_M and α given by Eq. (3.11). If the bubbles are spherical or nearly spherical, and $\alpha << 1$, it appears reasonable to assume $C_M = 0.5$. If the velocities of both the phases are equal, Eq. (6.17) reduces to

$$\frac{\partial}{\partial t}\{[u(1-\alpha)]\,[1 + {}^{p}/_{\rho_\ell a_{\ell p}^2}]\} + \frac{\partial}{\partial x}\{[u^2(1-\alpha)]\,[1 + {}^{p}/_{\rho_\ell a_{\ell p}^2}] + {}^{p}/_{\rho_\ell}\} = (1-\alpha)\left[g \sin\theta - \frac{f}{2D}\, u|u|\right] \tag{6.18}$$

which agrees with the momentum equation obtained by Kranenburg [5], who employed a homogeneous model for the analysis of transient cavitation. If the pipe friction and gravity terms are omitted in Eq. (6.17), and further if the added-mass terms are neglected relative to the other terms in Eq. (6.17)

$$\frac{\partial}{\partial t}\,[u(1-\alpha)] + \frac{\partial}{\partial x}\,[u^2(1-\alpha)] + \frac{1}{\rho_\ell}\frac{\partial p}{\partial x} = 0 \tag{6.19}$$

By combining Eqs. (6.19) and (6.8) we get

$$\rho_\ell(1-\alpha)\frac{du}{dt} + \frac{\partial p}{\partial x} = 0 \tag{6.20}$$

which agrees with the momentum equation obtained by Prosperetti and van

Wijngaarden [22] under the same assumptions.

Equation of Relative Bubble Motion

In order to introduce the effect of the relative motion between the gas bubble and the liquid phase an additional relationship is needed. For this purpose the bubble-dynamics model proposed by Prosperetti and van Wijngaarden [22] is employed. Their model was essentially based upon the model developed by Levich [31] for bubble motion through stationary liquids. Levich [31] defines various regimes of bubble motion, depending upon a Reynold's number vR/ν_ℓ, in which v is the bubble velocity, R is its radius and ν_ℓ the kinematic viscosity of the liquid. For Reynolds numbers above 800, gas bubbles no longer retain their spherical shape as pulsations frequently occur within the bubble. However, it is known that the velocity of rise of such bubbles remains almost constant at about 1 ft/sec, irrespective of the bubble size. In the current investigation Levich's model is only employed for spherical bubbles for which $50 < Re < 800$, corresponding to bubble diameters of 0.1 to 2 mm.

Due to negligible inertia of the gas, the bubbles can be assumed to offer no constraint to the tangential velocity of the liquid at the boundary of the bubble. The only constraints are the vanishing relative normal velocity, and the continuity of tangential stress at the boundaries. In other words, a peculiar boundary layer exists on the gas-liquid interface, allowing for viscous forces to establish a nonzero tangential velocity at the interface itself, which obviously differs from a solid-liquid interface. Furthermore, contrary to the case of a solid sphere, the size of the separation zone in the flow past a gas bubble is extremely small, indeed nearly negligible. Based upon potential theory, Levich

[31] shows that the rise velocity of a gas bubble is 1.5 times that of a solid sphere of the same size and density. Moreover, the viscous forces exerted by the liquid on a gas bubble has been shown to be twice that which would occur on a solid sphere under the same conditions. The form drag for a gas bubble is negligibly small, however.

Following Levich's approach, the viscous force acting on a single bubble moving with a relative translational velocity v-u can be expressed

$$F_v = -C' \mu_\ell R (v-u) \tag{6.21}$$

in which C' = a constant depending on bubble shape

(equal to 12 π for a spherical bubble)

μ_ℓ = dynamic viscosity of the liquid

The initial step in the development of the model is to formulate the equation of motion for a single bubble. The various forces acting on the bubble are: fluid inertia, viscous resistance, buoyancy, and the fictitious force due to the added-mass effect. The latter force is due to the rate of change of the liquid impulse, and is associated with the relative motion by the product of the relative velocity and the added mass. Further details on this force are available in Chapter V. Thus, the added-mass effect is given by the rate of change of the so-called Kelvin impulse (Lamb [35]). From the discussion in Chapter V, the rate of change of the Kelvin impulse is

$$\frac{D}{Dt} \{C_M \rho_\ell \forall (v-u)\} \tag{6.22}$$

in which D/Dt is defined by Eq.(5.13). The buoyancy force is the component of the weight of the displaced liquid in the direction of the bubble motion and is given by $\rho_\ell \forall\, g \sin\theta$. The inertial force of the liquid is $\rho_\ell \forall\, Du/Dt$. It may be noted that the acceleration term to be used in this development is Du/Dt rather than du/dt, as the liquid motion is being observed in a reference frame moving with the bubbles. This point has been stressed by Prosperetti and van Wijngaarden [22]. The equation for relative motion of a bubble may then be expressed by

$$\rho_g \forall \frac{Dv}{Dt} = -\rho_\ell \forall \frac{Du}{Dt} + \frac{D}{Dt}\{C_M \rho_\ell \forall (v-u)\}$$

$$+C' \mu_\ell R(v-u) + \rho_\ell \forall\, g \sin\theta \qquad (6.23)$$

The inertia of the bubble $\rho_g \forall \frac{Dv}{Dt}$ is very small compared to all the other terms of Eq. (6.23), and hence may be neglected, yielding

$$\frac{D}{Dt}\{C_M \rho_\ell \forall (v-u)\} = \rho_\ell \forall \frac{Du}{Dt} - C' \mu_\ell R(v-u) - \rho_\ell \forall\, g \sin\theta \qquad (6.24)$$

Upon multiplying Eq. (6.24) by n and replacing $n \forall$ by α

$$\frac{D}{Dt}\{C_M \rho_\ell \alpha (v-u)\} - C_M \rho \forall (v-u)\frac{Dn}{Dt}$$

$$= \rho_\ell \alpha \frac{Du}{Dt} - C' \mu_\ell n R(v-u) - \rho_\ell \alpha\, g \sin\theta \qquad (6.25)$$

Using the conservation of number density n, Eq. (6.15)

$$\frac{Dn}{Dt} = - n \frac{\partial v}{\partial x} \tag{6.26}$$

Substituting Eq. (6.26) in Eq. (6.25)

$$\frac{D}{Dt}\{ C_M \rho_\ell \alpha (v-u)\} + C_M \rho_\ell \alpha (v-u) \frac{\partial v}{\partial x}$$

$$= \rho_\ell \alpha \frac{Du}{Dt} - C' \mu_\ell n R (v-u) - \rho_\ell \alpha g \sin \theta \tag{6.27}$$

Eq. (6.27) can then be rearranged to

$$\frac{\partial}{\partial t} \{ C_M \rho_\ell \alpha (v-u)\} + \frac{\partial}{\partial x} \{ C_M \rho_\ell \alpha v (v-u) \}$$

$$= \rho_\ell \alpha \frac{\partial u}{\partial t} + \rho_\ell \alpha v \frac{\partial u}{\partial x} - C' \mu_\ell n R (v-u)$$

$$- \rho_\ell \alpha g \sin \theta \tag{6.28}$$

For spherical bubbles Eq. (6.28) can be simplified by replacing n, by using Eq. (5.22), and by noting that $\forall = 4 \pi R^3/3$ and $C' = 12 \pi$

$$\frac{\partial}{\partial t} \{ C_M \alpha (v-u)\} + \frac{\partial}{\partial x} \{ C_M \alpha v (v-u)\}$$

$$= \alpha \frac{\partial u}{\partial t} + \alpha v \frac{\partial u}{\partial x} - 9 \alpha \nu_\ell (v-u)/R^2$$

$$- \alpha g \sin \theta \tag{6.29}$$

Eq. (6.29) represents the equation of relative bubble motion, but obviously is not in the conservation form. It may be noted also that this equation has been derived not on the basis of a control volume concept, but instead by writing down the equation of relative motion for an individual bubble. Eq. (6.29) is valid only if the bubbles are of uniform size. However, for a nonuniform size distribution an average bubble size may be used as an approximation. If the bubble shape is not spherical, the deviation of C' from the theoretical value of 12 π is currently not known. Levich [31] has stated that for values of the bubble Reynolds number $vR/\upsilon_\ell > 800$, the bubbles tend to become nonspherical. Beyond this limit one has to be cautious regarding the use of Eq. (6.29) to represent the relative motion. Levich's model is strictly based on an individual bubble rising in a stationary liquid. In the case of mixtures the bubbles may interact; for example, if the flow is horizontal the bubbles have a tendency to travel along the top portion of the pipe. Clearly, the bubble distributions for vertically upward and downward flows may be different. All these factors together with possibility of bubble coalescence, or breakup due to shock waves, restrict the validity of Eq. (6.29) in a strict sense. Nevertheless, if the effect of translational relative motion of bubbles on the transient two-phase flow can not be ignored, a model using Eq. (6.29) may be a better representation than a homogeneous model which altogether neglects relative motion.

Prosperetti and Wijngaarden [22] have expressed Eq. (6.29) differently by using Eq. (6.20) to replace the term $\rho_\ell \alpha \frac{\partial u}{\partial t}$, resulting in an equation for relative bubble motion akin to a characteristic form

$$\frac{D}{Dt}\left[\alpha(v-u)\right] + \frac{\alpha}{C_M}(v-u)\frac{DC_M}{Dt} + \alpha(v-u)\frac{\partial v}{\partial x}$$

$$+ \frac{\alpha}{\rho_\ell C_M(1-\alpha)}\frac{\partial p}{\partial x} - \frac{\alpha(v-u)}{C_M}\frac{\partial u}{\partial x} = -\frac{C'n\,\nu_\ell R\,(v-u)}{C_M} \qquad (6.30)$$

As there is no advantage in changing the form of Eq. (6.29) in the present model, the characteristic approach was abandoned.

Bubble Velocity for Steady Flow

In satisfying Eq. (6.29) for the initial conditions of steady flow the liquid velocity u is assumed constant from section to section. It is reasonable to assume also that the bubble velocity v is constant for a constant inclination of the pipe θ, as v differs from u mainly because of buoyancy. Thus, for any inclination angle θ Eq. (6.29) is simplified to

$$v(v-u)\frac{\partial}{\partial x}\{C_M\alpha\} = -9\alpha\nu_\ell(v-u)/R^2 - \alpha\, g \sin\theta \qquad (6.31)$$

The value of $\partial(C_M\alpha)/\partial x$ as well as all other variables except v in Eq. (6.31) are known initially at each mesh point along the x axis. Thus Eq. (6.31) is simply a quadratic equation in v, and can be solved as follows.

If $\partial(C_M\alpha)/\partial x = C1$, $9\alpha\nu_\ell/R^2 = C2$

and $\alpha\, g \sin\theta = C3$, the result is

$$C1\ v(v-u) + C2\ (v-u) + C3 = 0 \tag{6.32}$$

Defining C4 = C1 u - C2 and C5 = C2u - C3 yields

$$C1\ v^2 - C4\ v - C5 = 0 \tag{6.33}$$

or

$$v = \frac{[C4 \pm (C4^2 + 4\ C1C5)^{1/2}]}{2\ C1} \tag{6.34}$$

The positive root on the radical is chosen as both v and u are positive for direction of the initial flow in the present study. As C1 is a very small quantity, Eq. (6.34) is rewritten for numerical treatment as

$$v = \frac{-2\ C5}{[C4 - (C4^2 + 4\ C1C5)^{1/2}]} \tag{6.35}$$

If the pipe line consists of reaches with different slopes v has to be evaluated for each section using Eq. (6.35).

The rise velocity of bubbles in a vertical pipe with the liquid stationary can also be obtained using Eq. (6.31). In this case, for which u = 0, $\partial(C_M\alpha)/\partial x = 0$, and sin θ = -1, Eq. (6.31) yields

$$9\nu_\ell \alpha\ v/R^2 = \alpha g \tag{6.36}$$

meaning that

$$v = \frac{g_R^2}{9\nu_\ell} \tag{6.37}$$

As would be expected Eq. (6.37) agrees with the corresponding expression obtained by Levich [31].

Numerical Analysis

The three conservation equations derived earlier, namely Eqs. (6.7), (6.13) and (6.17) can be expressed as

Conservation of liquid phase:

$$\frac{\partial Q_{11}}{\partial t} + \frac{\partial Q_{12}}{\partial x} = Q_{13} \tag{6.38}$$

in which $$Q_{11} = (1-\alpha)\left(1 + \frac{p}{\rho_\ell a_{\ell p}^2}\right) \tag{6.39}$$

$$Q_{12} = u\, Q_{11} \tag{6.40}$$

$$Q_{13} = 0 \tag{6.41}$$

Conservation of gas phase:

$$\frac{\partial Q_{21}}{\partial t} + \frac{\partial Q_{22}}{\partial x} = Q_{23} \tag{6.42}$$

in which $$Q_{21} = p^{1/\gamma_\alpha} \tag{6.43}$$

$$Q_{22} = vQ_{21} \tag{6.44}$$

$$Q_{23} = 0 \tag{6.45}$$

Conservation of momentum of the mixture:

$$\frac{\partial Q_{31}}{\partial t} + \frac{\partial Q_{32}}{\partial x} = Q_{33} \tag{6.46}$$

in which $$Q_{31} = [u(1-\alpha) + C_M\, \alpha(v-u)]\ (1 + \frac{p}{\rho_\ell a_{\ell p}^2}) \tag{6.47}$$

$$Q_{32} = [u^2(1-\alpha) + C_M\ \alpha v(v-u)]\ (1 + \frac{p}{\rho_\ell a_{\ell p}^2}) + p/\rho_\ell \tag{6.48}$$

$$Q_{33} = (1-\alpha)\ [g \sin\theta - \frac{f}{2D}\, u|u|] \tag{6.49}$$

Eqs.(6.38), (6.42), and (6.46), which are in the so-called conservation form, are a system of nonlinear hyperbolic partial differential equations. In principle, such a system could be numerically solved using the method of characteristics. However, because of the nonlinear nature of the problem as a result of the wave celerity varying as a function of pressure and the void fraction, the intersection of like characteristics and associated shock formation is quite possible, as shown earlier in Fig. 6. The resulting discontinuity has to be fitted into the continuous solution by prescribing shock equations as internal boundary conditions. This is a very difficult problem when there are several characteristics. The compatibility conditions are themselves complicated expressions. In fact,

in Chapter IV it has been pointed out that the evaluation of the characteristic roots for a two-phase flow problem itself is very difficult, not to mention the possibilities of the existence of complex roots. It was therefore decided not to use the method of characteristics but instead to resort to a gas-dynamics approach, for which many powerful numerical schemes are already in use for handling such discontinuities.

There are several numerical schemes for integrating the conservation equations under conditions for which discontinuities like shock waves can be treated. These methods usually embody a numerical viscosity, which in essence spreads the shock over a minimum number of mesh points, thereby suppressing the nonlinear instabilities. Most of the methods are second-order explicit schemes, as can be seen in Lax and Wendroff [40], Richtmyer [41], Gourlay and Morris [42], etc. Further descriptions may be found in Richtmyer and Morton [39] and Ames [38]. Of the accepted techniques the Lax-Wendroff method is quite well known, and has been successfully used by Kranenburg [5,43] for transient cavitation in pipe lines. When a shock wave exists, the Lax-Wendroff scheme causes certain oscillations behind the shock, which are inherent with the method. Based upon the work of Vliegenthart [47], Kranenburg [5,43] has explained a technique for smoothing out these oscillations without affecting the low frequency transients in the pipe line. A numerical Lax-Wendroff two-step scheme is used in this study with the smoothing procedure utilized by Kranenburg [5,43]. The scheme is explained in detail and verified for particular cases in Appendix C. Recently, there have been many implicit method suggested in the literature; for example, Gary [44], Gourlay and Morris [45], etc. These implicit methods possess an increased stability

range, but are more complicated as most of them necessitate the solution of a system of nonlinear equations. Recently, however, McGuire and Morris [46] have suggested a new, explicit-implicit scheme, which they claim retains the dissipation properties and ease of solution of the explicit scheme, but at the same time incorporates the optimal stability of the implicit methods.

Numerical Computational Procedure

Eqs. (6.38), (6.42), and (6.46) can be integrated numerically using the Lax-Wendroff two-step scheme described in detail in Appendix C. The finite-difference equations for the two steps are.

First step:

$$Q_{i1}(x + \Delta x,\ t + \Delta t) = \frac{1}{2}\ [Q_{i1}(x + 2\ \Delta x,\ t) + Q_{i1}\ (x,\ t)]$$

$$- \frac{\Delta t}{2\Delta x}\ [Q_{i2}(x + 2\ \Delta x,\ t) - Q_{i2}(x,\ t)] + \frac{\Delta t}{2}\ [$$

$$Q_{i3}(x + 2\Delta x,\ t) + Q_{i3}(x,\ t)]\ ;\ i = 1,\ 2,\ 3 \qquad (6.50)$$

Second step:

$$Q_{i1}(x,\ t + 2\Delta t) = Q_{i1}(x,\ t) - \frac{\Delta t}{\Delta x}\ [Q_{i2}(x + \Delta x,\ t + \Delta t)$$

$$- Q_{i2}(x - \Delta x,\ t + \Delta t)] + \Delta t\ [Q_{i3}(x + \Delta x,\ t + \Delta t)$$

$$+ Q_{i3}(x - \Delta x,\ t + \Delta t)]\ ;\ i = 1,\ 2,\ 3 \qquad (6.51)$$

The mesh length Δx has to be chosen small enough to obtain the desired accuracy as the numerical scheme spreads a shock front over a few reaches. Once Δx is fixed Δt is evaluated from the Courant-Friedrichs-Levy (CFL) convergence condition

$$\frac{\Delta t}{\Delta x} |\lambda| \leq 1 \tag{6.52}$$

in which λ is the maximum modulus eigenvalue of the coefficient matrix A of the linearized version of the above system of equations, which is written in the form

$$\frac{\partial q}{\partial t} + A \frac{\partial q}{\partial x} = z \tag{6.53}$$

in which q and z are vectors. As the exact evaluation of λ is very difficult for the complex system at hand a reasonable approximation of $|\lambda|$ equal to $|u| + |v| + a_{mp}$ is used. For more details on this Appendix C may be referred to. Δt is determined at each step by taking the maximum value of $|u| + |v| + a_{mp}$ at that step. Considering all the mesh points and using the CFL condition yields

$$\Delta t = \Delta x / (|u| + |v| + a_{mp})_{max} \tag{6.54}$$

The smoothing procedure described in Appendix C can be employed to eliminate any over shooting of shock wave-fronts and the high frequency damped oscillations following it. This procedure is actually accomplished by

adding numerical viscosity. The values of Q_{i1}, i = 1, 2, 3, are corrected in order to obtain the smoothed values at each step of the scheme.

The boundary conditions can be prescribed using the characteristic equations for the homogeneous model. This approximation was employed because of the difficulties involved in obtaining the eigenvalues of the four-by-four matrix, as well as the derivation of the compatibility conditions when relative motion is considered.

The characteristic equations (5.52), (5.53), (5.56), and (5.57) of the homogeneous model yield values of u and α if p is prescribed, or p and α if u is prescribed at the boundary. The value of v at the boundary nodes can be reasonably assumed to be same as that at the adjacent node.

From the known values of Q_{11} and Q_{21}, as defined by Eqs. (6.39) and (6.43), p and α can be evaluated. Eliminating α from Eq. (6.39) and using Eq. (6.43)

$$\frac{Q_{21}}{\rho_\ell a_{\ell p}^2}\, p - \frac{1}{\rho_\ell a_{\ell p}^2}\, p^{1 + 1/\gamma} + p^{1/\gamma}\,(Q_{11} - 1) + Q_{21} = 0 \qquad (6.55)$$

To obtain p, Eq. (6.55) can be solved numerically by Newton's method. Upon substituting p into Eq. (6.43), α can also be evaluated. The value of Q_{31} is known from the Lax-Wendroff integration of Eq. (6.46). From Eq. (6.47), which defines Q_{31}

$$u = \{Q_{31}/[(1 + p/\rho_\ell\, a_{\ell p}^2)\,(1 - \alpha - C_M\alpha)]\} -$$

$$[C_M\alpha/(1 - \alpha - C_M\alpha)]v \qquad (6.56)$$

Eq. (6.56) actually gives the relationship between u and v at the nodes of the x - t plane. The solution for u and v can be effected if one more relationship between the two can be formulated. This second relationship is derived by expressing the equation of relative bubble motion (6.29) in a central finite-difference form

$$[C_M\,\alpha(v-u)]_{x,\,t+\Delta t} = [C_M\,\alpha(v-u)]_{x,\,t} - \frac{\Delta t}{2\Delta x}\{$$

$$[C_M\,\alpha v(v-u)]_{x+\Delta x,\,t} - [C_M\,\alpha v(v-u)]_{x-\Delta x,\,t}\}$$

$$+ (\alpha v)_{x,t}\,\frac{\Delta t}{2\Delta x}\{(u)_{x+\Delta x,\,t} - (u)_{x-\Delta x,\,t}\} - \Delta t$$

$$\{[\,9\alpha\upsilon_{\ell}(v-u)/R^2]_{x,\,t}\} - \frac{\Delta t}{2}\{(\alpha\ g\ \sin\theta)_{x,\,t} + (\alpha\ g\ \sin\theta)_{x,\,t+\Delta t}\}$$

$$+ 1/2\{[(\alpha)_{x,\,t} + (\alpha)_{x,\,t+\Delta t}]\,[(u)_{x,\,t+\Delta t} - (u)_{x,\,t}]\} \qquad (6.57)$$

In Eq. (6.57) the value of C_M is only a function of α and hence is known at each time step. The value of bubble radius R can be obtained at each time step by the adiabatic law as the pressure is known. Thus Eq. (6.57) simply represents a relationship between $(u)_{x,\,t+\Delta t}$ and $(v)_{x,\,t+\Delta t}$. However, a relationship between these two quantities already exists in Eq. (6.56), which may be written in the finite-difference form

$$(u)_{x,\,t+\Delta t} = C6 - C7\,(v)_{x,\,t+\Delta t} \qquad (6.58)$$

in which C_6 and C_7 are known quantities at $(x, t + \Delta t)$. Eqs. (6.57) and (6.58) can be solved simultaneously to give the values of u and v at each time step. Thus, all four variables can be evaluated at each time step and the computations can be carried out for any desired period of time.

CHAPTER VII

DRIFT-FLUX MODEL

In this chapter a one-dimensional model based on the drift-flux concepts is developed for transient analysis of air-water mixtures in long pipe lines. Unlike the bubble-dynamics model developed in the previous chapter the drift-flux model should be valid for bubbly, slug, or drop regimes. Furthermore, the effect of the velocity and concentration profiles can be accounted for in this model, which essentially consists of time-smoothed and area-averaged one-dimensional equations of continuity of the gas phase, continuity of the mixture, and momentum of the mixture. Also needed are several constitutive relations relating the various variables involved. The time-averaging, area-averaging and weighting procedure adopted here corresponds to that proposed and explained in detail by Ishii [48, 49]. Due to the very extensive and elaborate nature of the techniques involved, a full description of the averaging procedure is not included herein, however.

Wallis [20] has given a detailed description of the drift-flux theory. The drift-flux term is defined as the volumetric flux of either component relative to a surface moving at the volumetric average velocity. It is analogous to the molecular diffusion flux in the molecular diffusion of gases. A drift-flux model is a modified homogeneous model where the attention has been given to the relative motion between the phases. It differs from a separated-flow model in that attention is focused on the relative motion, and not on the motion of individual phases themselves.

The expressions for the drift velocity and the various relations between the numerous variables are discussed by Zuber and Findlay [50], and summarized by Wallis [20]. These expressions are used in this model as outlined later. The three-field equations are in the so-called conservation form and can be numerically integrated using the Lax-Wendroff finite-difference scheme described in Appendix C.

Assumptions

The following assumptions are made in deriving the one-dimensional equations for the drift-flux model:

(a) Any mass transfer and heat transfer between the phases is not allowed.

(b) The gas is assumed to obey an isentropic adiabatic law.

(c) The gas and liquid pressures are assumed to be equal at a cross section.

(d) No cavitation is allowed.

(f) The pipe-wall expansion and the water compressibility are neglected to avoid complexities in defining the area-averaging and weighting techniques.

(g) A constant value of the drift velocity of the gas phase is assumed for each section of a pipe with a constant slope.

(h) Surface tension effects are neglected.

(i) The temperature rise across a dynamic wave is assumed to be negligibly small, and the energy equation is not incorporated into the model.

Definition of Variables

All the variables defined below are time-averaged and area-averaged weighted mean values. Both averaging procedures are disscussed in Appendix D. The subscript g is used to note the gas phase, ℓ the liquid phase, and m the mixture. With k = ℓ, g or m, ρ_k denotes the density, v_k the flow velocity, and j_k the volumetric flux. If k = ℓ or g, V_{kj} is the drift-velocity, and V_{km} is the diffusion velocity. The void fraction is α, and $\Delta\rho$ is the difference in densities $\rho_\ell - \rho_g$. Let A be the area of cross section of the pipe, and Q_k the volumetric rate of flow with k = ℓ or g. Referring to Wallis [20], Zuber and Findlay [50], and Ishii [48, 49] the following relationships can be formulated

$$\rho_m = \alpha\rho_g + (1-\alpha)\ \rho_\ell \tag{7.1}$$

$$v_m = [\alpha\rho_g\ v_g + (1-\alpha)\ \rho_\ell v_\ell]/\rho_m \tag{7.2}$$

$$v_r = v_g - v_\ell \tag{7.3}$$

$$j_g = \frac{Q_g}{A} = \alpha v_g \tag{7.4}$$

$$j_\ell = \frac{Q_\ell}{A} = (1-\alpha)\ v_\ell \tag{7.5}$$

$$j_m = j_g + j_\ell = \alpha v_g + (1-\alpha)v_\ell \tag{7.6}$$

$$V_{gm} = v_g - v_m = (1-\alpha)\ \frac{\rho_\ell}{\rho_m}\ v_r \tag{7.7}$$

$$V_{\ell m} = v_{\ell} - v_m = - \alpha \frac{\rho_g}{\rho_m} v_r \tag{7.8}$$

$$V_{gj} = v_g - j_m = (1-\alpha)\, v_r \tag{7.9}$$

$$V_{\ell j} = v_{\ell} - j_m = - \alpha\, v_r \tag{7.10}$$

$$j_m = v_m + \alpha \frac{\Delta\rho}{\rho_m} V_{gj} \tag{7.11}$$

$$v_g = C_o\, j_m + V_{gj} \tag{7.12}$$

in which C_o is the distribution parameter defined by Zuber and Findlay [50]. For the bubbly-churn turbulent flow regime

$$V_{gj} = 1.41 \left[\frac{\sigma g \Delta\rho}{\rho_{\ell}^2}\right]^{1/4} \tag{7.13}$$

in which σ is the surface tension. For the slug-flow regime

$$V_{gj} = 0.35 \left[\frac{g \Delta\rho D}{\rho_{\ell}}\right]^{1/2} \tag{7.14}$$

Expressions given by Eqs. (7.13) and (7.14) are empirical in nature and suggest that the weighted-mean drift velocity of the gas phase is independent of the gas-phase concentration. The parameter C_o in Eq. (7.12) actually takes into account the velocity and concentration profiles across a cross section. Zuber and Findlay [50] have observed that C_o varies from 1.5 to 1.0 as long as the gas concentration is greater at

the center of the pipe than near the pipe wall. If the concentration near the wall is greater than that at the center, C_o can be less than unity. In the absence of experimental data C_o can be assumed to be 1.2 for bubbly flow, a value that actually is identical to that for the ratio of maximum fluid velocity to average velocity of turbulent flow in a conduit.

The weighted mean velocities defined by v_m, V_{gm}, and $V_{\ell m}$ are based on the center of mass of the mixture concept, where as j_m, V_{gj} and $V_{\ell j}$ are based on a center of volume of the mixture concept. As stressed by Zuber [51], the center of mass concept is more appropriate in the derivation of field equations, and the corresponding variables are used to express the continuity and momentum equations.

The Field Equations

The field equations for the drift-flux model are obtained by time averaging and area averaging the equations that describe the flow characteristics at a particular point. The time and area-averaged field equations have terms which are functions of the time and area-averaged weighted mean values of the variables. The averaging method employed here has been adopted from that proposed by Ishii [48,49].

If the interfacial mass transfer and the surface-tension effects are neglected the problem is simplified considerably. The time-averaged and area-averaged continuity equation for the gas phase can be expressed

$$\frac{\partial}{\partial t}(\alpha \rho_g) + \frac{\partial}{\partial x}(\alpha \rho_g v_g) = 0 \qquad (7.17)$$

Using Eq. (7.7) the term v_g can be replaced by $v_m + V_{gm}$, resulting in

$$\frac{\partial}{\partial t} (\alpha \rho_g) + \frac{\partial}{\partial x} [\alpha \rho_g (v_m + V_{gm})] = 0 \tag{7.18}$$

The time and area-averaged continuity equation for the mixture is

$$\frac{\partial}{\partial t} (\rho_m) + \frac{\partial}{\partial x} (\rho_m v_m) = 0 \tag{7.19}$$

Omitting the momentum transfer due to turbulence in this one-dimensional formulation, the mixture momentum equation may be written as

$$\frac{\partial}{\partial t} (\rho_m v_m) + \frac{\partial}{\partial x} (\rho_m v_m^2) = - \frac{\partial p}{\partial x} - \frac{f_m}{2D} \rho_m v_m |v_m|$$

$$+ g \rho_m \sin \theta - \frac{\partial}{\partial x} \left[\frac{\alpha}{1-\alpha} \frac{\rho_g \rho_\ell}{\rho_m} V_{gj}^2 \right] \tag{7.20}$$

Upon rearranging,

$$\frac{\partial}{\partial t} (\rho_m v_m) + \frac{\partial}{\partial x} \left(\rho_m v_m^2 + \frac{\alpha}{1-\alpha} \frac{\rho_g \rho_\ell}{\rho_m} V_{gj}^2 + p\right)$$

$$= - \frac{f_m}{2D} \rho_m v_m |v_m| + g \rho_m \sin \theta \tag{7.21}$$

The last term in Eq. (7.20) represents a drift stress, which comes from the time averaging and area averaging of the convective term, as shown in Appendix D. Actually, Eq. (7.20) has the same form as the momentum equation obtained by Zuber [51]. The drift-stress term is not present in the

momentum equation of a homogeneous model, constituting the basic difference between the two models. Equations (7.18), (7.19), and (7.21) are the field equations used for the present model. The constitutive equations (7.1) to (7.14) are used to relate the variables.

The thermal equations of state for the gas phase is in general

$$\rho_g = \rho_g (p_g , T_g) \tag{7.22}$$

in which p_g is the pressure and T_g the temperature of the gas. As reported earlier, Campbell and Pitcher [16] have shown for a stationary shock wave that the temperature rise across the wave is negligibly small. Hence, ρ_g may be considered to depend only on p_g. In this model the pressure p_g is assumed to be equal to the pressure p_ℓ of the liquid. As the mixture pressure p_m is defined by $\alpha\, p_g + (1-\alpha)\, p_\ell$, the respective pressures $p_g = p_\ell = p_m = p$, allowing for the omitting of any subscript for p in the momentum equation (7.21). Based upon the experimental observations of the shock speeds to be presented in the next chapter, an isentropic adiabatic law for the following gas behavior is assumed

$$p^{1/\gamma}/\rho_g = \text{constant} \tag{7.23}$$

Equations (7.18), (7.19), and (7.21) embody eight dependent variables; namely, α, ρ_g, ρ_m, v_m, v_g, V_{gm}, V_{gj} and p, as the liquid density ρ_ℓ is assumed constant. Using the constitutive equations (7.1) to (7.14), and Eq. (7.23), the variables can be related to each other, reducing the unknown variables to three--α, ρ_m, and v_m.

Numerical Computations

The three main field equations of the model, Eqs. (7.18), (7.19), and (7.21) are all in the so-called conservation form. As discussed earlier in the numerical analysis of the bubble-dynamics model, there are many explicit, implicit or combined numerical schemes for integration of the equations in this form. The Lax-Wendroff two-step scheme described in Appendix C has been used for the numerical computations in this study. At this point, it may be noted that Eq. (7.18), (7.19), and (7.21) can be mathematically simplified to a three variable system, for which a system of characteristic equations may be obtained. But the possibility of shock formation and the consequent complication in devising shock fitting, interpolations etc., discourages attempts in the use of the method of characteristics. Instead, a rather simple gas-dynamic approach may be adequate.

One of the initial steps in the solution is to choose a finite-difference grid that satisfies the conditions of stability of the Lax-Wendroff scheme. In choosing the mesh size Δx it must be realized that the accuracy in obtaining the shock profiles increases as the number of increments along the pipe length, $L/\Delta x$, increases. The time interval Δt can be evaluated to satisfy the CFL convergence condition, Eq. (6.52), at each time step by equating $\Delta x/\Delta t$ to the corresponding maximum value of the eigenvalue $|\lambda|$. The exact value of λ is not known for the present system of equations; hence, the value of λ for the homogeneous model $v_m + a_{mp}$ has been used, indeed yielding adequate computational stability.

Initial Steady Flow Conditions

All the eight variables involved in the field equations are to be

defined for the initial steady flow. Usually, the available information will be the average volumetric rate of flow of the liquid, the initial pressure distribution, and the mass rate of flow of the gas, from which the initial volumetric quality β at each mesh point can be defined. The void fraction α may be obtained using, for example, the relationship proposed by Zuber and Findlay [50]

$$\frac{\beta}{\alpha} = C_o + \frac{V_{gj}}{j_m} \tag{7.24}$$

The values of β, α, and j_m are the area-averaged values and V_{gj} is the time and area-averaged weighted value. For $\alpha << 1$, v_m may be approximated by the average water discharge divided by the cross-sectional area of the pipe. The term V_{gj} may be evaluated by using the empirical relations, Eq. (7.13) or (7.14) with $\Delta\rho \simeq \rho_\ell$, an approximation that is reasonable for $\rho_g << \rho_\ell$. To apply Eq. (7.24) a value of C_o has to be assumed. If data on velocity and concentration profiles are available, the value of C_o can be determined by referring to the relationships given in Zuber and Findlay [50]. Otherwise, a value must be estimated. Considering the approximate nature of Eq. (7.24) it is probably permissable to replace j_m by v_m for the evaluation of β/α. From the known pressures at various points, the density ρ_g of the gas phase may be evaluated from Eqs. (7.1-7.12). Thus, the initial conditions are fully described.

Boundary Conditions

To satisfy the boundary conditions at the ends of the test pipe the characteristic equations of the homogeneous model are again used.

Leaving the drift-stress term in Eq. (7.21), Eqs. (7.21) and (7.19) can be employed to obtain the pair of characteristic equations. The knowledge that the mass of gas per unit mass of the mixture is constant for a homogeneous model provides an additional relation between ρ_g and α. The adiabatic relations between p and ρ_g are also used. The characteristic equations have the same form as Eqs. (5.56) and (5.57) if $\rho_\ell(1-\alpha)$ is replaced by ρ_m and u by v_m. At the boundaries, the following relationships are used to evaluate v_m, α, and p. From the continuity of gas phase, Eq. (7.17), and $v_g = v_\ell = v_m$

$$\frac{d}{dt}\left(\frac{p^{1/\gamma_\alpha}}{1-\alpha}\right) = 0 \tag{7.25}$$

The characteristic equations become

$$\frac{dp}{dt} \pm \rho_m a_{mp} \frac{d v_m}{dt} \mp \frac{f_m}{2D} \rho_m a_{mp} v_m |v_m| = 0 \tag{7.25}$$

$$\frac{dx}{dt} = v_m \pm a_{mp} \tag{7.27}$$

The positive sign is used for the forward C^+ characteristic and the negative sign for the backward C^- characteristic. If either v_m of p is prescribed at the respective boundaries, the other can be evaluated using C^+ equations for a downstream boundary, and the C^- relationships for an upstream boundary.

CHAPTER VIII

RESULTS ON BUBBLE-SIZE DISTRIBUTION AND SHOCK WAVES

The experimental results reported in this chapter have been obtained using the plexiglass-piping apparatus described earlier. Based on the photographs of the bubbles obtained at different locations along the test pipe, the general bubble-size distribution pattern in the test pipe will be discussed. Finally, formation of shock waves, their speed of propagation, and structure, will be considered in detail.

Bubble-Size Distribution

The size and distribution of bubbles across a cross section of the pipe can have a considerable influence on the velocity of propagation and the structure of shock waves in a bubbly mixture. Fig. 7 shows typical photographs of bubbles at three locations along the test pipe: the riser, the horizontal leg, and the downcomer. For the entire bubbly-flow regime in which experimental observations on shock waves have been made, similar photographs have been obtained for different air concentrations and flow conditions.

As seen in the photograph of Fig. 7, the riser has a more or less uniform distribution of bubbles across the entire cross section. The bubbles are spherical, but not of uniform size, ranging in diameter from 0.5 to 2 mm. For the bubbles shown in the riser of Fig. 7 a statistical distribution is represented in Fig. 8. It is noted that the average bubble size d_{50} is 1.37 mm and the standard deviation is $\pm$ 0.41 mm. For

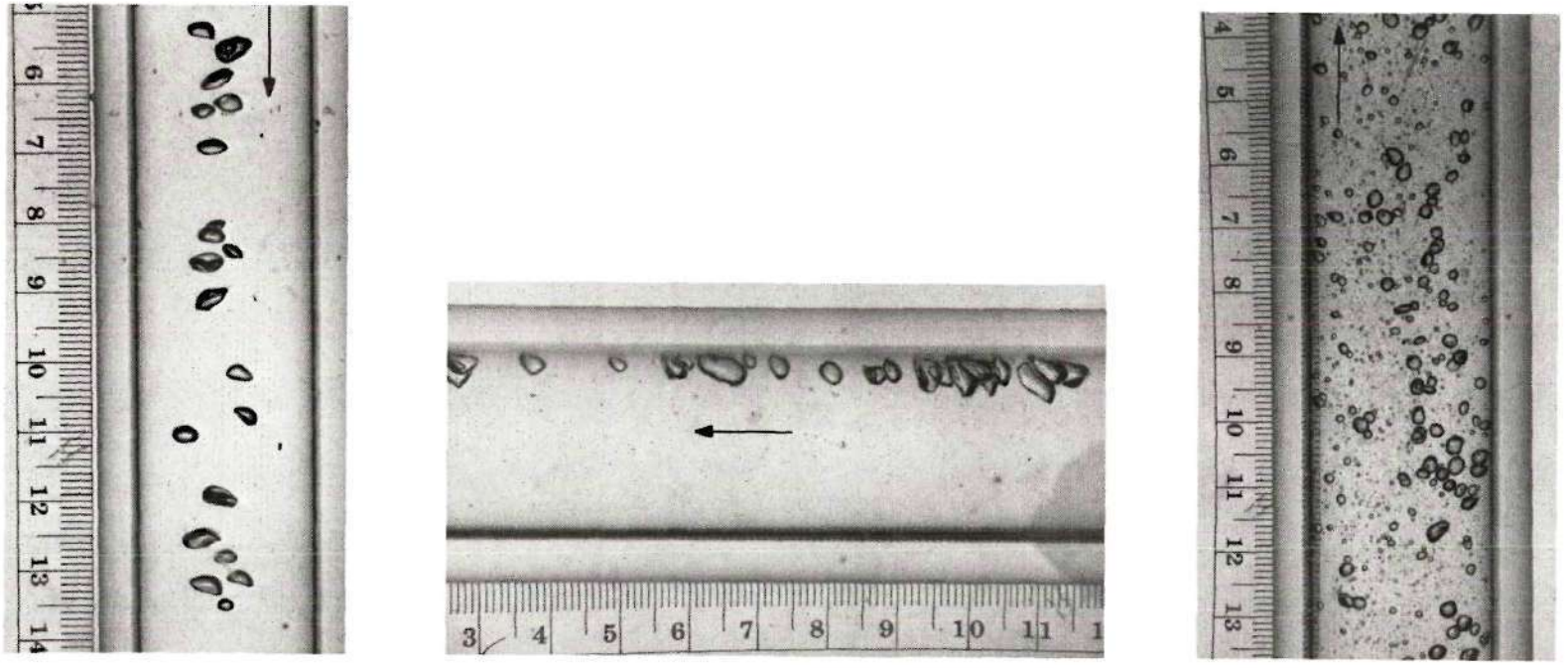

Figure 7. Typical Bubble-Distribution in Three Legs of the Plexiglass Test Pipe.

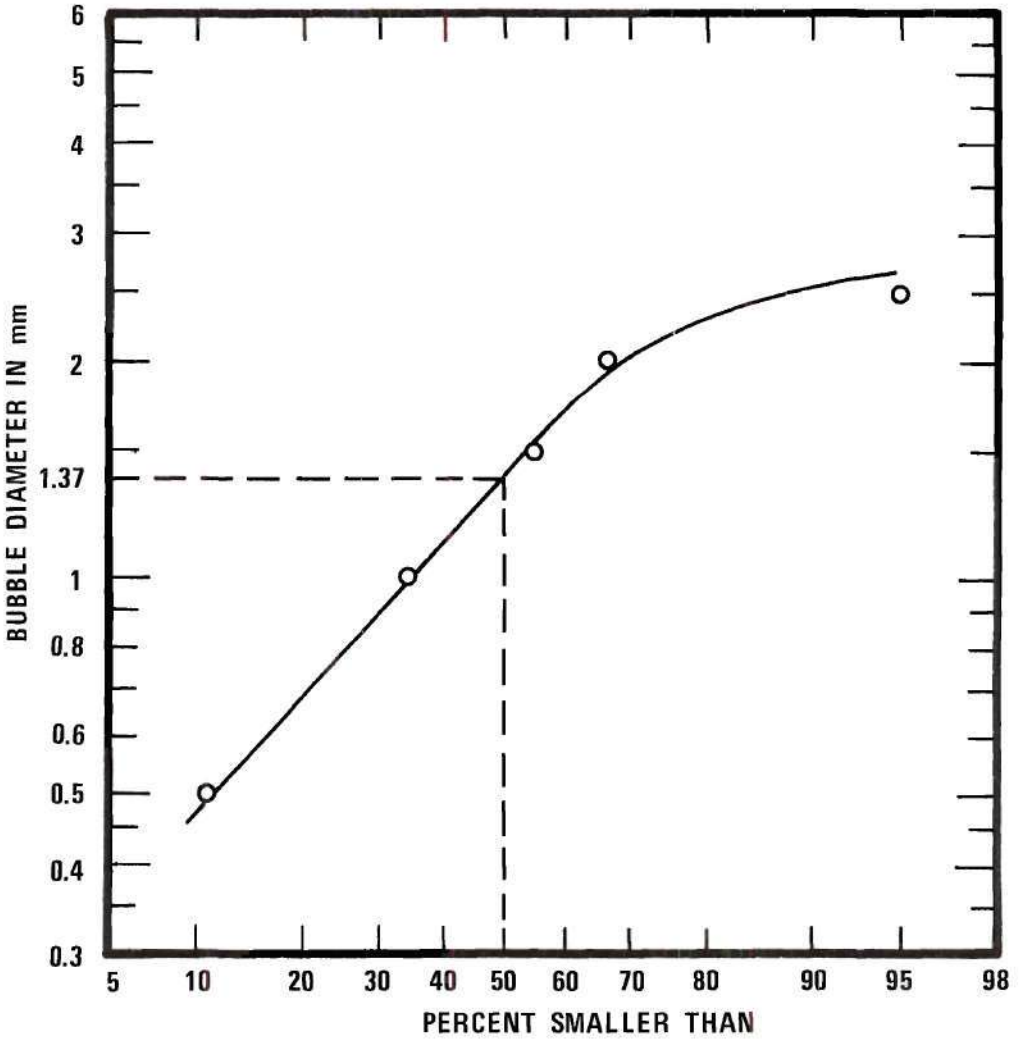

Figure 8. Typical Bubble-Size Distribution Curve for the Riser: u_o = 5.2 ft/sec, p_o = 39 psig, β_o = 0.01.

use in the study of the shock waves and transients, the representative bubble sizes are determined from the bubble-size distribution curves in this manner. As the water discharge, the reservoir pressure, and hence the initial steady-flow pressure distribution are not varied much for the experiments reported herein, the main concern is the influence of the air concentration on the bubble sizes. It has been observed that as the air concentration is increased the average bubble size also increases, but only slightly. In fact, the range of the average bubble size is from 1 mm to 1.5 mm for the range of $0.005 < \beta < 0.08$.

In the horizontal portion, as shown in Fig. 7, the bubbles occupy the top portion of the pipe and to some extent coalescence takes place. Also, it may be noted that the bubbles lose their spherical shape, and are larger in size. Because of the large nonuniformity in size and distribution, and the coalescence taking place, it was found to be too difficult to choose any representative bubble diameter for the horizontal portion. Consequently, limited attention has been paid to the study of the shock structure in this portion of the test pipe.

In the vertical downcomer the bubbles are large and mainly concentrated along the center of the pipe. They appear to flow intermittently with a tendency to form clusters. Pulsating motion of the bubbles has also been observed. Even though the bubbles are large and nonspherical they are more or less of the same size, with an average dimension of about 3 mm. For lower air concentrations the intermittency of the bubbles was dominant, but for higher air concentrations a formation of clusters was observed. The bubbles ultimately transformed into slugs at approximately $\beta = 0.09$. Slugs formed in this manner in the downcomer even when

a bubbly flow existed in the other portions of the pipe.

From the above description it may be concluded that the bubble sizes and the bubble distribution varied from portion to portion of the test pipe. This variation can be expected to affect the characteristics of the shock waves formed as well as the celerity of the disturbances in the medium.

Shock Waves

Formation of Shock Waves

Inasmuch as the wave speed depends upon the pressure and the void fraction, both of which vary during a transient, a compression wave propagating in a gas-liquid mixture undergoes a change in form continuously, resulting in the steepening of its front. In a long pipe this steepening process may result in a shock wave which itself may undergo changes in its structure as it propagates. The phenomenon of steepening of a compression wave has been illustrated in Fig. 9 for three cases of different air concentrations. In these experiments a compression wave was generated by a rapid closure of the valve at the downstream end of the pipe. Fig. 9 shows photographs of oscilloscope traces of a compression wave near the valve and the same wave after it has travelled a distance of 5.5 ft up the pipe, for three different cases. The steepening of the wave front is noticeable in all the cases. In case (a) a weak shock formation is seen, as the strength of the wave p_1/p_o is relatively small. In case (b) a high degree of steepening is noticeable. In fact, a shock has already formed, exhibiting its significant features of a steep front and damped oscillations behind it. Case (c) represents a lower air concentration, and consequently higher wave strength and speed. Because of the higher

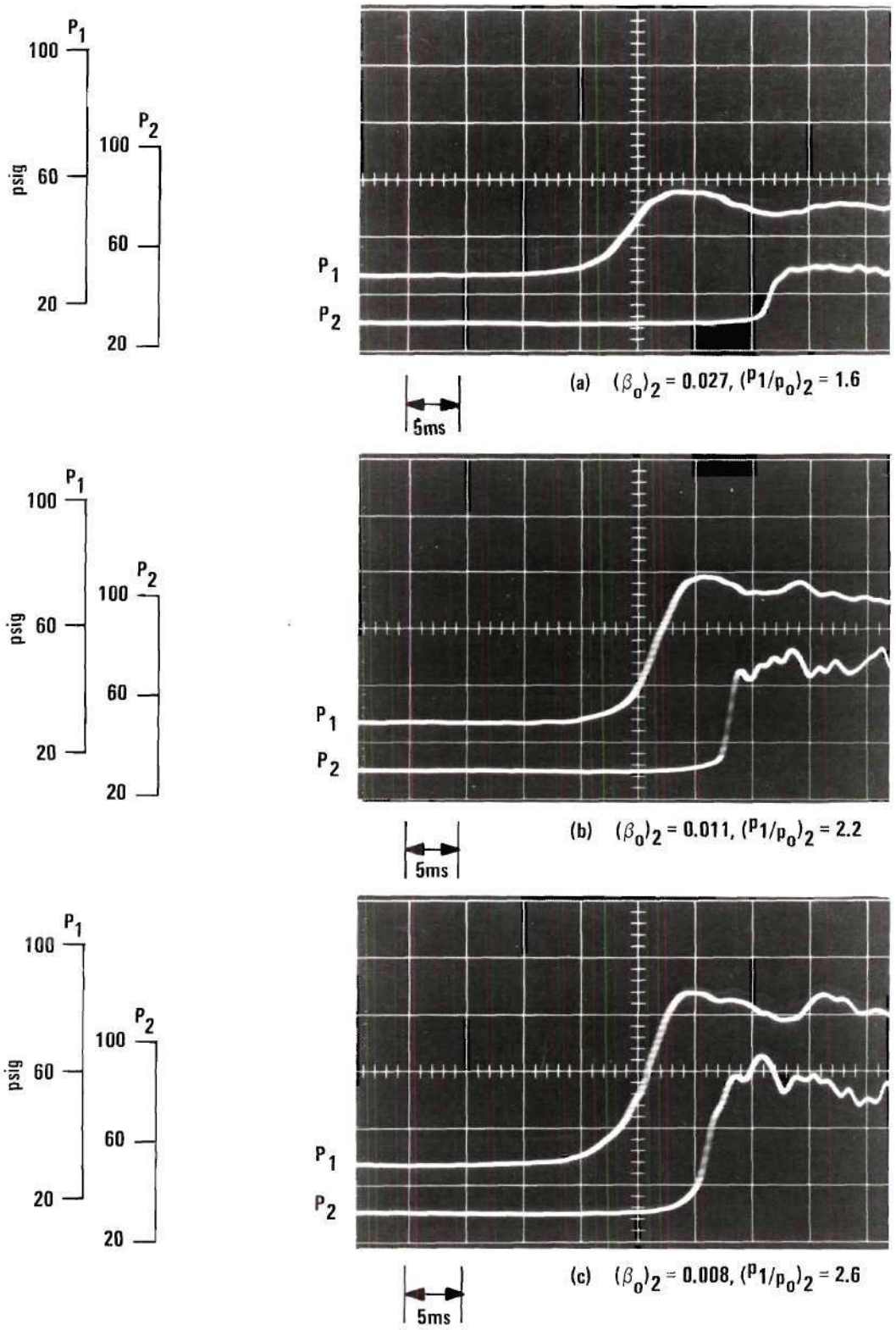

Figure 9. Compression Wave Steepening and Resulting Shock Wave Formation. Piezometers P1 and P2 at x = 60.5 ft and 55.0 ft, Respectively, u_o = 4.4 ft/sec.

speed the compression wave has not yet fully steepened in its travel of 5.5 ft. Nevertheless, the steepening phenomenon is very significant.

It may be noted that the steepening process is dependent on the pressure, the void fraction, and the form of the initial compression wave, which in this case is governed by the time of closure of the valve. Obviously, the distance over which the steepening takes place and the consequent formation of shock waves is affected by the above factors, which also influence the shock characteristics. In a long pipe with a mixture flowing the formation of shock waves is very likely for a rapid closure of a downstream valve. The time of closure of the valve has a significant influence on the shock formation. A compression wave of greater thickness takes more time to transform to a shock wave, and the inception of the shock takes place further away from the valve end.

In a grid of characteristics the shock inception is denoted by the intersection of like characteristics, as illustrated in Fig. 6. It can be shown by considering different cases that this intersection occurs almost near the valve end for an instantaneous closure, whereas it takes place further and further from the valve as the time of closure is increased, all other conditions being the same. At this point it may be noted that the exact inception point of a shock wave as predicted by the grid of characteristics is very sensitive to the mesh size used and can not necessarily be taken to represent the real point of shock inception as observed by experiments.

Speed of Propagation of Shock Waves

The velocity of propagation of a dynamic wave in a two-phase medium is dependent on the pressure and void fraction. In the case of shock

waves the strength of the shock p_1/p_o also affects the speed of propagation. In the case of bubbly mixtures the behavior of the bubbles may be isothermal or adiabatic, depending on the range of frequencies of bubble oscillations, Plesset [25]. In the present experiments, with the shock speeds of the order 10^2 m/sec and thicknesses of the order 10^{-2} m, the thermal penetration depth, $(D_g/\omega)^{1/2}$, as defined by Plesset [25], is of the order 10^{-4} m, the value of D_g for air being about 1.8×10^{-5} m^2/sec. The acoustical wave length in air, λ_g, is of the order 10^{-2} m. With the bubble radius R_o of the order of 10^{-3} m, it is evident that for the present experimental conditions $(D_g/\omega)^{1/2} << R_o$ and $\lambda_g > R_o$. For this range an adiabatic behavior of the bubbles is to be expected, based on the study of Plesset [25].

Eqs. (4.13) and (4.14) give the speed of the shock waves based on the adiabatic and isothermal laws, respectively. It is intended to verify which of these equations gives the best agreement with the experimental values of the corresponding shock speed. From the photographs of the oscilloscope traces of the shock wave at two locations 4 ft apart, average shock speeds have been measured. For better accuracy, the pressures before and after the passage of the shock are noted from the plotted records rather than from the photographs. The average void fraction α_o at pressure p_o is obtained from the known volumetric quality β_o, using Eq. (7.24) with the distribution parameter $C_o = 1.2$. From Eq. (3.9) the acoustical velocity based on homogeneous theory a_h is evaluated for both isothermal and adiabatic behavior with m equal to 1 and 1.4, respectively. Using Eqs. (4.13) and (4.14) the theoretical shock speeds are calculated. In Figs. 10 to 12 the theoretical and experimental values are compared.

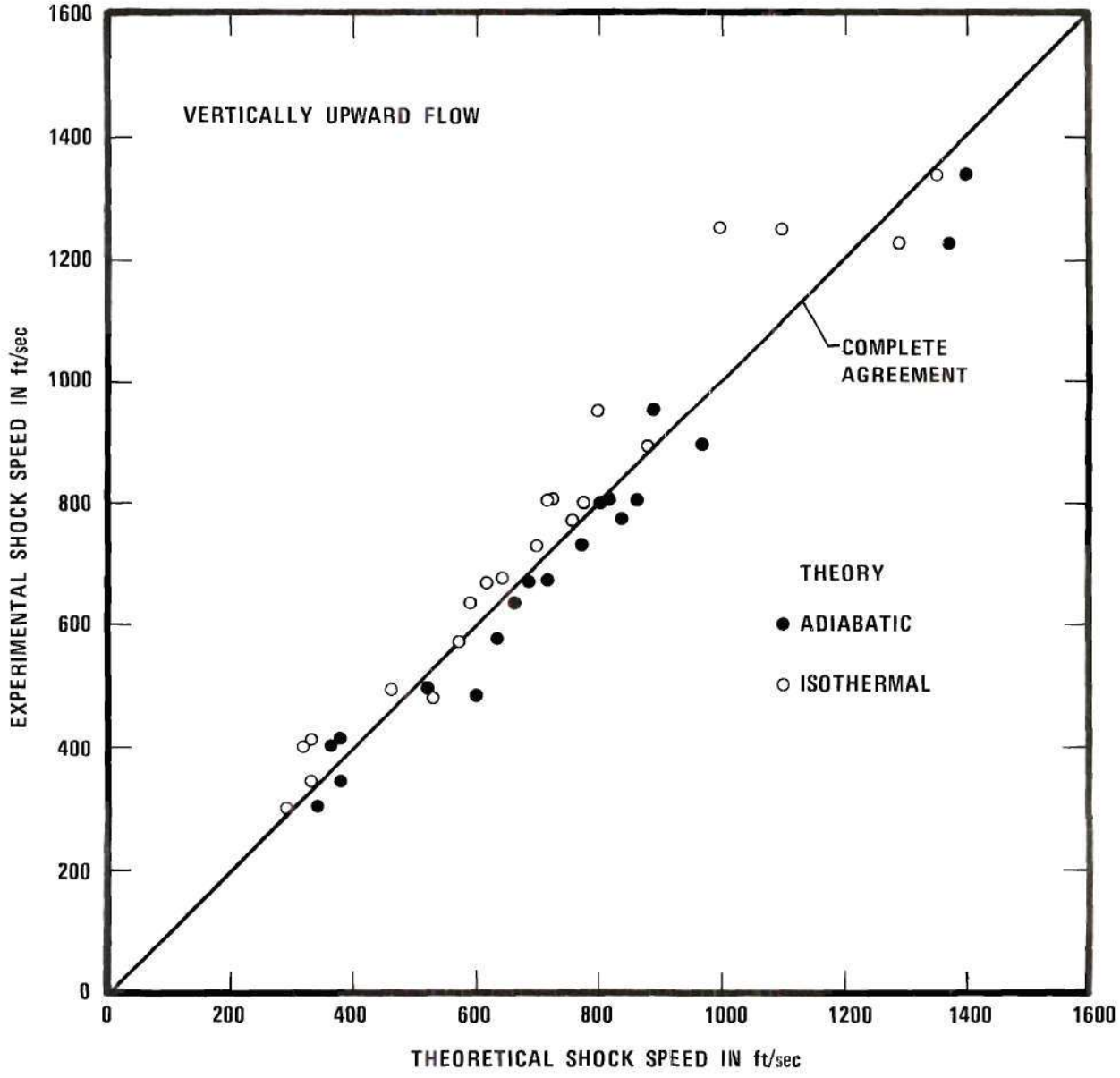

Figure 10. Comparison of Experimental and Theoretical Shock Speeds in the Riser.

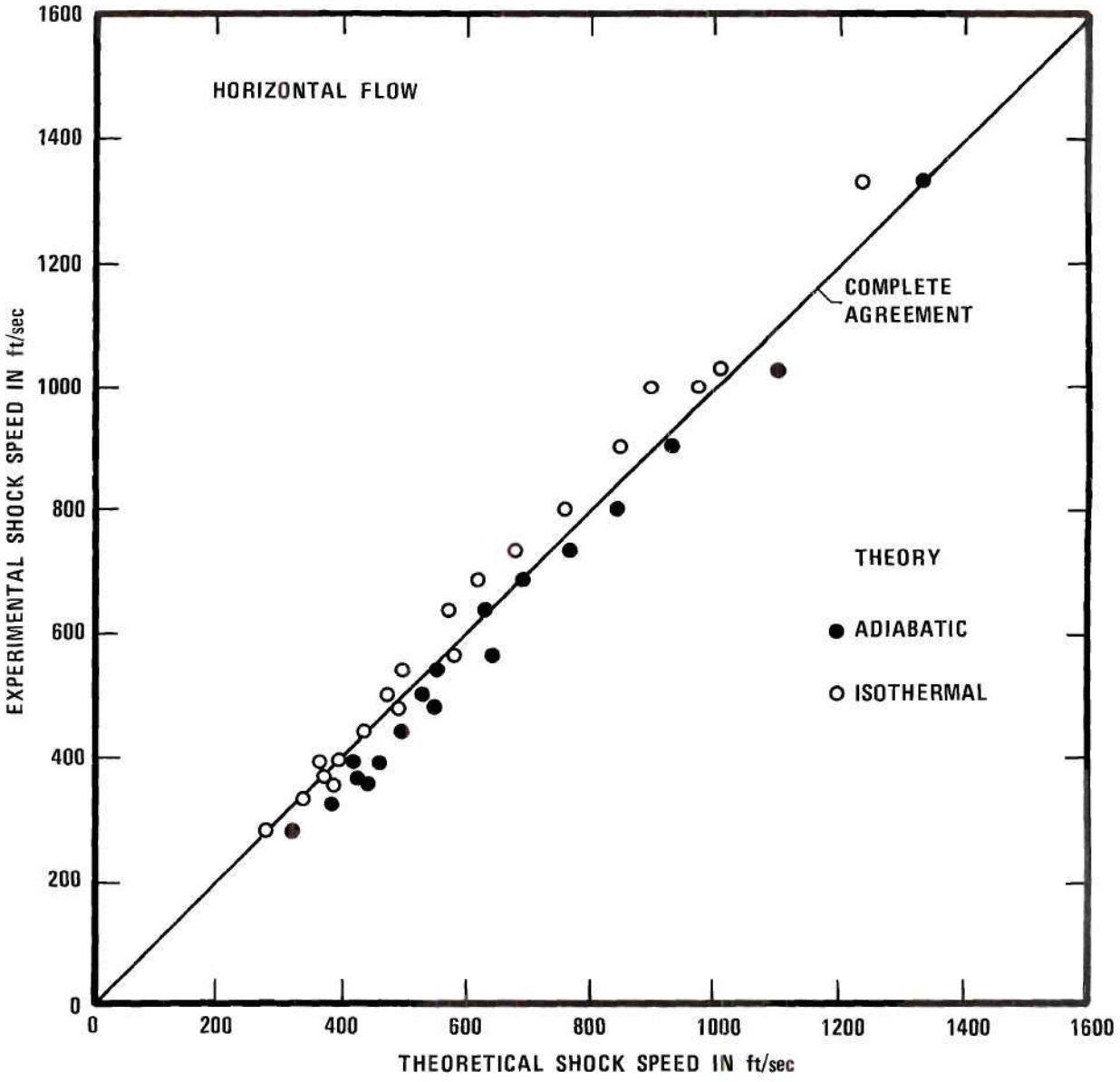

Figure 11. Comparison of Experimental and Theoretical Shock Speeds in the Horizontal Leg.

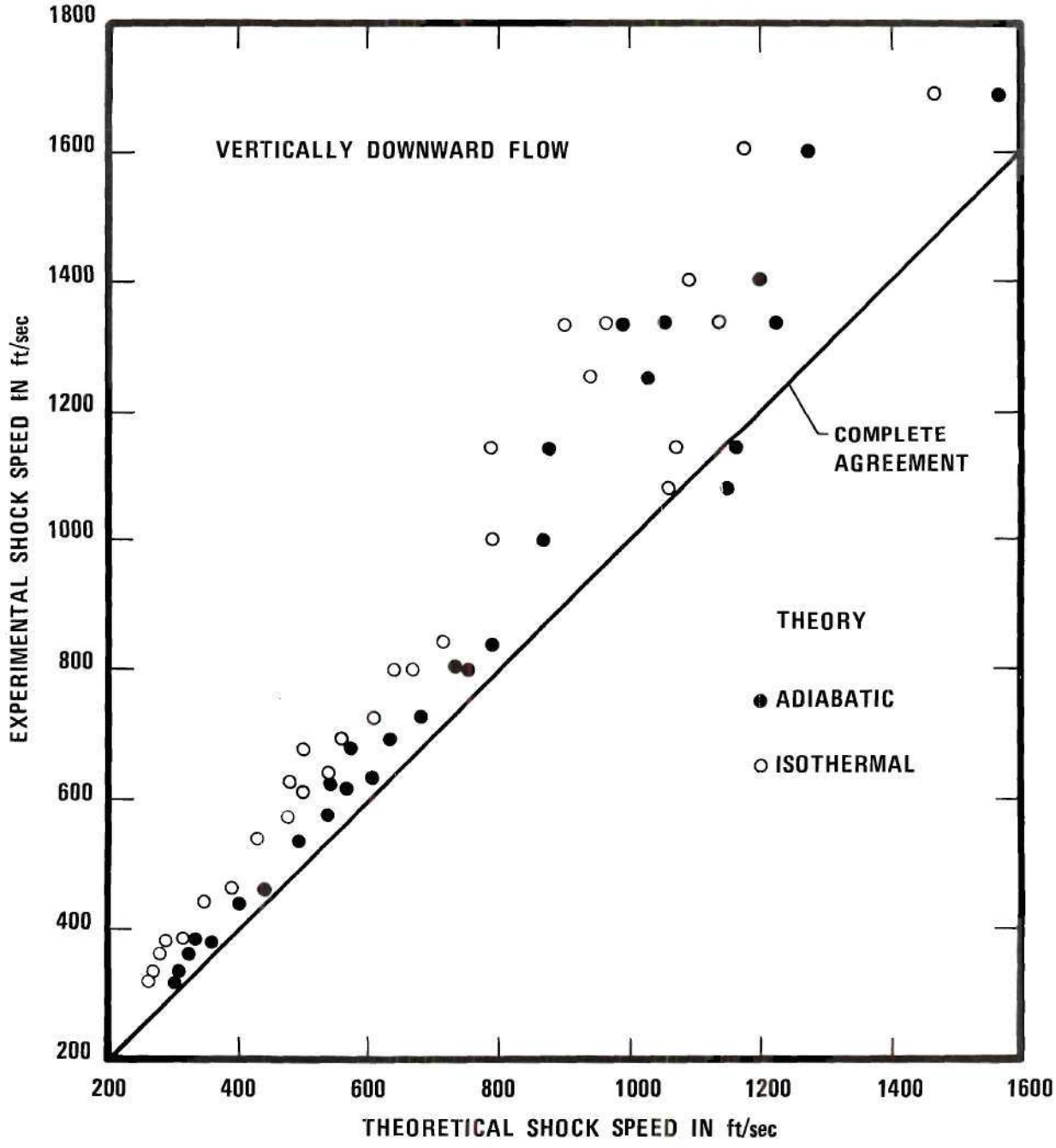

Figure 12. Comparison of Experimental and Theoretical Shock Speeds in the Downcomer.

It may be noted that the adiabatic theory gives values closer to the experimental ones for all the three portions of the pipe. However, for the downcomer the experimental values are consistently higher than the theoretical values--even those from adiabatic theory. This discrepancy may be caused by the very nonhomogeneous and nonspherical features of the bubbles in the downcomer relative to the other legs of the pipe, as seen in Fig. 7. The bubbles are concentrated at the center of the pipe and are intermittent in the flow. This situation may be visualized as a type of flow in between the bubbly and slug-flow regimes, for which it is reasonable to expect higher wave speeds. In general, it may be concluded that, for the experimental conditions of the present investigation, the adiabatic theory shows better agreement for the prediction of the celerity of shock waves than isothermal theory.

Structure of Shock Waves

In the present investigation photographs of the shock waves at different locations along the test pipe have been obtained for air concentrations varying from $\beta = 0.005$ to 0.05. The initial steady-flow water velocity was maintained at about 4 to 5 fps. Shock waves of weak to moderate strengths with p_1/p_o varying from 1.4 to 3.2 have been observed. Average bubble sizes for each of these cases have also been obtained from photographs similar to those of Fig. 7. However, the nonuniformity of the bubble sizes, as well as their nonspherical shape and wide distribution resulted in a great scatter of the experimental values of shock thickness, wave lengths of oscillations, etc. Futhermore, the values of the wave speed measured from the oscilloscope traces are of limited accuracy because of approximations involved in judging the beginning

of the shock, the end of the steep portion, etc. Considering all these inaccuracies, it was decided to follow a qualitative approach in presenting and discussing the results on the structure of shock waves. Nevertheless, as far as possible, the shock parameters were measured and are reported in Appendix E. No attempt has been made to develop any theoretical relationships, however. Figs. 13 to 18 show typical shock photographs at different locations along the pipe, which will be used for further discussion on the structure of shock waves.

The classifications of shock wave has been discussed in Chapter IV, following the procedure of Noordzij and van Wijngaarden [28]. A-type shocks, which are characterized by a very steep front with the pressure shooting above the equilibrium level, have not been observed in the present study. Noordzij [32] has observed A-type of shocks in his experiments on shock tubes to be very near the end of the tube where the shock was generated. A-type shocks are described to form when the relative bubble motion is not resisted by viscous forces. For a typical relaxation time τ defined by Eq. (4.30), the relative motion is likely to be resisted by viscosity, and the shock structure may well change from A-type to B-type, as explained by Noordzij and van Wijngaarden [28]. In the case of shock-tube experiments, a shock is generated almost instantaneously, giving it a very steep front, which undergoes changes all along the tube. But in the case of the present study, a compression wave of moderate thickness transforms itself into a shock wave by steepening. The steepening process is opposed by the viscous resistance to the radial and translational relative motions of the bubbles, as well as by the dispersion effects. Hence, the physical process of shock formation by

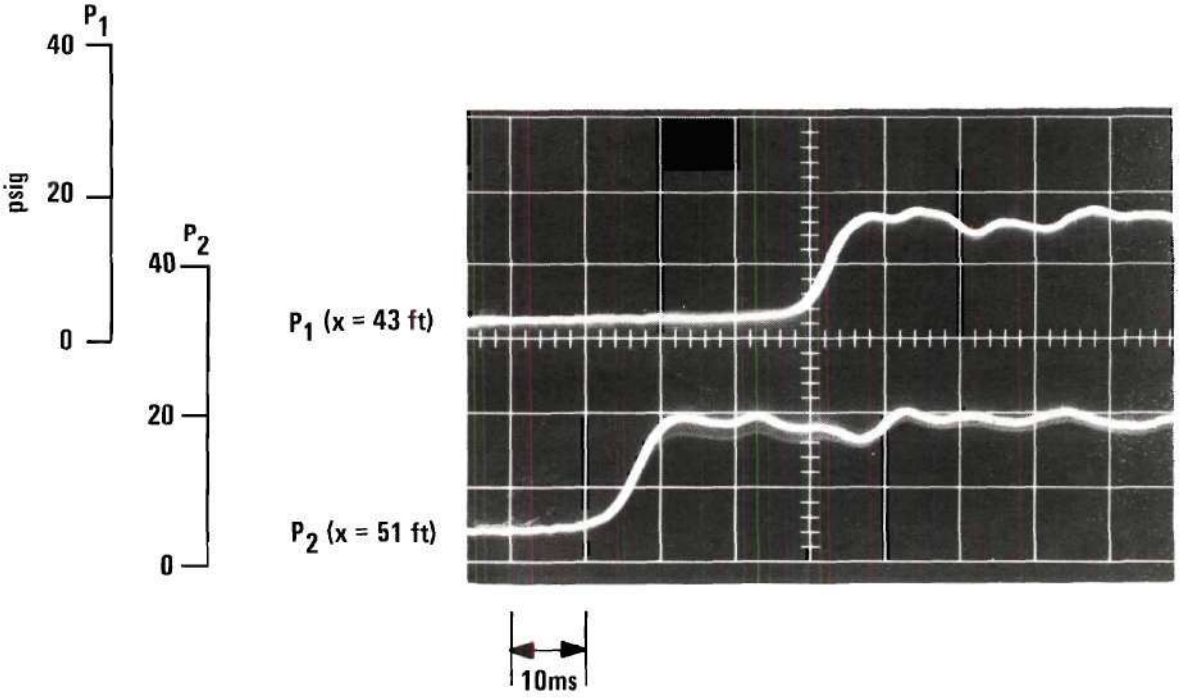

Figure 13. Profile of Shock Wave Propagating up the Downcomer. u_o = 3.7 ft/sec, $(\beta_o)_2$ = 0.053, and $(p_1/p_o)_2$ = 1.45.

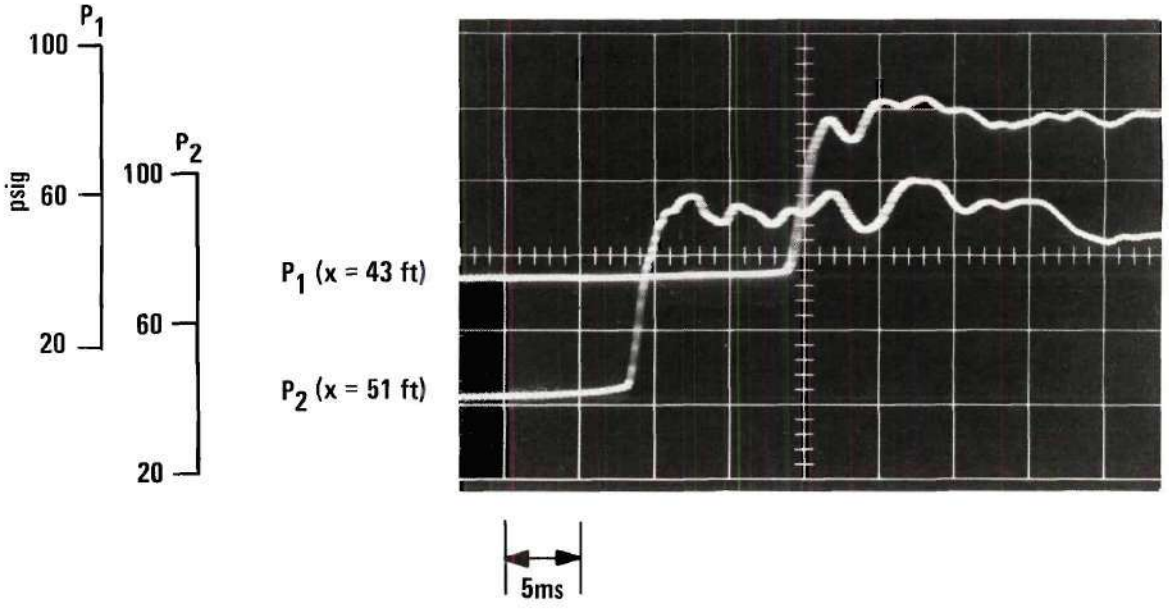

Figure 14. Profile of Shock Wave Propagating up the Downcomer. u_o = 5.0 ft/sec, $(\beta_o)_2$ = 0.016, and $(p_1/p_o)_2$ = 2.08.

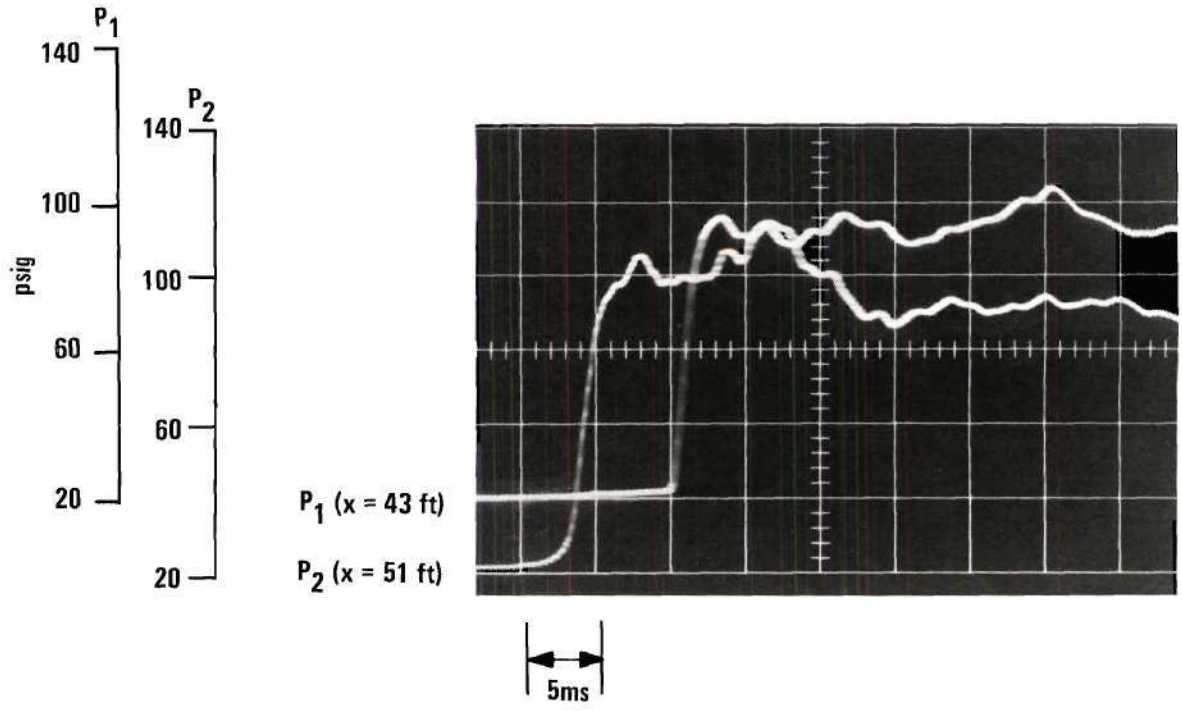

Figure 15. Profile of Shock Wave Propagating up the Downcomer. u_o = 5.1 ft/sec, $(\beta_o)_2$ = 0.006, and $(p_1/p_o)_2$ = 2.76.

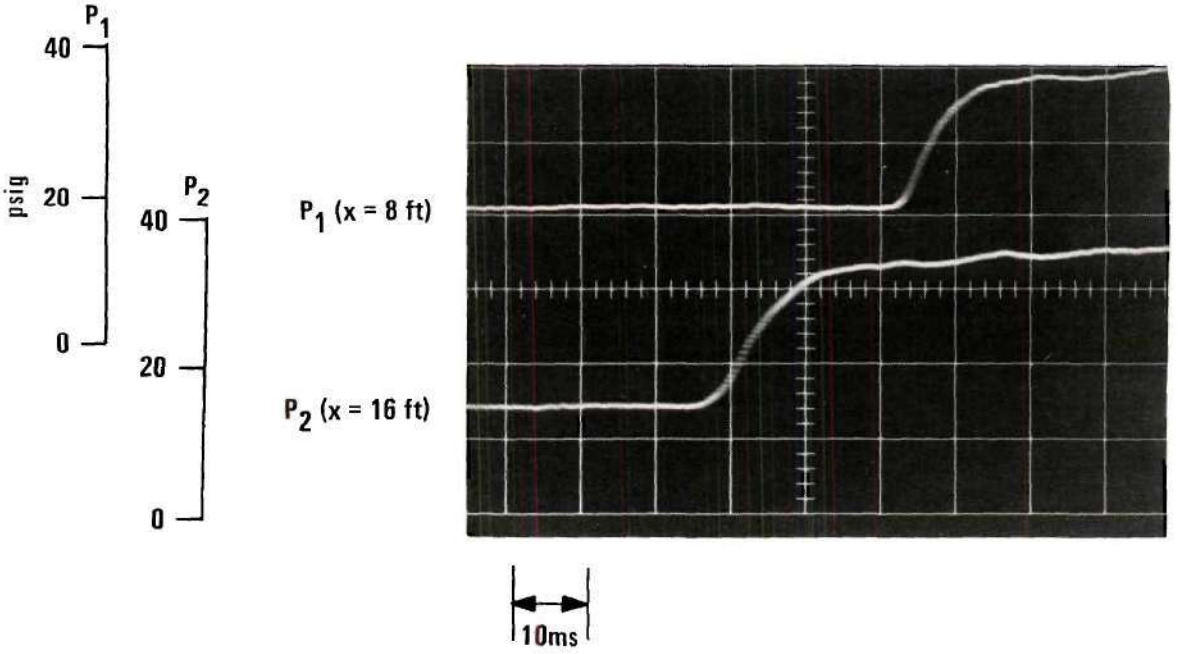

Figure 16. Profile of Shock Wave Propagating down the Riser. u_o = 4.3 ft/sec, $(\beta_o)_2$ = 0.037, and $(p_1/p_o)_2$ = 1.60.

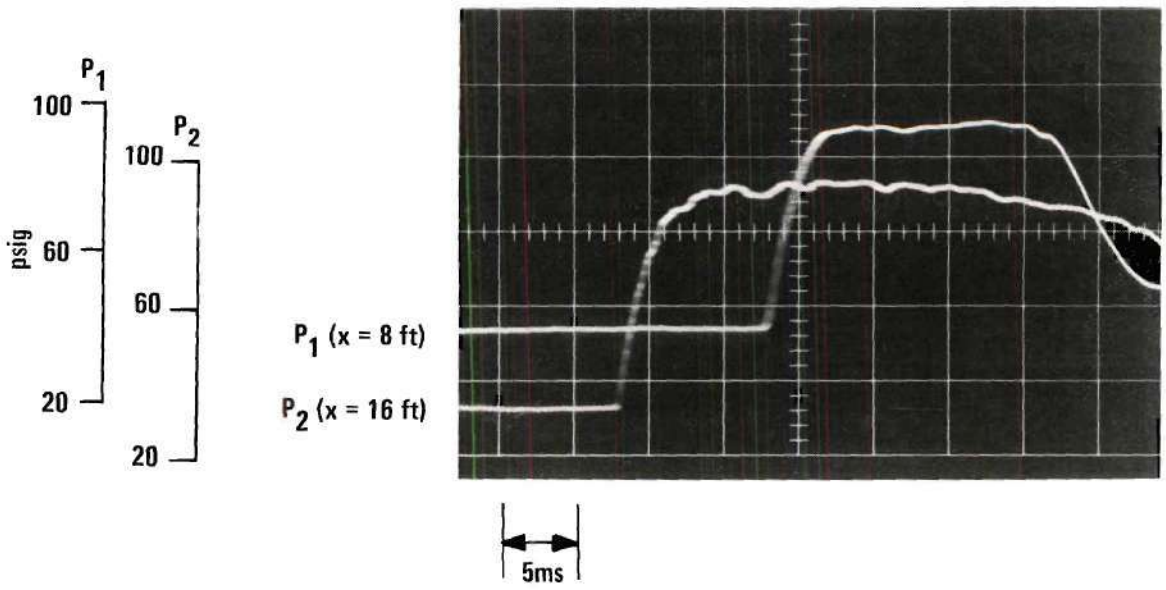

Figure 17. Profile of Shock Wave Propagating down the Riser. u_o = 5.1 ft/sec, $(\beta_o)_2$ = 0.010, and $(p_1/p_o)_2$ = 2.40.

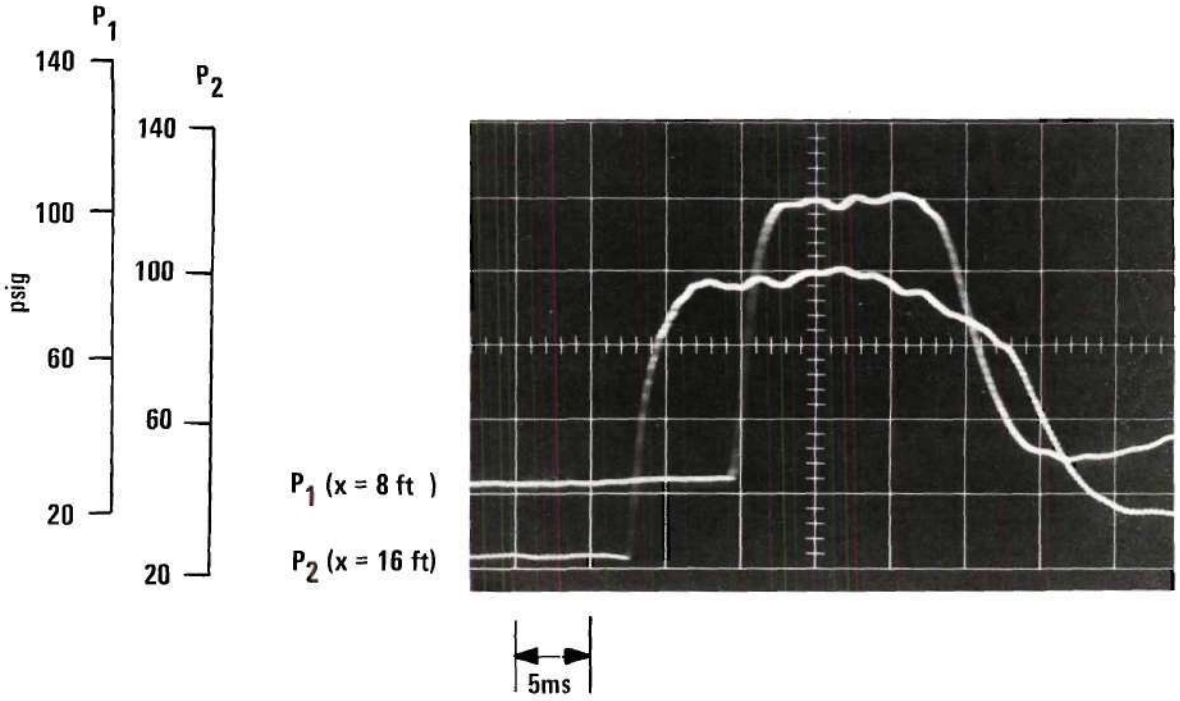

Figure 18. Profile of Shock Wave Propagating down the Riser. u_o = 5.1 ft/sec, $(\beta_o)_2$ = 0.006, and $(p_1/p_o)_2$ = 2.83.

steepening of a compression wave makes the shock waves of this study different from those generated in shock tubes. Probably one could expect A-type shocks in this situation only when the initial compression wave produced by the valve closure itself has a very steep front. Apparently, only a instantaneous closure producing a shock right at the valve could produce this condition. For the present study the typical time of closure for a spring-actuated closure of the valve is 10 ms, for which no A-type shocks were observed.

Fig. 13 shows a weak shock with p_1/p_o = 1.45 at 10.5 ft and 18.5 ft from the valve end. It is seen that there is very little steepening of the front of the shock over this 8 ft of travel. The profile is very smooth with a gradually rising front. Except for the low amplitude oscillations seen behind the shock, the profile resembles a C-type shock. In fact, as the shock reached the vertical portion near the reservoir end of the pipe system, these oscillations were observed to be practically absent, and the shock had the appearance of a C-type shock, similar to that shown in Fig. 16, for which a weak shock with p_1/p_o = 1.6 is shown propagating vertically downwards. For a lower pressure p_o and a higher void fraction α_o as is the case with the weak shocks of Figs. 13 and 16, the steepening process is relatively slow. Fig. 16 shows that the steepening is still occuring even after the wave has travelled almost 53.5 ft. Fig. 14 shows the propagation of a shock with p_1/p_o = 2.08. It is seen that the shock profile is almost steady, possessing a steep front and a gradually rising poriton, followed by oscillations. This shock may be classified as the B-type, for which a balance between steepening, dispersion and dissipation exists. The oscillations behind the shock do not

possess a definite perodicity. Noordzij and van Wijngaarden [28] have described the influence of the bubble sizes on the period of these oscillations. It is to be expected that with a nonuniformity in bubble sizes the oscillations would be irregular. However, it is seen that the oscillations are not completely random. The first two crests are utilized in obtaining the approximate wave lengths reported in Appendix D. For shocks of this kind no noticeable change in structure has been observed for their complete passage along the pipe. Fig. 17 shows a similar shock wave propagating down the downcomer toward the reservoir end. It may be observed that the shock is more or less steady. A stronger shock wave with $p_1/p_o \simeq 2.8$ is shown propagating upwards near the valve end in Fig. 15 and propagating downwards near the reservoir end in Fig. 18. In Fig. 15 it is seen that the steepening is taking place, whereas in Fig. 18 the shock profile is practically steady. Compared to the shock of Fig. 14, the shock of Fig. 15 has a higher propagation speed, and consequently, for the duration over which the steepening takes place the latter travels a longer distance along the pipe.

The effect of gravity on the shock structure is extremely small, as discussed in Chapter III. Hence, no definite conclusions can be drawn from the photographs of the shocks. However, a very careful observation of the almost steady profiles of shock waves in Figs. 17 and 18 reveals possibly that there is a very small stretching of the profile as the wave travels downwards into the region of a positive pressure gradient. This agrees with the observations made by Noordzij [32].

The transformation of shock waves from B-type to C-type was only observed in the present study in the case of very weak shocks, for which p_1/p_o was less than about 1.6. For all of the moderate shocks with p_1/p_o

ranging from 1.6 to 3.3 no change of the shock type was observed as the wave propagated along the test pipe. Noordzij [32] has reported the changes from A-type to B-type and C-type for shock waves propagating down a shock tube through liquids of higher viscosity than tap water. However a few of his experiments with tap water did not show these changes in the shock structure, meaning that the viscosity of the liquid has a great influence upon the shock structure. As the viscous dissipation due to the relative motion of the bubbles increases with the viscosity of the liquid, and since dissipation has a considerably higher influence than dispersion, a balance between the steepening phenomenon and the dissipation can exist, resulting in C-type shocks.

The oscillations behind a B-type shock are damped in a few wave lengths and are very small compared to the overall pressure rise produced by the shock. From the photographs of B-type shocks of different strengths, different flow velocities, and air concentrations, the thickness d_B of the steep front and a representative wave length Λ_B of the oscillations were measured and reported in Appendix E. The thickness of the observed few C-type shocks are also measured and tabulated therein. It may be noted that these quantities are measured in time units and are multiplied by the average wave speed obtained experimentally to express them in terms of linear units. As mentioned earlier the quantities are very approximate due to the limited accuracy associated with the measurements from photographs.

The form of the initial compression wave is observed to have an influence on the structure of the shock wave. Noordzij [32] has derived theoretical expressions for the shock parameters in terms of its strength,

initial pressure, initial void fraction, and the bubble radius. The viscosity of the liquid is also considered for C-type shocks, and the gradually rising part of B-type shocks. A brief description of the theoretical expressions have already been incorporated in Chapter IV. For the sake of comparison with the present study, Eqs. (4.36) (4.39), and (4.40) have been used to evaluate the values of d_B and Λ_B of B-type shocks and d_c of C-type shocks. The calculated values are included in Appendix E. It has been noted that the experimental values of d_B and Λ_B are consistently higher than the theoretical values, suggesting that the shock parameters have different values from those for shocks encountered in shock tubes. The difference may be due to the influence of the profile of the original compression wave on the parameters of the subsequent shock wave.

From Appendix E it may be noted that the theoretical values of the shock thickness d_C of C-type shocks are consistently higher than those predicted by experiments. In fact, Noordzij [32] has indicated that the theoretical values can be as much as three times experimental values based on experiments in shock tubes. The reason for this large discrepency has been attributed to nonspherical nature of bubbles causing a higher drag force than that represented in the theoretical development. Also, thermal relaxation effects have not been accounted for in the theory.

Based on Crespo's theory [17] on thermal relaxation, Noordzij and van Wijngaarden [28] have shown that if thermal relaxation is present the smooth profile of a C-type shock may be expected when $p_1/p_o < 1.4$. As smooth profiles are seen to exist in the present study for p_1/p_o less than about 1.6, it appears that thermal relaxation may be important, at

least for weak shock waves. In fact, this can also be explained by a simple argument. In the present study, C-type shocks are mainly observed in the riser near the reservoir end of the pipe. The average bubble radius R_o is about 0.75 mm. Hence, the relaxation time τ associated with visocus relaxation can be calculated to be 0.03 sec from Eq. (4.30). With the thermal diffusivity D_g for air equal to 18×10^{-5} ft^2/sec, the relaxation time associated with thermal relaxation is also 0.03 sec, Eq. (4.41). Thus, it appears that thermal relaxation is equally important in the present case, and C-type shocks are indeed to be expected if p_1/p_o is approximately 1.4.

CHAPTER IX

BUBBLY-FLOW TRANSIENT RESULTS

Experimental results of pressure transients at different locations along the plexiglass pipe were obtained over the entire bubbly-flow regime for a variety of air concentrations, flow velocities, and pressures. The transients were generated by the rapid spring-activated closure of a downstream valve. Two springs could be adjusted to obtain desired times of closure ranging from 10 to 100 ms. The details on the experimental procedure and instrumentation have already been reported in Chapter II. Five typical experimental runs, covering a range of the volumetric quality $0.006 < \beta < 0.09$, will be presented and analyzed. The details of the runs are given in Table 1, while the pertinent characteristics of the pipe are listed in Table 2. These data have been used in the numerical simulation of the results by the bubble-dynamics and the drift-flux models. Numerical results are also included for the velocity transients, followed by a discussion on the relative advantages and disadvantages of the proposed models.

In the numerical computation of transient flow, the initial distribution of the average void fraction α along the pipe is required. With the known mass rate of flow of air, volumetric rate of flow of water and the measured pressure gradient, the distribution of the volumetric quality β was computed. Using Eq. (7.24) to describe the relationship between β and α, the initial variation of α along the pipe was ascer-

Table 1. Experimental Data for Bubbly Flow

Run Number	Water Discharge in cfs	Mass Rate of Air Flow slugs/sec $X10^5$	Reservoir Pressure in psig	Time of Closure in seconds	Average Bubble Diameter in mm
1	0.0234	0.1129	40	0.03	0.530
2	0.0286	0.2996	40	0.03	0.675
3	0.0268	0.5526	40	0.04	0.680
4	0.0302	1.0463	40	0.03	0.690
5	0.0232	1.4702	40	0.03	0.690

Table 2. Characteristics of Plexiglass Pipe

Total Length of the test pipe	61.5 ft
Length of the riser	20.75 ft
Length of horizontal portion	17.50 ft
Length of the downcomer	23.25 ft
Diameter of the pipe	1.025 inch
Average thickness of wall	0.25 inch
Celerity of a disturbance through only water (α=o)	2033 ft/sec

tained. In the absence of velocity and concentration profiles, the distribution parameter C_o in Eq. (7.24) was assumed to be 1.2. Eq. (7.13) gives a value of V_{gj}, the drift velocity, equal to 0.8 ft/sec for the riser, zero for the horizontal, and -0.8 ft/sec for the downcomer, resulting in a different β/α ratio for each portion of the pipe. As this difference caused initial undesirable discontinuities in α at the junctions between the different portions of the pipe, a constant representative value of β/α for the entire test pipe was employed instead.

The methods of numerical computations and the procedure involved have been described in detail in Chapter VI for the bubble-dynamics model, and in Chapter VII for the drift-flux model. The Lax-Wendroff two-step finite-difference scheme was used for numerical integration of the equations in the so-called conservation form, and smoothing was accomplished as described in Appendix C. The mesh length Δx selected for all the computations was 1.025 ft, corresponding to 60 divisions. In both of the numerical models the gas phase was assumed to behave in accordance with the isentropic adiabatic law. For the bubble-dynamics model, the bubble radii at each mesh point for the initial steady flow were evaluated from the average bubble radius d_{50} at the particular location in the upward-flow portion of the pipe. The available information on bubble sizes in the horizontal and downward-flow portions was not used in the bubble-dynamics model because of the requirement of prescribing a uniform distribution, and the constraint of no coalescence or breakup of the bubbles. The bubble sizes are not required in the applications of the drift-flux model, however.

Simulation of Transients with Bubble-Dynamics Model

The experimental and numerical transient pressure records are plotted in Figs. 19 to 23. These time histories show the transient pressures at different locations along the pipe for each of the five experimental runs listed in Table 1. A reasonably good agreement is realized in both amplitude and phase, especially for the last three runs, which correspond to relatively higher air concentrations. For the lower air concentrations depicted in Figs. 19 and 20, the experimental record shows a much higher damping. The increased dispersion and dissipation exhibited by runs with lower void fractions can be attributed to frequency-dependent friction, viscoelastic wall response, or effects of the long-radius elbows and pipe flanges. These factors apparently play a greater role for lower values of α, which correspond to higher pressure changes in the case of rapid valve closure.

The results of increased dispersion and dissipation is clearly shown on Fig. 24 for the case of pure waterhammer, or $\alpha = 0$. Although the other nonlinear factors mentioned above may also play a role, the use of steady-state friction in the Lax-Wendroff solution does not allow for any dispersion. Zielke [52] clearly demonstrates the difference between solutions that include frequency-dependent solution effects and those that employ steady-state friction. Although Zielke's technique is quite effective for transient laminar flow, there is no comparable method for turbulent flow. Regarding the theoretical results represented on Fig. 24, it should be noted that is has been proved in Appendix C that the Lax-Wendroff scheme yields exactly the same results as the fixed grid of characteristics for single-phase flow with a constant wave speed.

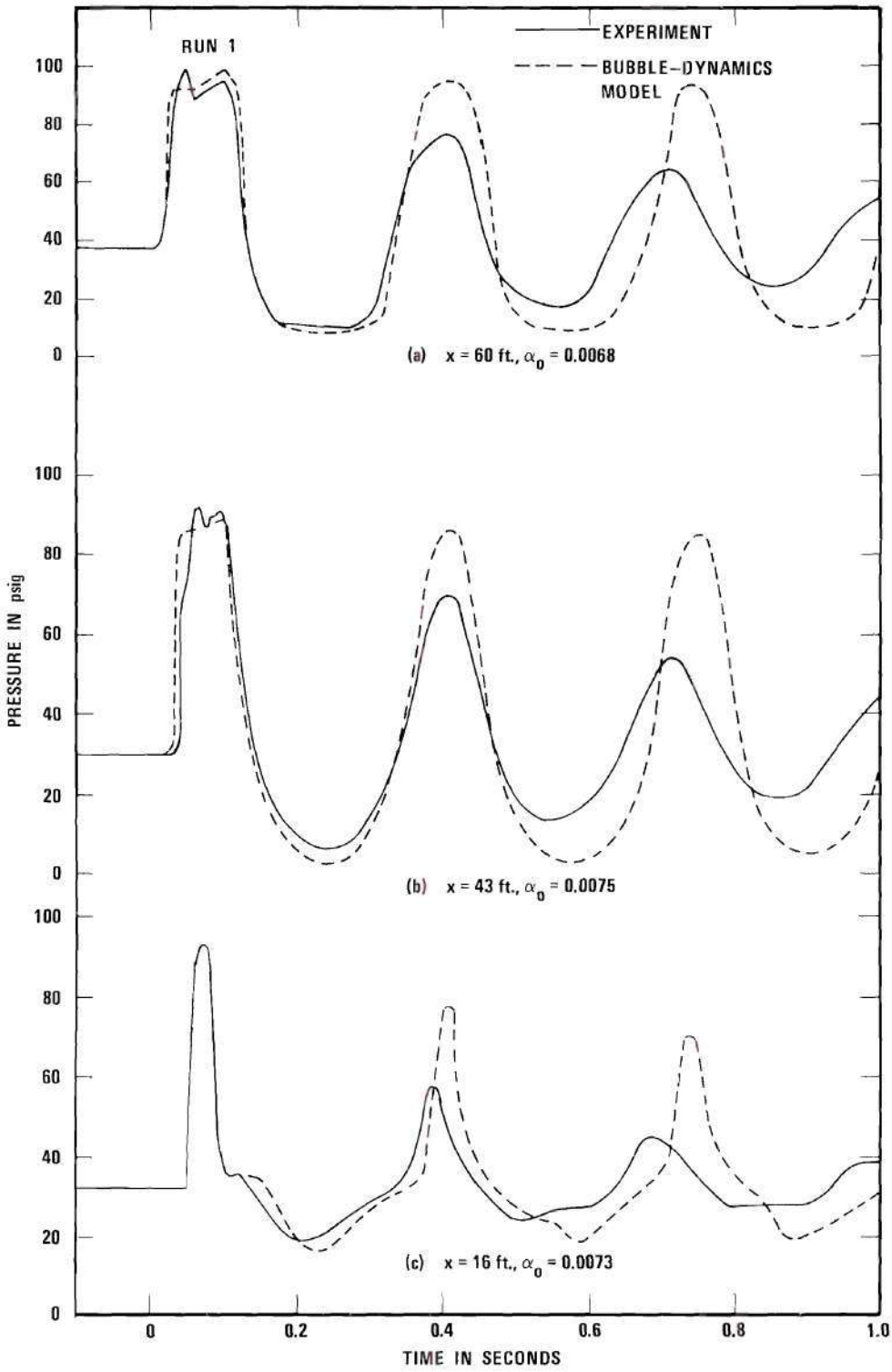

Figure 19. Comparison of Measured Transient Pressures in Bubbly Flow with Bubble-Dynamics Model. Rapid Valve Closure with u_o = 4.10 ft/sec in Plexiglass Pipe.

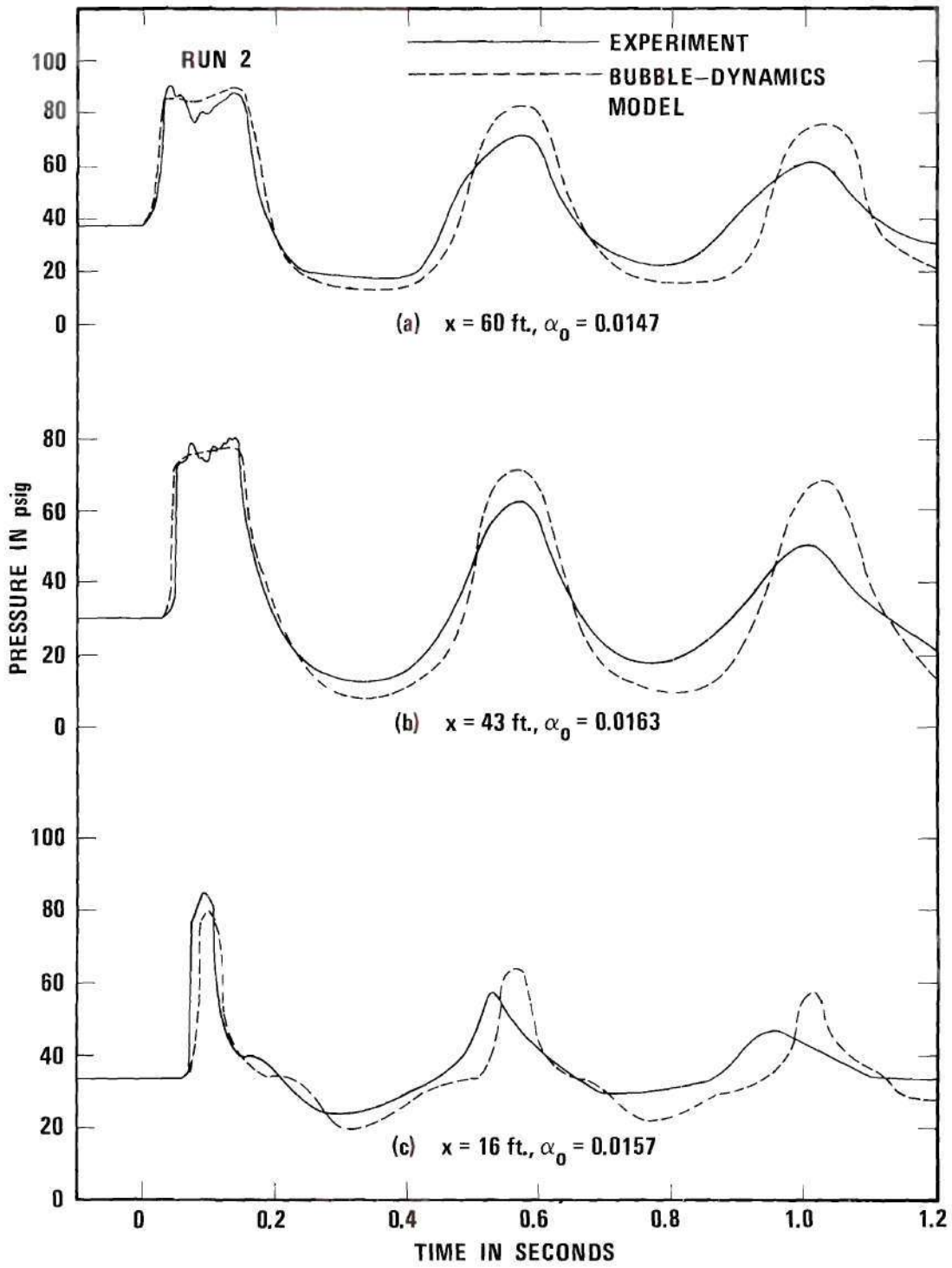

Figure 20. Comparison of Measured Transient Pressure in Bubbly Flow with Bubble-Dynamics Model. Rapid Valve Closure with u_o = 5.00 ft/sec in Plexiglass Pipe.

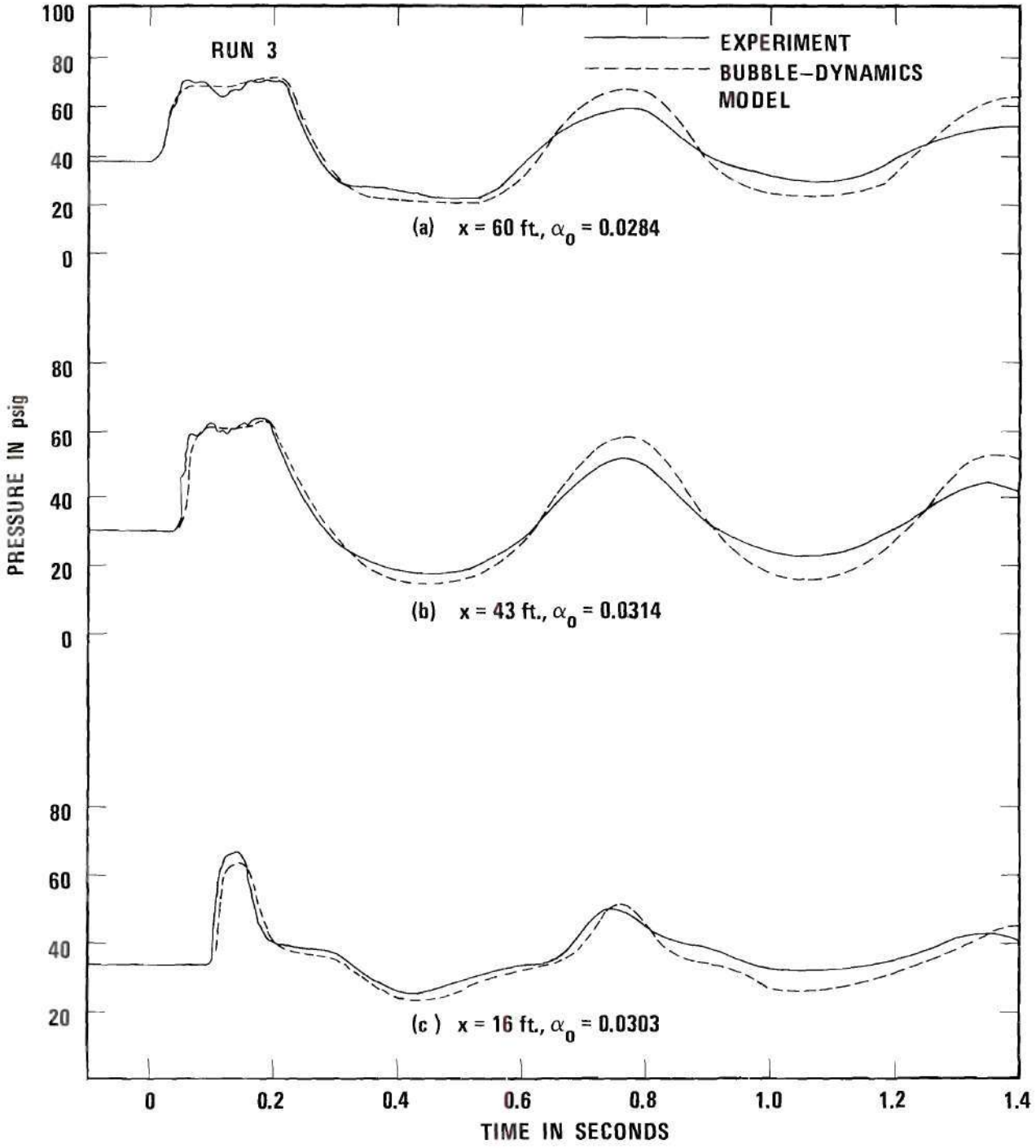

Figure 21. Comparison of Measured Transient Pressures in Bubbly Flow with Bubble-Dynamics Model. Rapid Valve Closure with u_o = 4.69 ft/sec in Plexiglass Pipe.

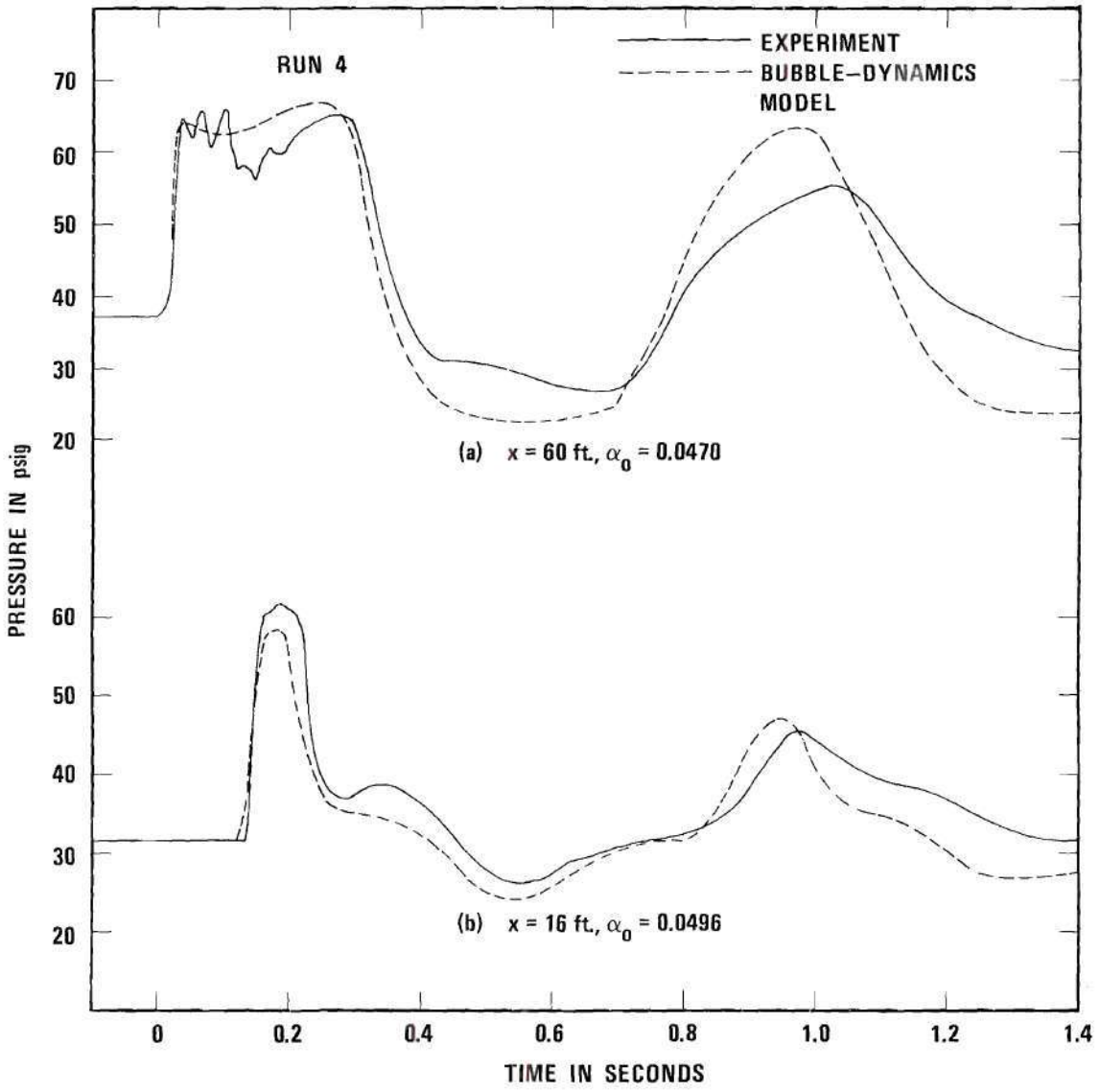

Figure 22. Comparison of Measured Transient Pressures in Bubbly Flow with Bubble-Dynamics Model. Rapid Valve Closure with u_o = 5.29 ft/sec in Plexiglass Pipe.

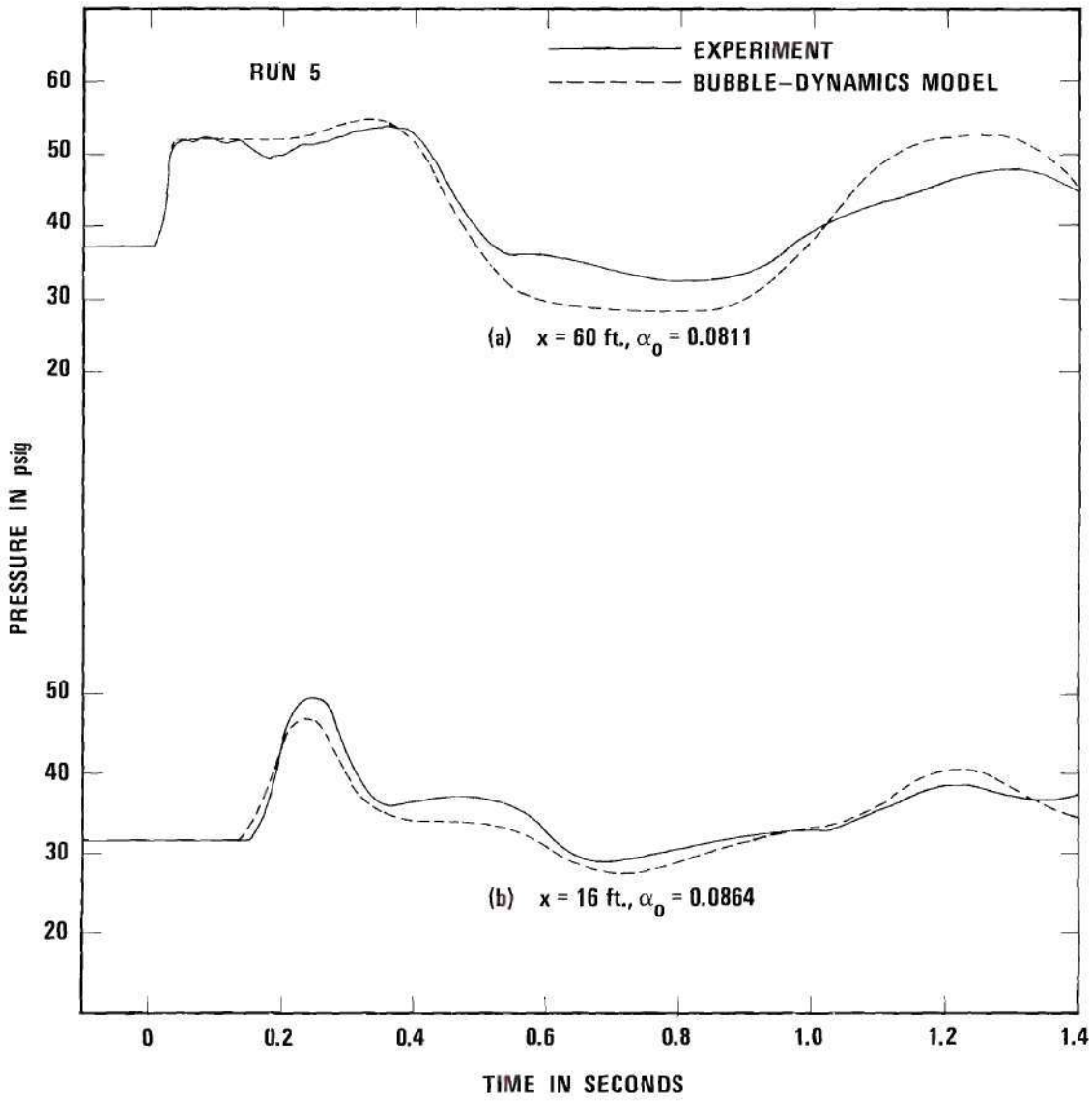

Figure 23. Comparison of Measured Transient Pressures in Bubbly Flow with Bubble-Dynamics Model. Rapid Valve Closure with u_o = 4.05 ft/sec in Plexiglass Pipe.

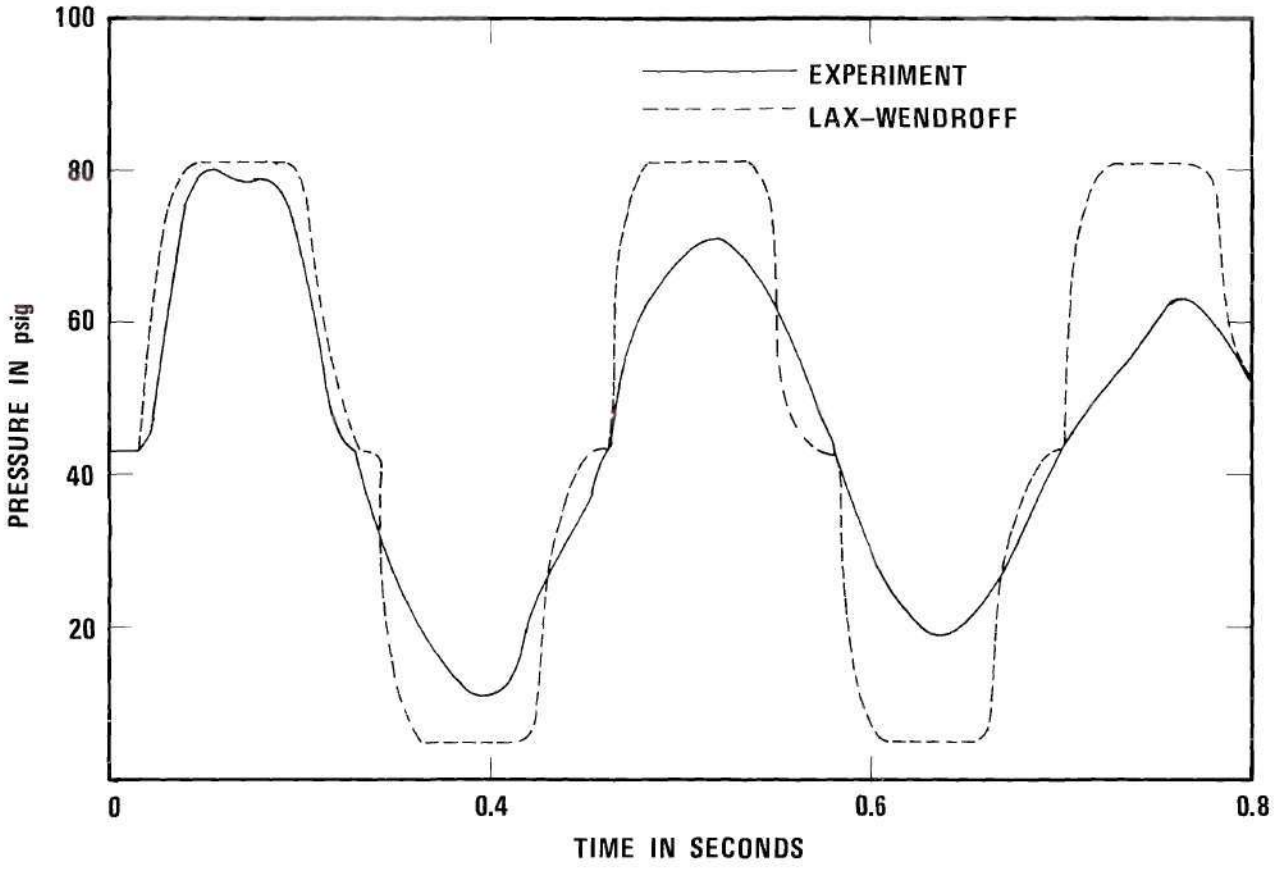

Figure 24. Comparison of Measured Transient Pressures at x = 43 ft with Lax-Wendroff Solution for Pure Waterhammer (α = 0). Rapid Valve Closure with u_o = 1.4 ft/sec in Plexiglass Pipe.

The bubble-dynamics model may be considered superior to the homogeneous model on the one hand, in that the relative bubble motion with respect to the liquid is accounted for. On the other hand, however, the assumption of uniform-sized bubbles is not satisfied, as witnessed by the irregularly-shaped bubbles shown on Fig. 7. In fact, in most practical cases it is seldom possible to have bubbles of uniform size at every cross section. However, this does not necessarily preclude the use of the bubble-dynamics model as far as the prediction of transient pressures is concerned. For air-water mixtures the effect of relative motion itself is indeed very small. This point is made clear upon inspection of Figs. 25 and 26, where comparisons between the homogeneous and bubble-dynamics models are made at two locations along the pipe. In the bubble-dynamics model an average bubble size has been used to correspond to the d_{50} size obtained from photographs. Practically very little difference in the predicted transients are seen. Considering the very small effect of relative velocity itself, the error involved in assuming an average bubble size in the bubble-dynamics model may be expected to be negligible.

Inasmuch as the gas bubbles possess much less mass than the liquid, it is obvious that the transient velocity of the bubbles must differ in both amplitude and phase from the corresponding velocity of the liquid. Figs. 27 to 29 show the velocity transients for Run 3 at three different locations, one at each leg of the test pipe. From these figures it is clear that the acceleration or deceleration caused by the transients occur at a much faster rate for the air bubbles than that for the liquid. In fact, the shock wave decelerates the liquid at a very fast rate to zero velocity, imparting a higher deceleration to the bubbles. The de-

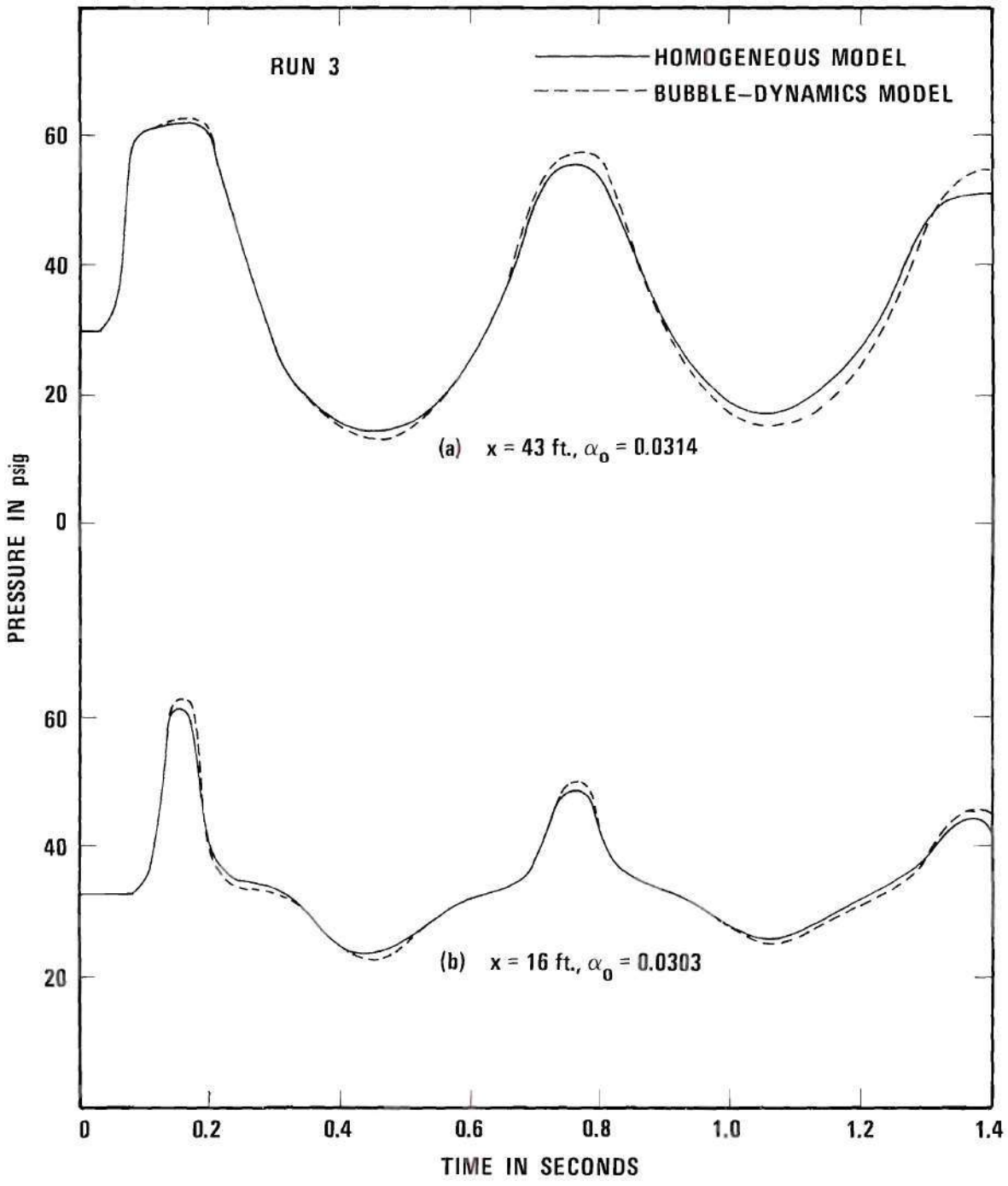

Figure 25. Effect of Relative Bubble Motion on Transient Pressures. u_o = 4.69 ft/sec.

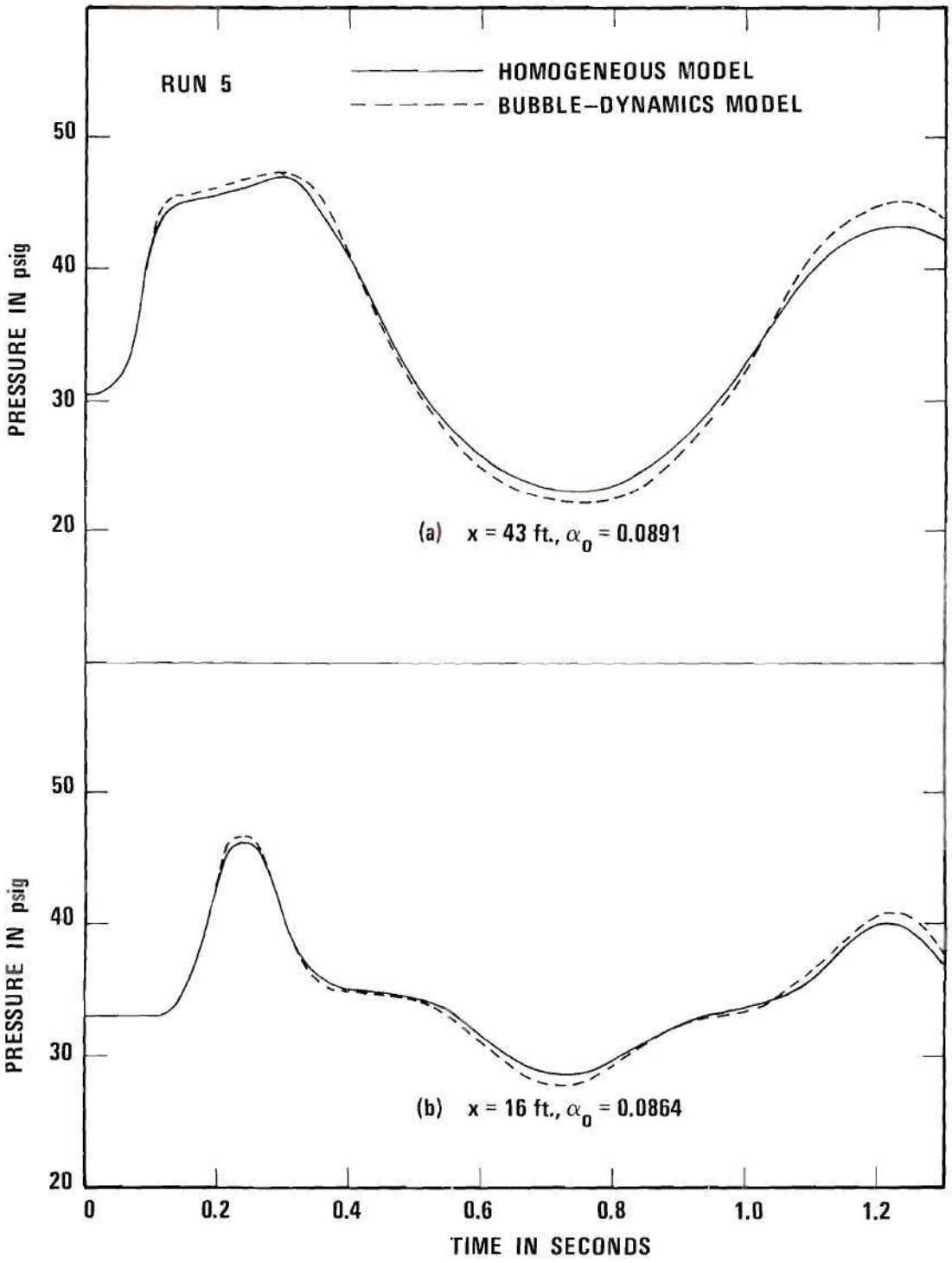

Figure 26. Effect of Relative Bubble Motion on Transient Pressures. u_o = 4.05 ft/sec.

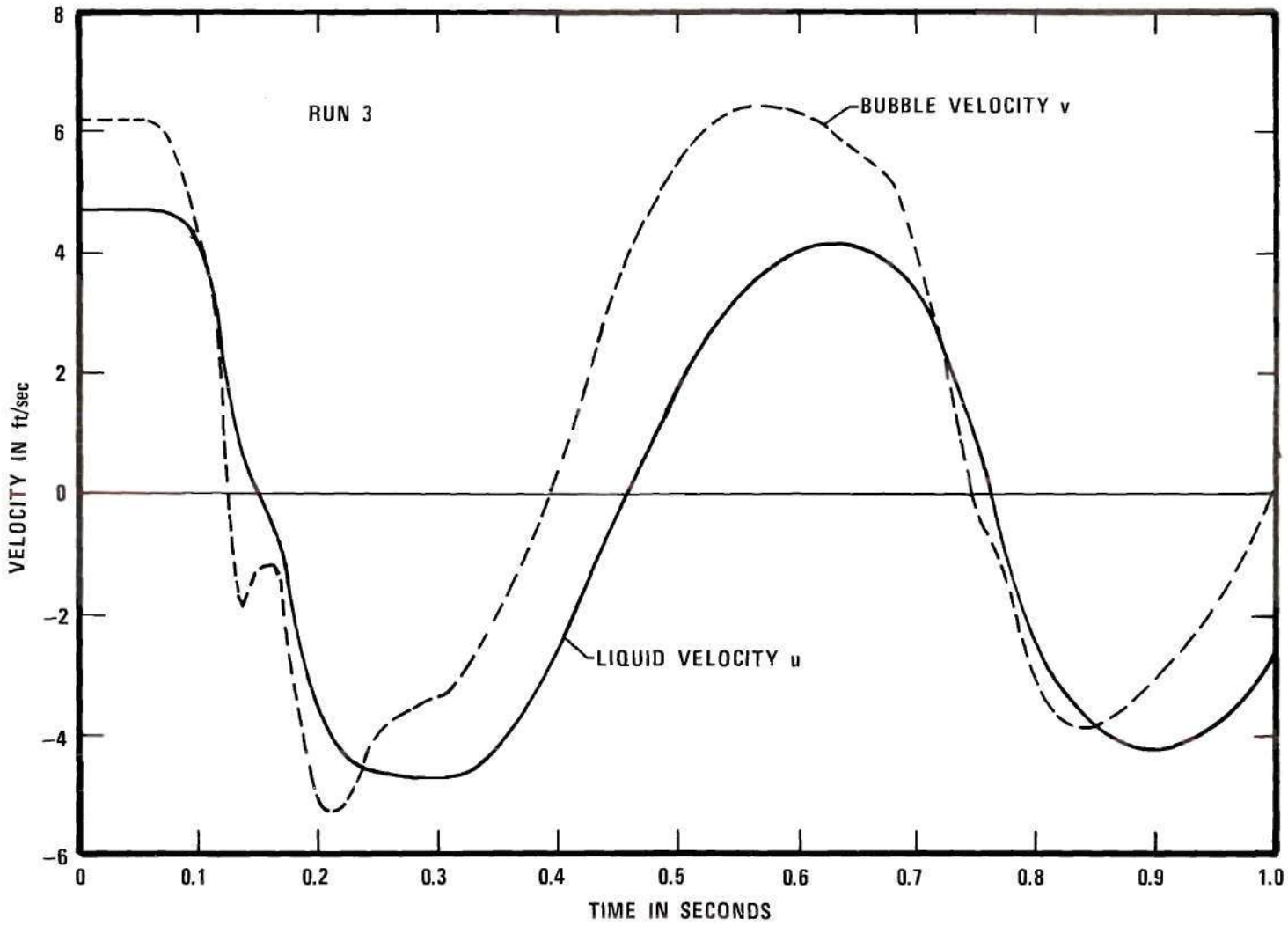

Figure 27. Prediction of Transient Liquid and Bubble Velocities in Riser (x = 15.4 ft) with Bubble-Dynamics Model. u_o = 4.69 ft/sec.

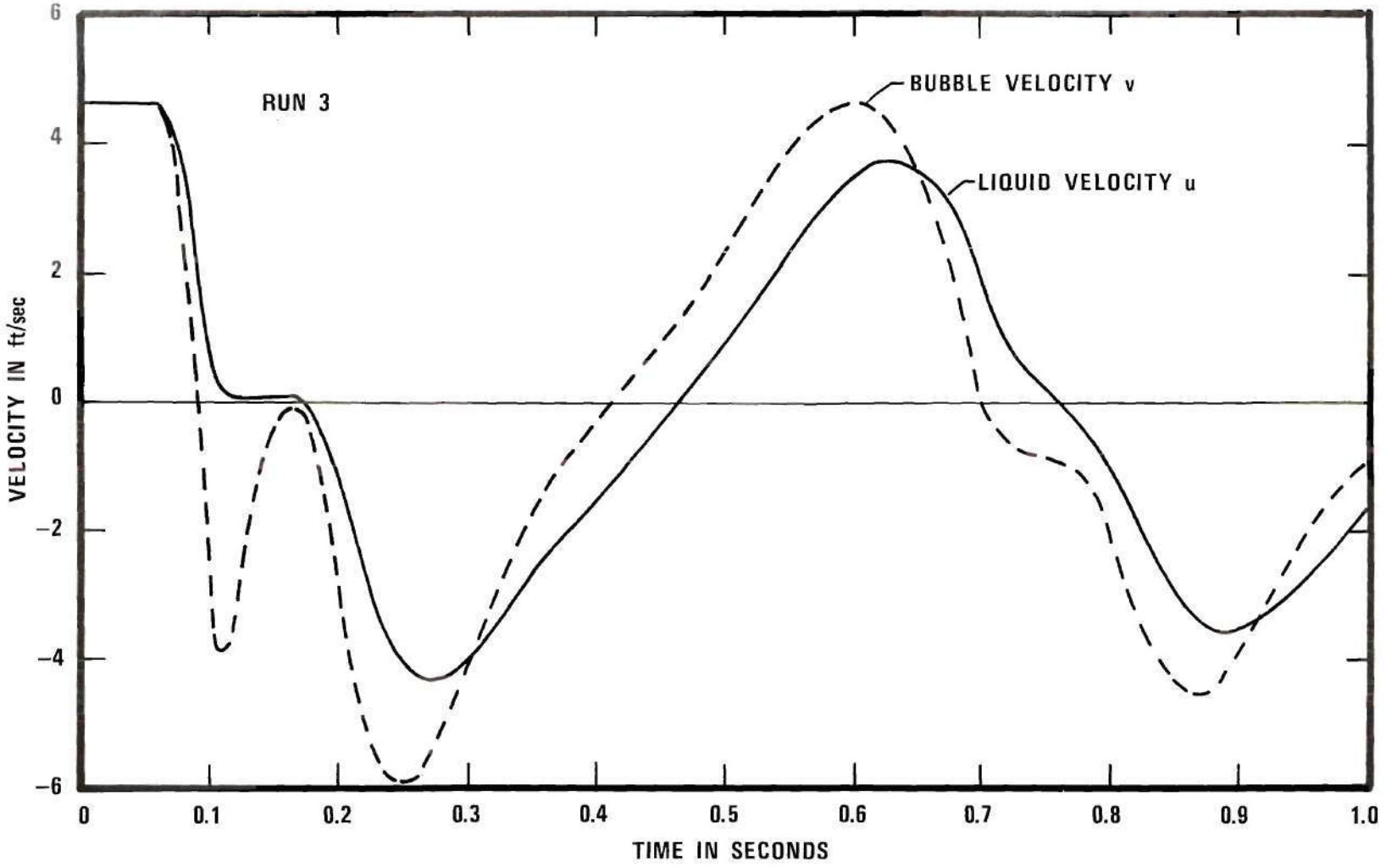

Figure 28. Prediction of Transient Liquid and Bubble Velocities in Horizontal Leg (x = 30 ft) with Bubble-Dynamics Model. u_o = 4.69 ft/sec.

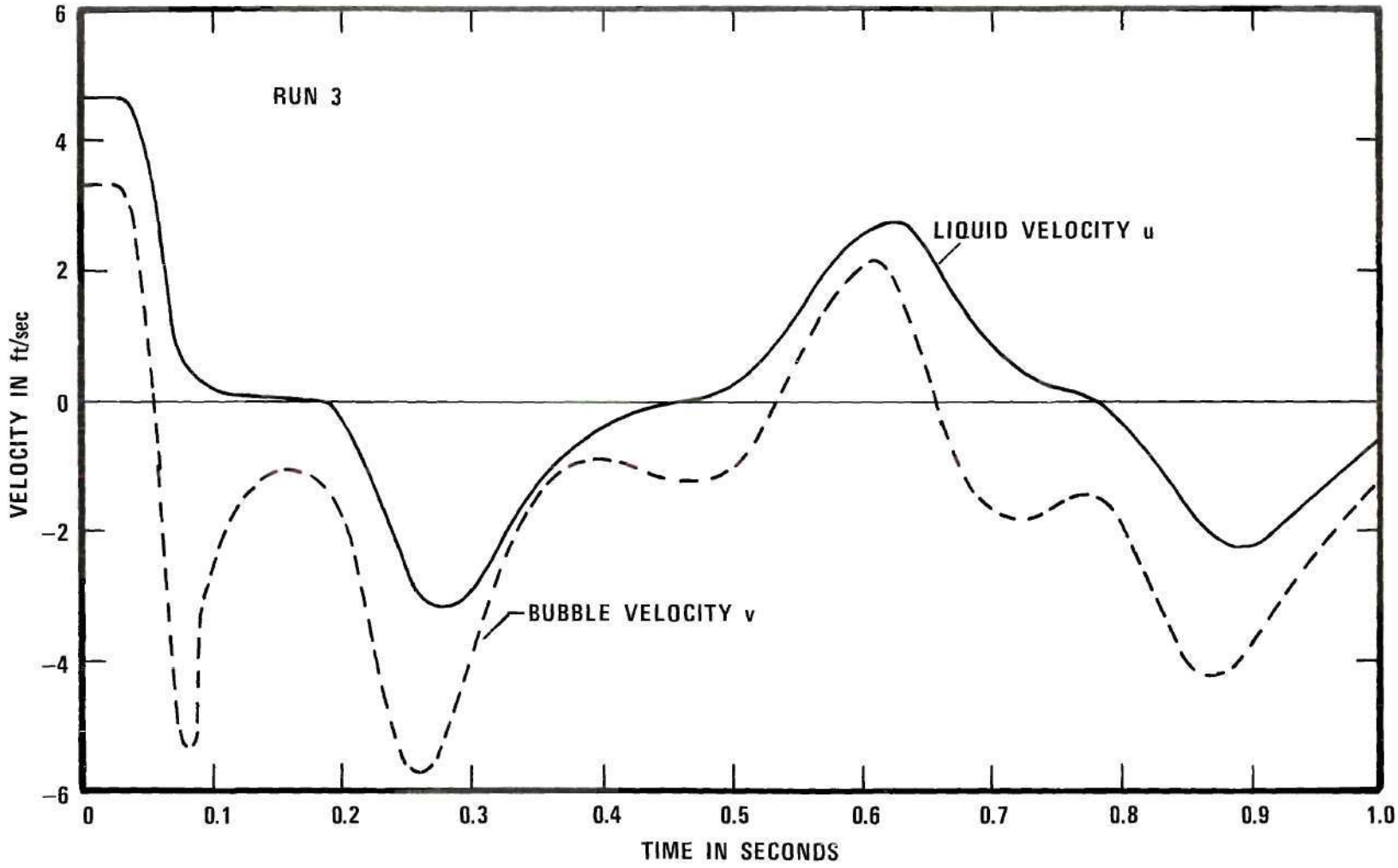

Figure 29. Prediction of Transient Liquid and Bubble Velocities in Downcomer (x = 43 ft) with Bubble-Dynamics Model. u_o = 4.69 ft/sec.

celeration results in a negative velocity peak before the bubbles start adjusting to the motion of the liquid. This shock-induced relative velocity is apparent in Fig. 28, which shows the transients in the horizontal leg, in which buoyancy effects should not exist. In this case, the positive and negative regions of the transient velocity records exhibit more or less the same amplitude and phase difference between the velocities of the two phases. Fig. 27 shows the velocity transient records in the riser. Here the initial relative velocity v-u is positive and is entirely due to buoyancy. During the transients the amplitude difference is higher in the positive-velocity region than in the negative-velocity region. The opposite situation exists in the downcomer, as shown in Fig. 29. It may also be noted that, in the riser, the phase shift between the velocities of the two phases is greater during acceleration than during deceleration, and vice versa in the downcomer. Thus, Figs. 27 and 29 establish the effect of buoyancy on the relative bubble motion. It may also be observed from Fig. 29 that the shock wave induces a very high negative bubble-velocity peak in the downcomer, wherein the buoyancy favors the deceleration of the air bubbles; whereas, as seen in Fig. 27, this negative bubble-velocity peak is not so pronounced in the riser, wherein buoyancy resists the deceleration.

Simulation of Transients with Drift-Flux Model

Figures 30 to 34 show the transient pressure records computed with the drift-flux model for each of the five experimental runs listed in Table 1. As shown by Figs. 30 and 31 the measured damping exceeds that predicted by theory. For higher air concentrations reasonable agreement between the experimental and computed pressures is obtained, as

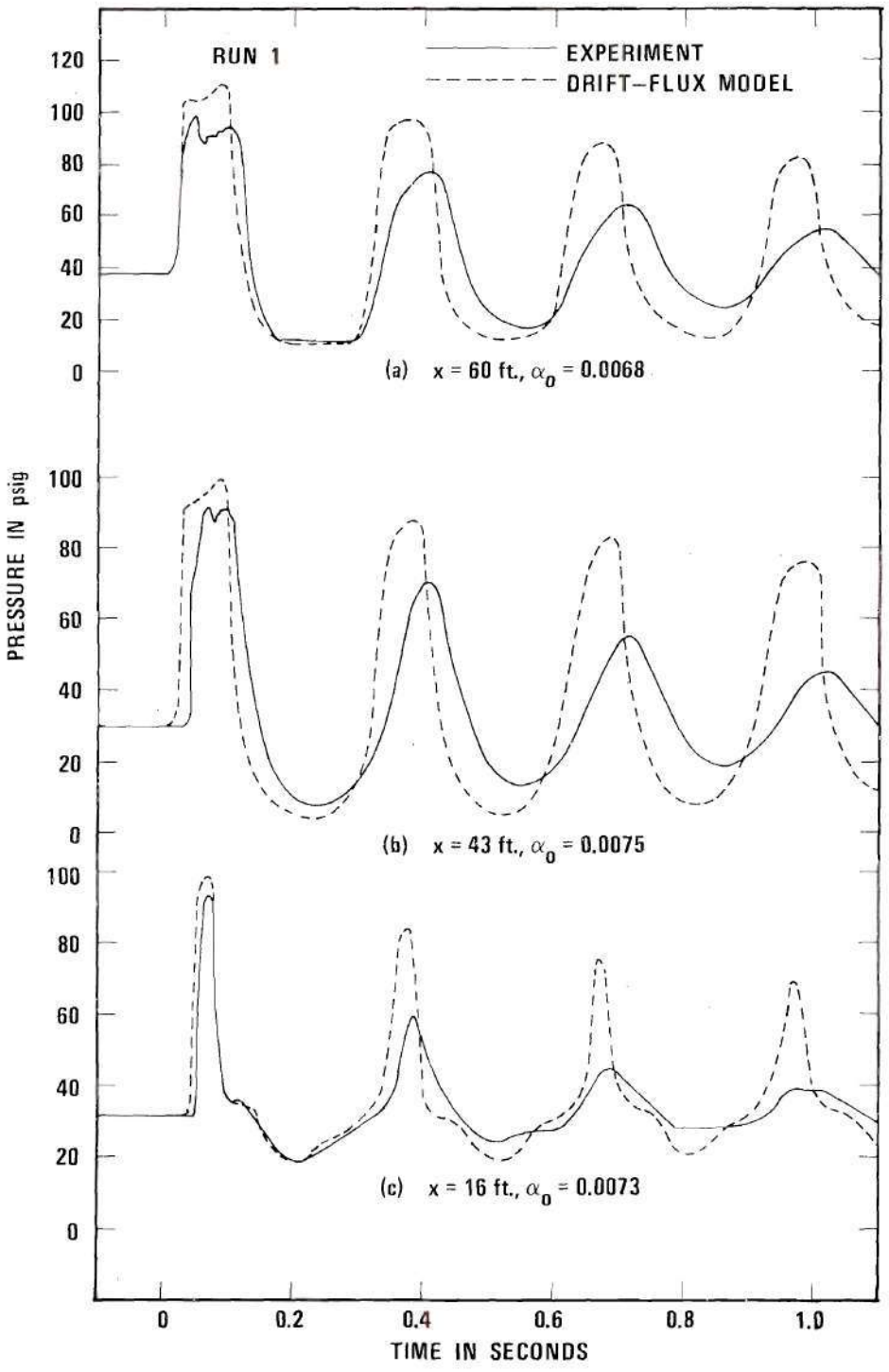

Figure 30. Comparison of Measured Transient Pressures in Bubbly Flow with Drift-Flux Model. Rapid Valve Closure with u_o = 4.10 ft/sec in Plexiglass Pipe.

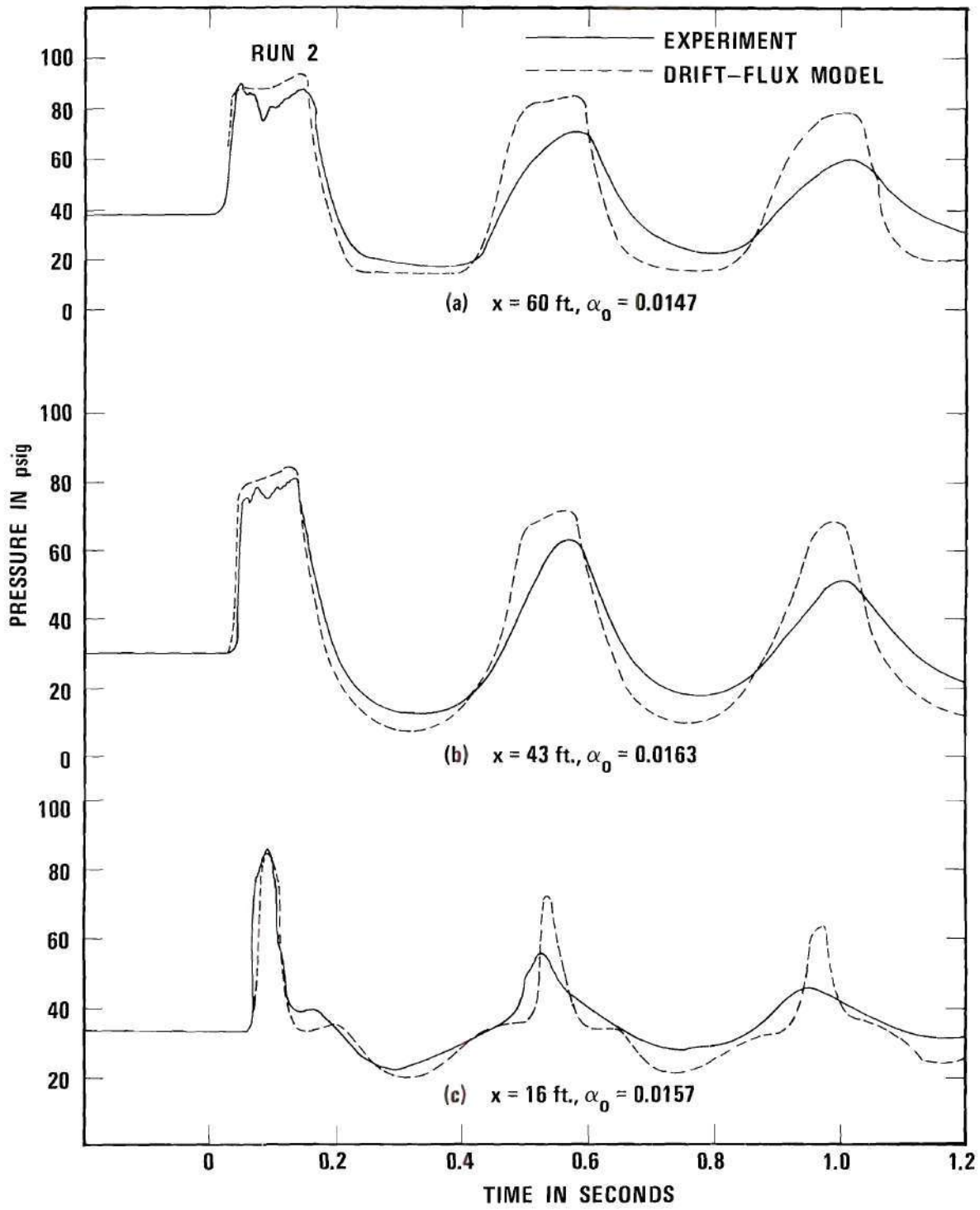

Figure 31. Comparison of Measured Transient Pressures in Bubbly Flow with Drift-Flux Model. Rapid Valve Closure with u_o = 5.00 ft/sec in Plexiglass Pipe.

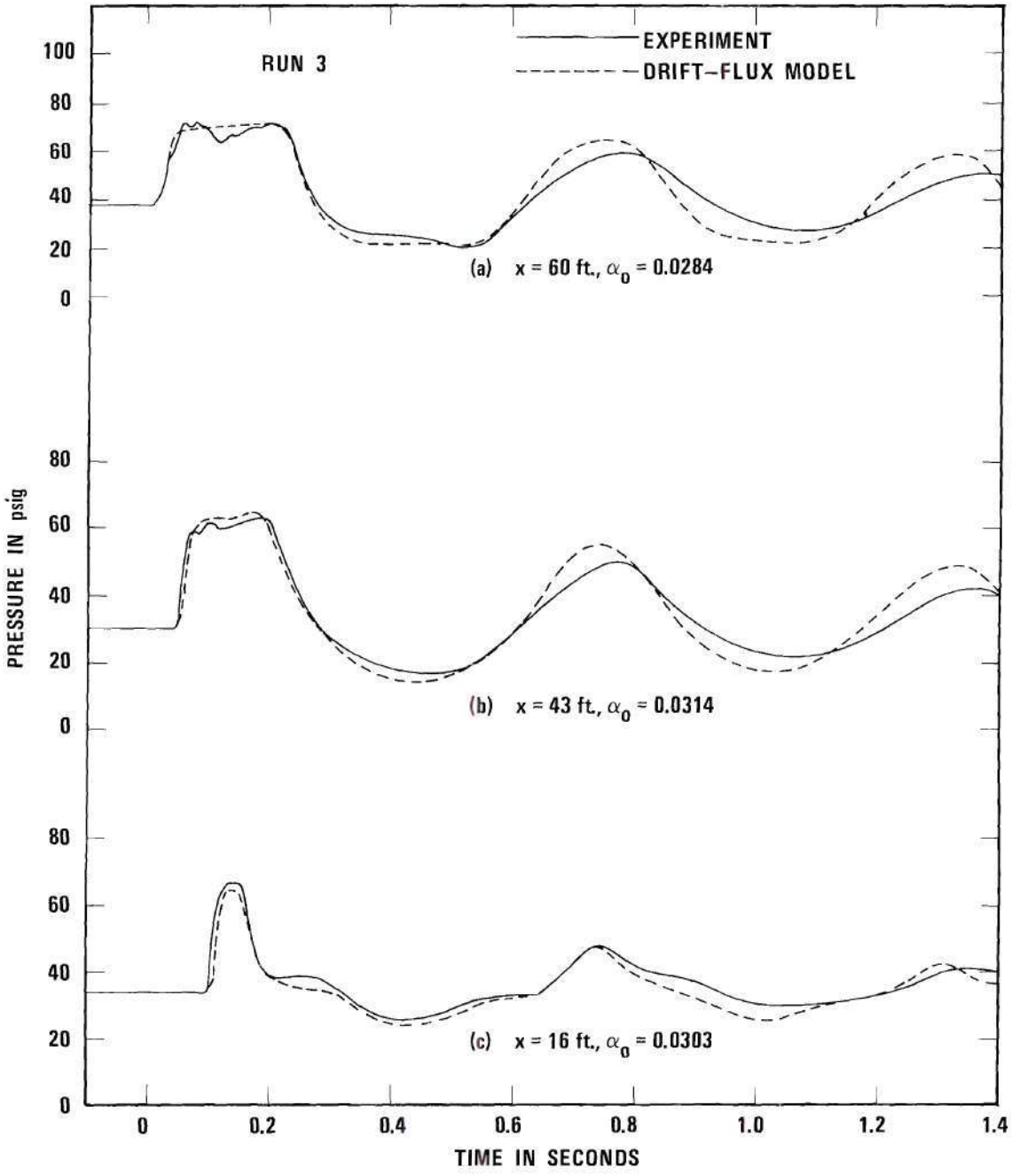

Figure 32. Comparison of Measured Transient Pressures in Bubbly Flow with Drift-Flux Model. Rapid Valve Closure with u_o = 4.69 ft/sec in Plexiglass Pipe.

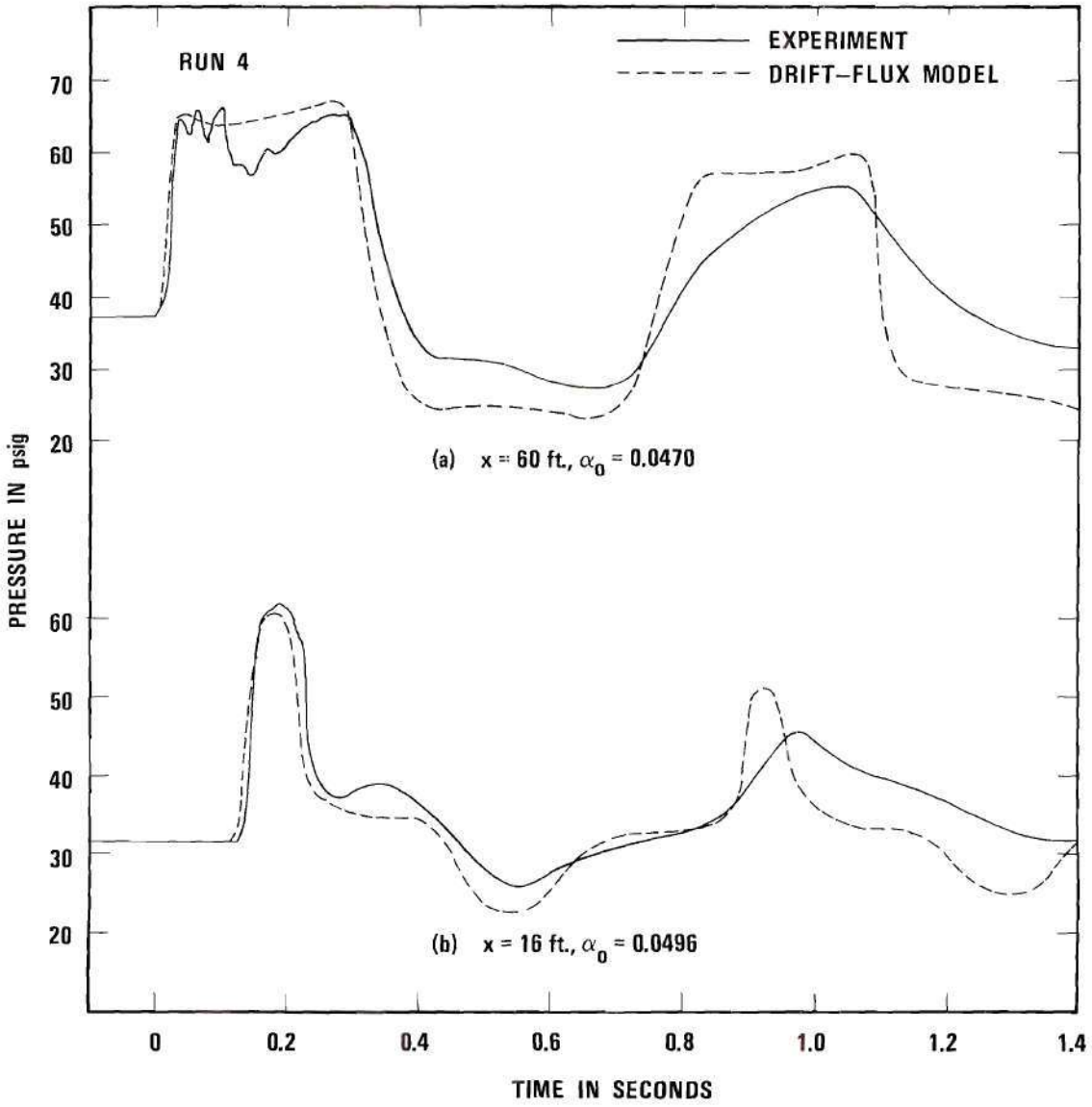

Figure 33. Comparison of Measured Transient Pressures in Bubbly Flow with Drift-Flux Model. Rapid Valve Closure with u_o = 5.29 ft/sec in Plexiglass Pipe.

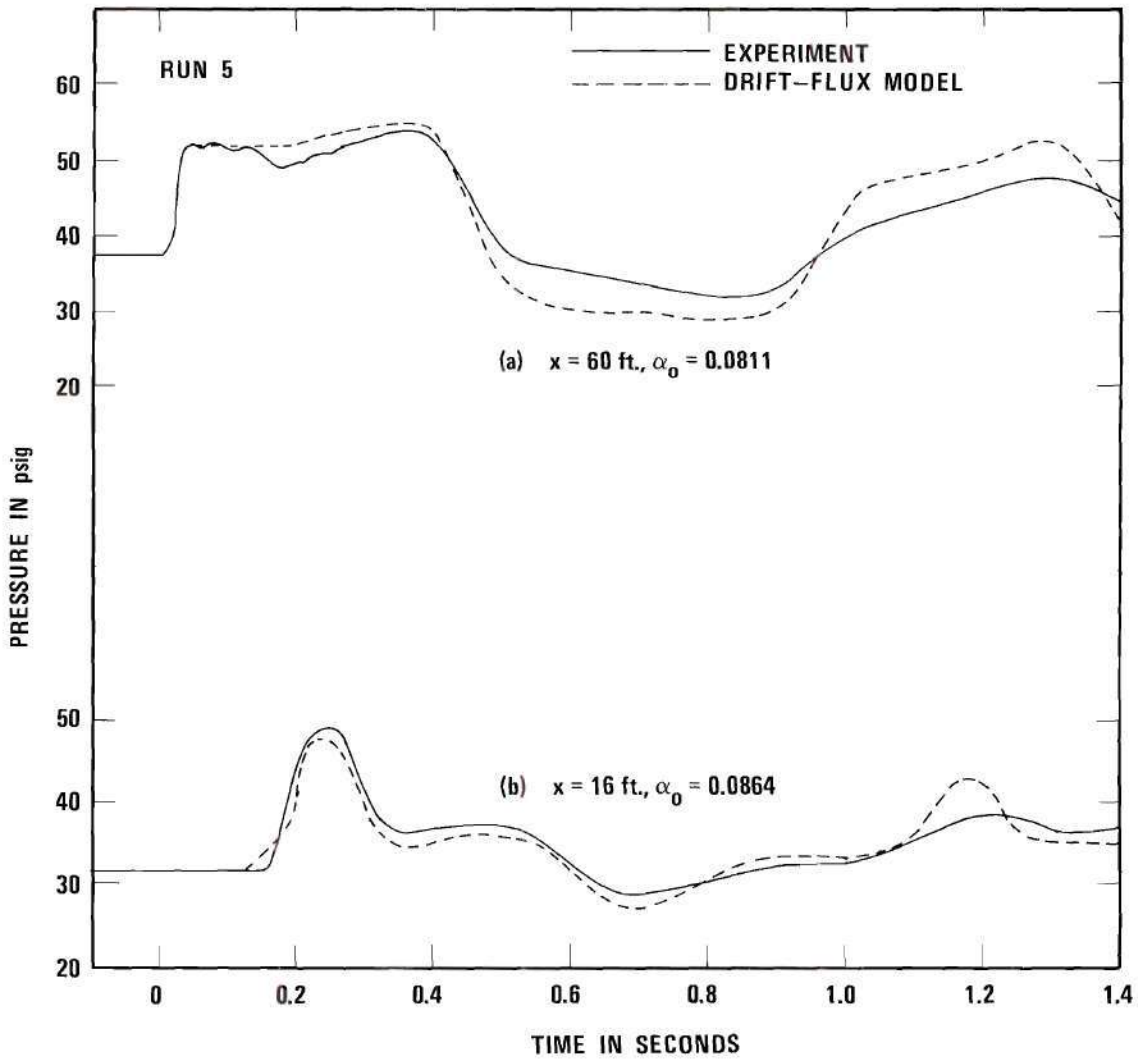

Figure 34. Comparison of Measured Transient Pressures in Bubbly Flow with Drift-Flux Model. Rapid Valve Closure with u_o = 4.05 ft/sec in Plexiglass Pipe.

evident from Figs. 32 to 34. The computed transients exhibit a wave form which resembles a rectangular one, whereas the experimental records show smoother fronts and backs of the waves. Upon comparing with Figs. 21 to 33, it may be noted that the bubble-dynamics model yields results that appear closer to reality. The bubble-dynamics model is also seen to induce slightly higher damping than that predicted by the drift-flux model.

As explained in detail in Chapter VII, the drift-flux model does not consider the motion of the individual phases themselves, but instead accounts for the relative motion indirectly by the drift-flux theory. The velocities of the two phases are time and space-averaged weighted quantities. The velocity of the gas phase v_g does not represent that of the bubbles. This point may be established by comparing the velocity transients shown in Figs. 35 to 37, which were based upon the drift-flux model, with the corresponding records shown in Figs. 27 to 29, which were obtained using the bubble-dynamics model. The drift-flux model predicts practically no phase shift between the time of occurrence of the maximum velocities of the phases. As evident from Fig. 36, which shows the velocity transients in the horizontal leg, where the drift velocity is zero, the drift-flux model does not predict the relative velocity induced by the shock wave. In fact, both phases are seen to attain zero velocities at the same instant.

Critical Evaluation of the Two Proposed Models

The advantages and disadvantages of the two proposed models may be outlined as follows.

(a) The transient pressures are predicted by both models reasonably well in amplitude and phase. The bubble-dynamics model is seen to

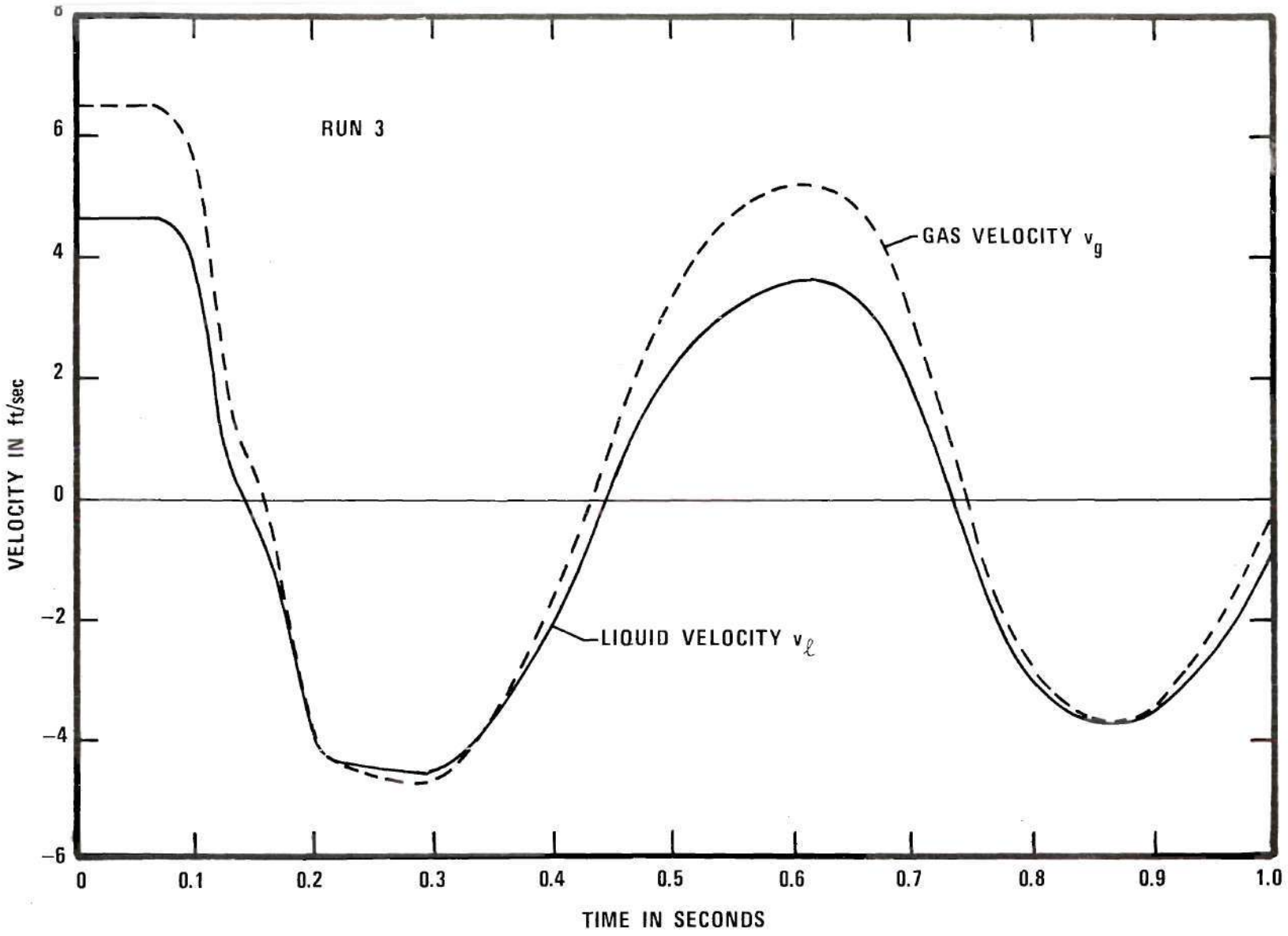

Figure 35. Prediction of Transient Liquid- and Gas-Phase Velocities in Riser (x = 15.4 ft)with Drift-Flux Model. u_o = 4.69 ft/sec.

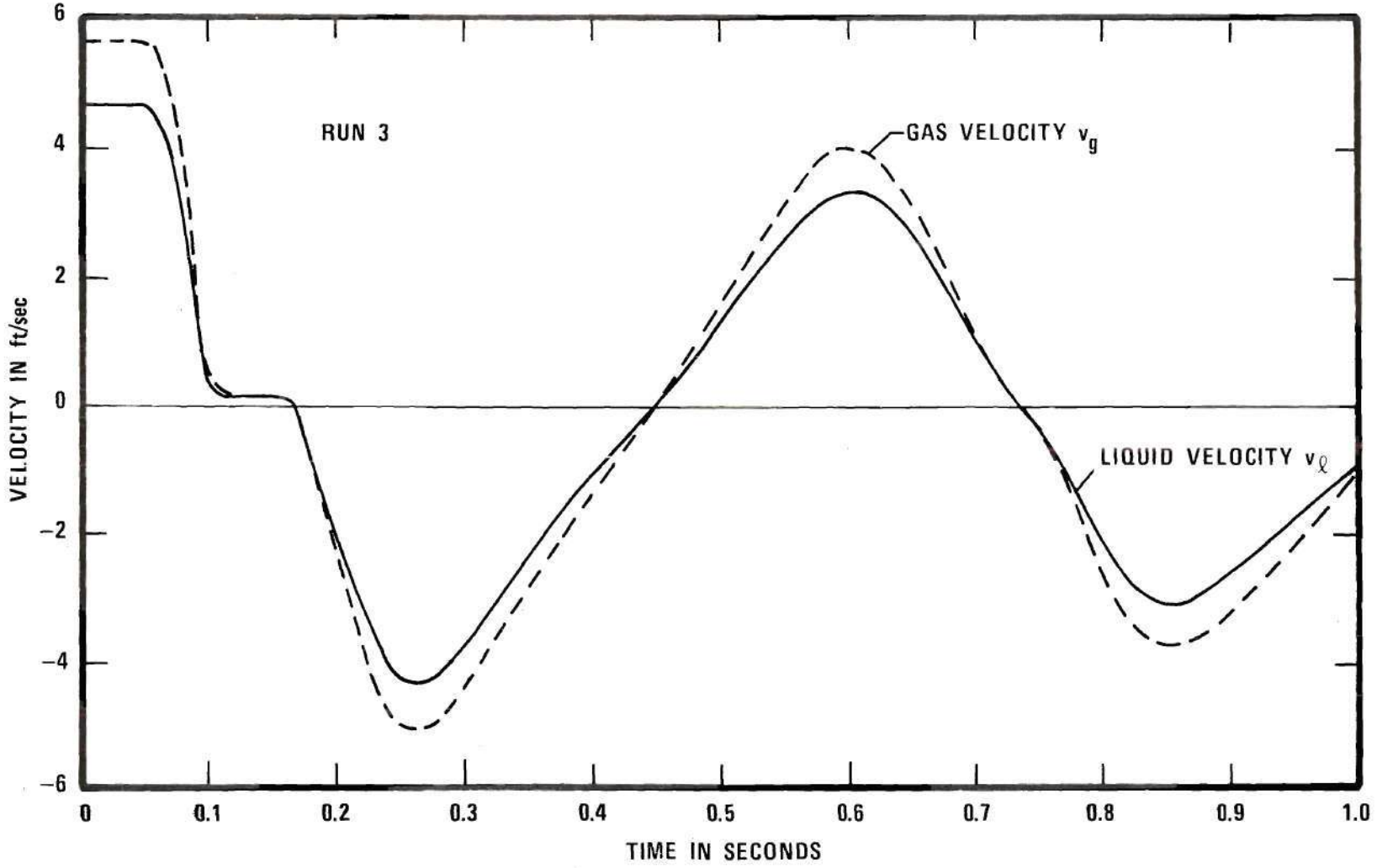

Figure 36. Prediction of Transient Liquid- and Gas-Phase Velocities in Horizontal Leg (x = 30 ft) with Drift-Flux Model. u_o = 4.69 ft/sec.

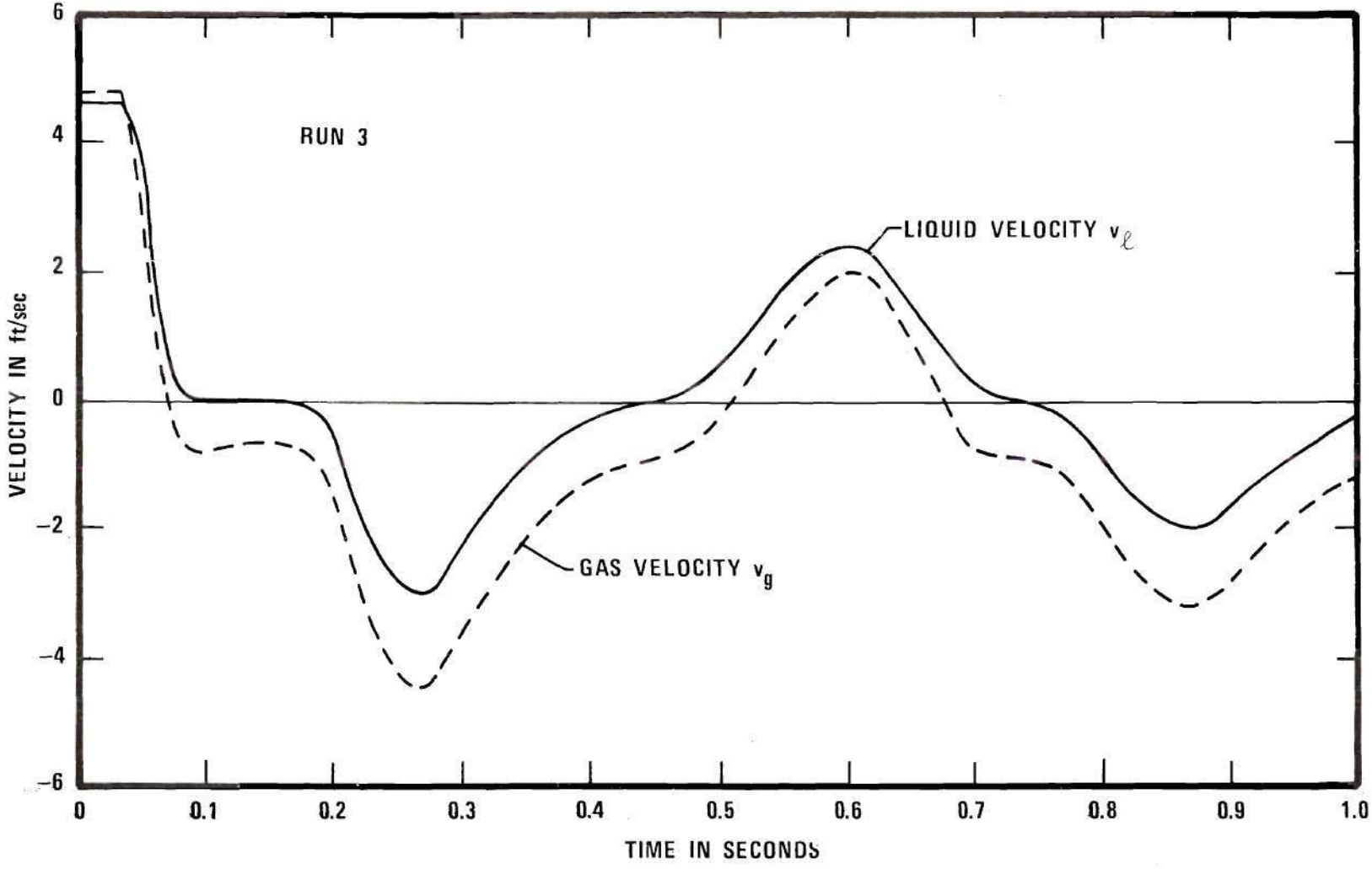

Figure 37. Prediction of Transient Liquid- and Gas-Phase Velocities in Downcomer (x = 43 ft) with Drift-Flux Model. u_o = 4.69 ft/sec.

produce smooth wave forms, resembling the actual experimental records of the pressure traces. Furthermore, the bubble-dynamics model produces greater damping than the drift-flux model.

(b) The motion of the individual phases is well predicted by the bubble-dynamics model. The velocity of the gas phase used in the drift-flux model does not represent the velocity of the bubbles, and consequently the model does not provide any information on the motion of the individual phases.

(c) The effects of concentration and velocity profiles on the transients can be incorporated into the drift-flux model, a very definite advantage.

(d) The bubble-dynamics model, strictly speaking, is valid only when the bubbles are of the same size and shape, and are well distributed across a cross-section. However, for the prediction of pressure transients, the use of an average bubble size and a spherical shape appears to produce reasonable results, at least for the range of bubble sizes and concentrations investigated in this study.

(e) The bubble-dynamics model is valid only for bubbly flows, whereas the drift-flux model may also be applied to slug flows with very little modifications.

(f) The use of Levich's model restricts the bubble-dynamics model to bubble Reynolds numbers less than about 800.

(g) The drift-flux model is simpler as only the field equations, all in the conservation form, are used. The bubble-dynamics model requires an additional equation based upon the relative bubble motion. This equation can not be put in conservation form, and consequently only a

first-order accuracy is achieved with respect to time derivatives in the numerical integration.

(h) The coalescence and breaking up of bubbles are not allowed in the bubble-dynamics model. The drift-flux model is not affected by these factors.

(j) The bubble-dynamics model includes the pipe-wall expansion and liquid compressibility. In the drift-flux model these effects have not been included due to the area-averaging techniques and weighting procedures involved.

(k) The bubble-dynamics model requires the knowledge of bubble sizes, which in a practical case may not be readily available.

(l) The drift-flux model also involves a distribution parameter, C_o, the exact determination of which requires the knowledge of the velocity and concentration profiles at a cross section. Furthermore, the weighted-average drift velocities are evaluated using empirical equations, the validity of which may likewise have to be checked for individual cases.

CHAPTER X

SLUG-FLOW TRANSIENT RESULTS

The slug-flow regime is characterized by a series of individual large bubbles which fill nearly the entire pipe cross-section. The obvious difference between observed bubbly flow and slug flow suggests that a homogeneous model would probably be more applicable to the former regime. For the latter, however, a separated-flow model would appear to be more representative. In both instances the bubble velocity is a function of the average volumetric flux of the mixture j_m, the pipe geometry, the fluid properties, and the body force field. The drift velocity V_{gj} of the gas is the bubble velocity minus the overall volumetric flux j_m, and hence is independent of the void fraction. Actually, the drift velocity is independent of j_ℓ and j_g individually, depending only upon their sum, j_m. The distribution parameter C_o used in the drift-flux model in constitutive equation (7.12), and in the relationship between α and β given by Eq. (7.24), will have different values for vertically upward and downward slug flow. Wallis [20], and Zuber and Findlay [50] have provided detailed discussions on the distribution parameter C_o for slug flows. A study was conducted by Martin [53] on steady vertically downward slug flow in the downcomer of the same plexiglass-piping apparatus used in the present investigation. Of especial concern was the determination of experimental data for the evaluation of the distribution parameter C_o for downward slug flow. Details on this particular investigation are given in Martin [53] in which the value of C_o for downward slug flow is

reported to be 0.93.

Preliminary studies were conducted with the copper-tubing apparatus to ascertain the possible formation of shock waves in slug-flow mixtures. Later, transient pressure tests were performed using both the plexiglass-piping and the copper-tubing apparatuses. In both setups the transients were created by the rapid closure of a valve at the downstream end of the respective pipe. Using the drift-flux model, transient pressures were predicted for a few experimental runs for comparison with the experimental results.

Shock-Wave Formation

The preliminary pressure-transient tests performed with the copper-tubing apparatus revealed the possible formation of shock waves. These tests were conducted by first establishing an equilibrium steady flow of water and air in the copper tubing, and then rapidly slamming the quick-acting gate valve at the discharge end of the pipe. Depending upon the fraction of air to water present, a shock wave may or may not form at some distance upstream from the valve. If the void fraction is great enough no shock forms because of the large elasticity of the mixture. Figure 38 is a composite of the results of the pressure traces at nine pressure taps for one set of conditions; namely, an initial reservoir pressure, p_o = 30 psig, and an initial volume concentration, or quality, β_o = 0.005.

The steepening of the compression wave as it propagates up the pipe suggests the formation of a shock wave. The increase in the wave-propagation speed as the pulse moves in the negative x-direction is also apparent when the loci of the initial rise of the pressure traces are plotted

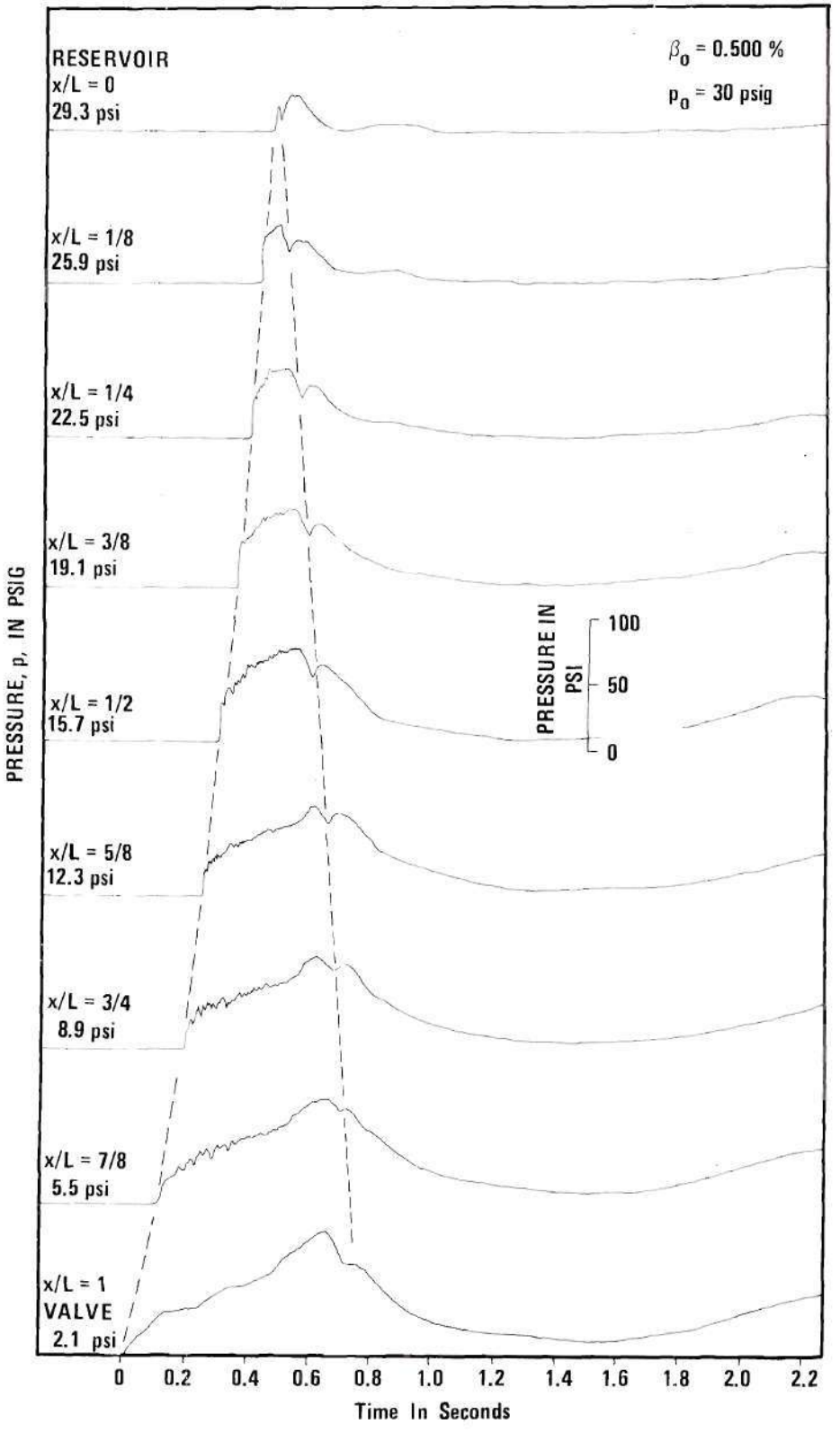

Figure 38. Pressure Traces in Copper Tubing for Very Rapid Valve Closure. u_o = 4.00 ft/sec.

on a space-time plane (x-t plane), shown in Fig. 39 for seven different sets of initial conditions. Especially for those data on Fig. 39, for which β is relatively small, it appears that the shock apparently reaches equilibrium conditions corresponding to a constant shock speed. The data for the run shown on Fig. 38 suggests that, even though a shock probably formed in the vicinity of $x/L = 7/8$, its corresponding speed and thickness varied continuously to a location beyond $x/L = 1/2$. A further evidence of shock formation before $x/L = 7/8$ is the appearance of higher frequency pressure fluctuations behind the compression wave on all the traces except $x/L = 1$. As indicated by the pressure traces on Fig. 38 the steep shock wave that reaches the pressure tank reflects back as an initially sharp rarefaction wave, which gradually flattens out as it propagates toward the valve. Upon studying the results of various runs it became apparent that this rarefaction wave propagated at nearly a constant speed until it reached the valve. The space-time plane data shown on Fig. 40 are extensions of the shock propagation data for the same runs on Fig. 39. Apparent missing data points on Fig. 40 correspond to tests for which the usually sharp dip in the pressure trace associated with the rarefaction wave did not occur. All of the data for Figs. 38, 39, and 40 correspond to test conditions for which the pressure at the reservoir end was 30 psig.

Slug-Flow Transients

Plexiglass-Piping Apparatus

Transition from bubbly flow to slug flow was noticed in the downcomer and the horizontal leg of the plexiglass piping for air concentrations $\beta > 0.09$. For qualtities greater than $\beta = 0.16$ annular flow was observed

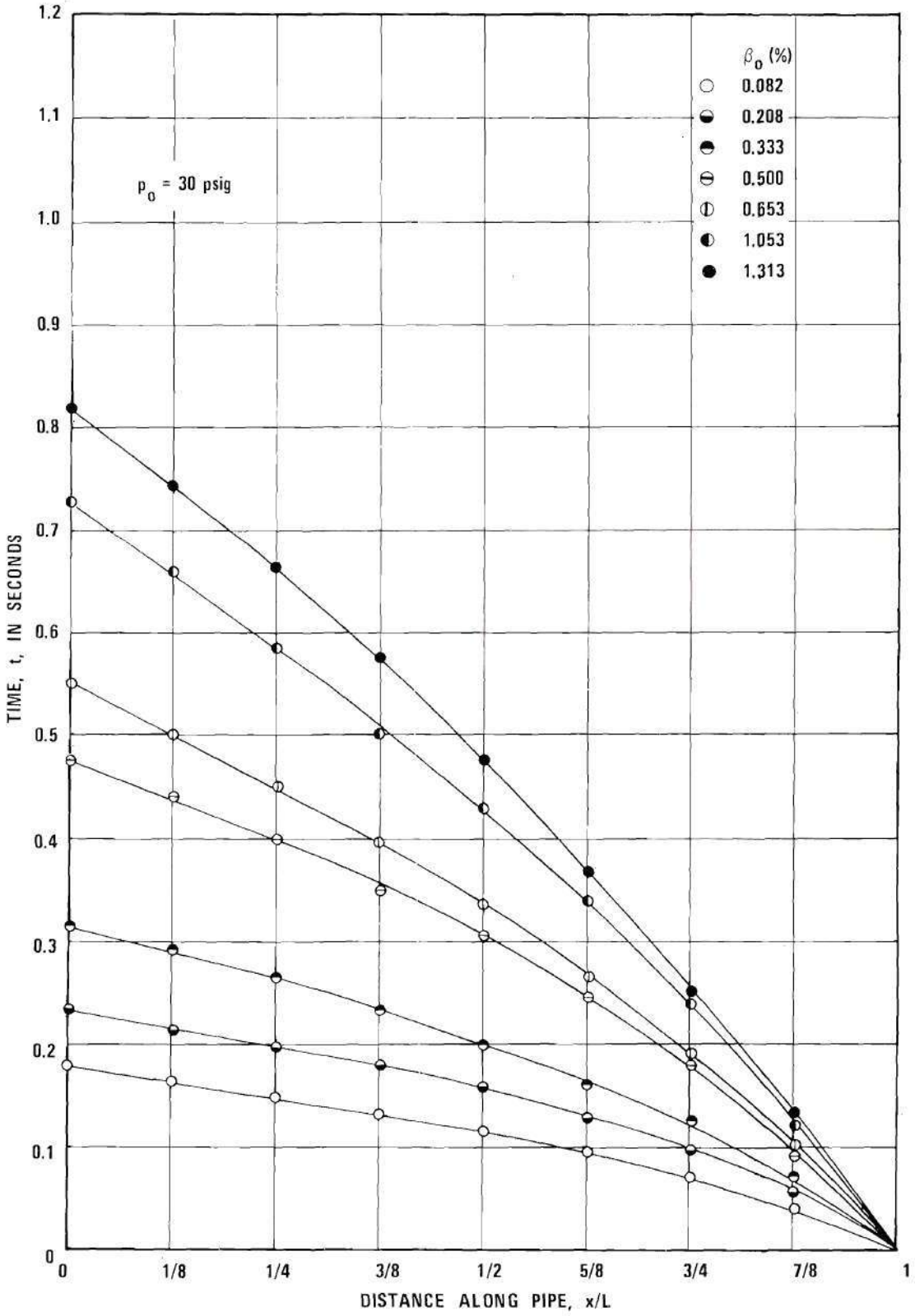

Figure 39. Space-Time Representation of Shock Wave Propagation in Copper Tubing. u_o = 4.00 ft/sec.

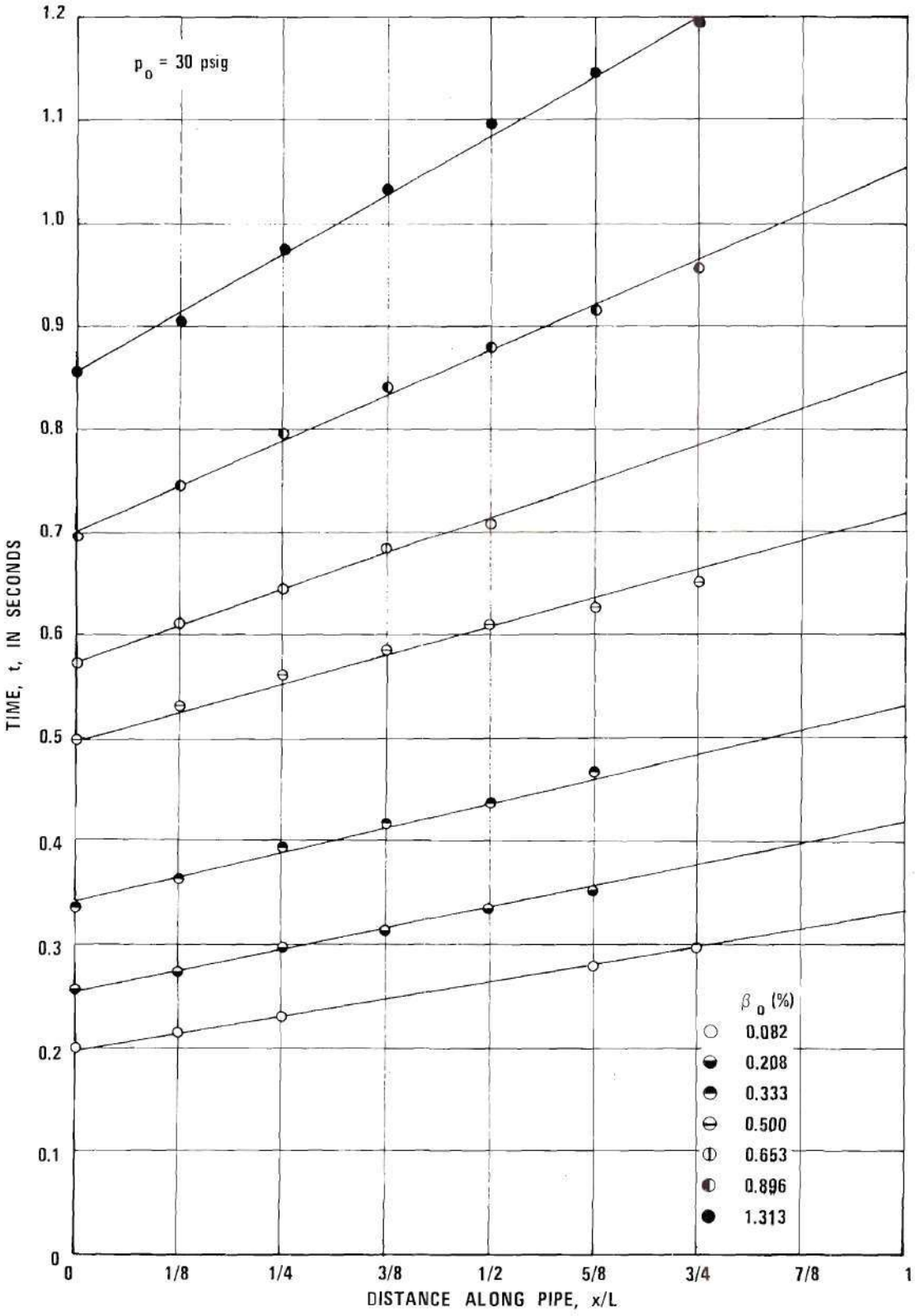

Figure 40. Space-Time Representation of Reflected Shock Wave of Fig. 39.

near the bend in the upper portion of the downcomer. Hence, all the experiments on transients in slug flow have been conducted for a range of $0.10 < \beta < 0.16$, even though the flow in the riser was in a transition state from bubbly to slug. The flow was always in the turbulent regime as the initial water velocity was maintained between 2 and 3 ft/sec. Data for two typical experimental runs considered for discussion are listed in Table 3. Figures 41 and 42 show the experimental records for these runs.

For the numerical analysis, the set of field equations employed are the same as those for transient computations in bubbly flow, except that Eq. (7.14) has been used rather than Eq. (7.13) for calculation of the drift flux. Knowing the initial distribution of β, the initial distribution of α for the steady flow has been obtained from Eq. (7.24). The value of the distribution parameter C_o for the downward slug flow has been chosen as 0.93, as explained in Appendix E. Following the same procedure adopted in the case of computations of transients in bubbly flow, an average value of β/α has been chosen for the entire pipe in order to avoid discontinuities in α at the junctions between the respective legs of the pipe. Sixty Δx divisions were used for the computations. The Lax-Wendroff two-step scheme was used for numerical integration; smoothing of overshooting of the shock fronts was accomplished as described in Appendix C. The numerical results are shown in Figs. 41 and 42 for comparison. Obviously, the agreement between the experimental and computed pressure transients is not as good as that obtained for bubbly flow. One possible reason is the fact that the vertically downward slug flow possessed irregularities in bubble length and spacing, which varied from

Table 3. Experimental Data for Slug Flow

Run Number	Apparatus Used	Water Discharge in cfs	Mass Rate of Air-Flow in Slugs/sec $x10^5$	Reservoir Pressure in psig	Time of Closure in sec
1	Plexiglass	0.0111	1.0530	40	0.02
2	Plexiglass	0.0113	1.2513	40	0.02
3	Copper tubing	0.0075	0.0587	50	0.05
4	Copper tubing	0.0074	0.1313	50	0.05

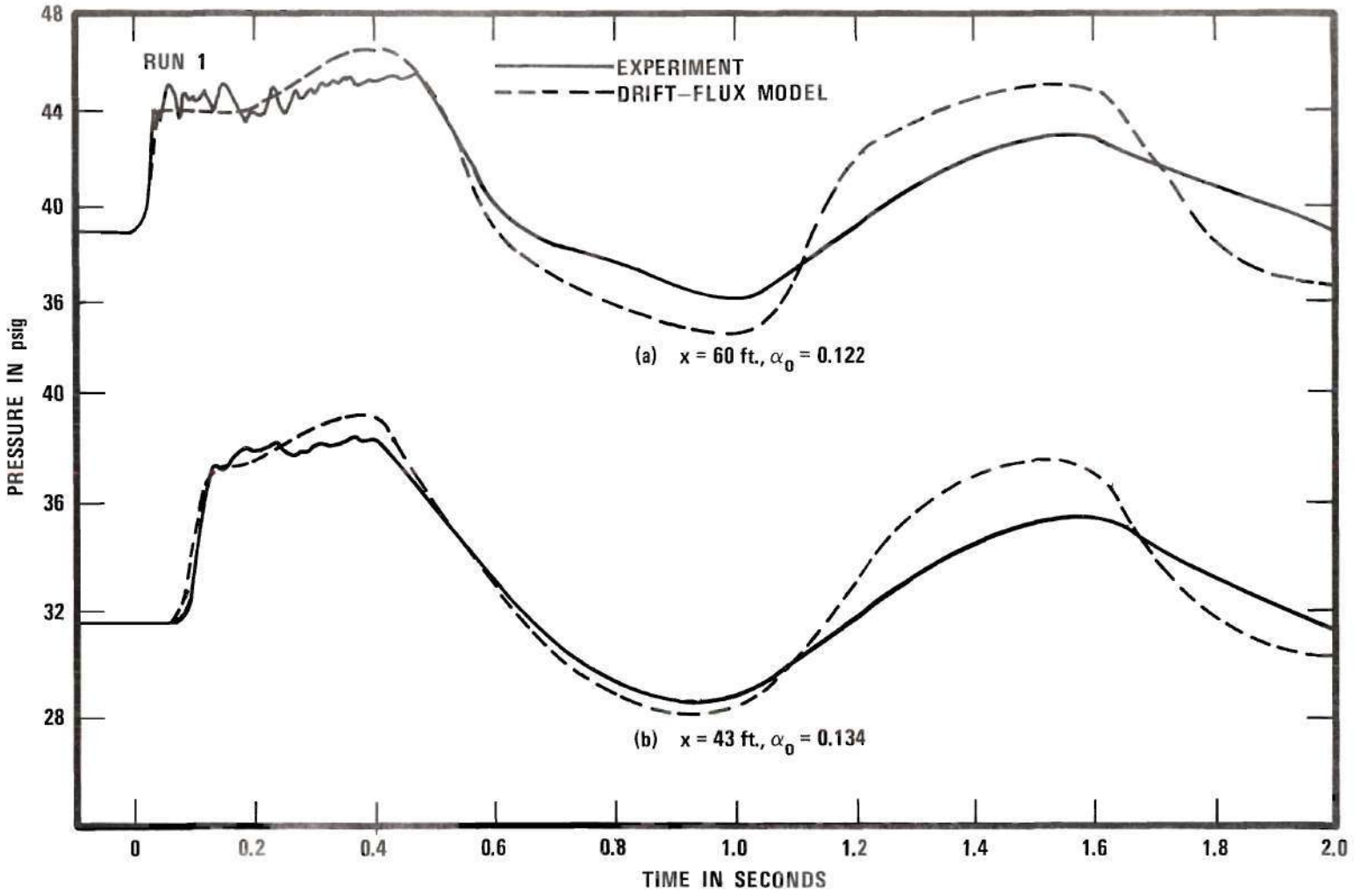

Figure 41. Comparison of Measured Transient Pressures in Slug Flow with Drift-Flux Model. Rapid Valve Closure with u_o = 1.94 ft/sec in Plexiglass Pipe.

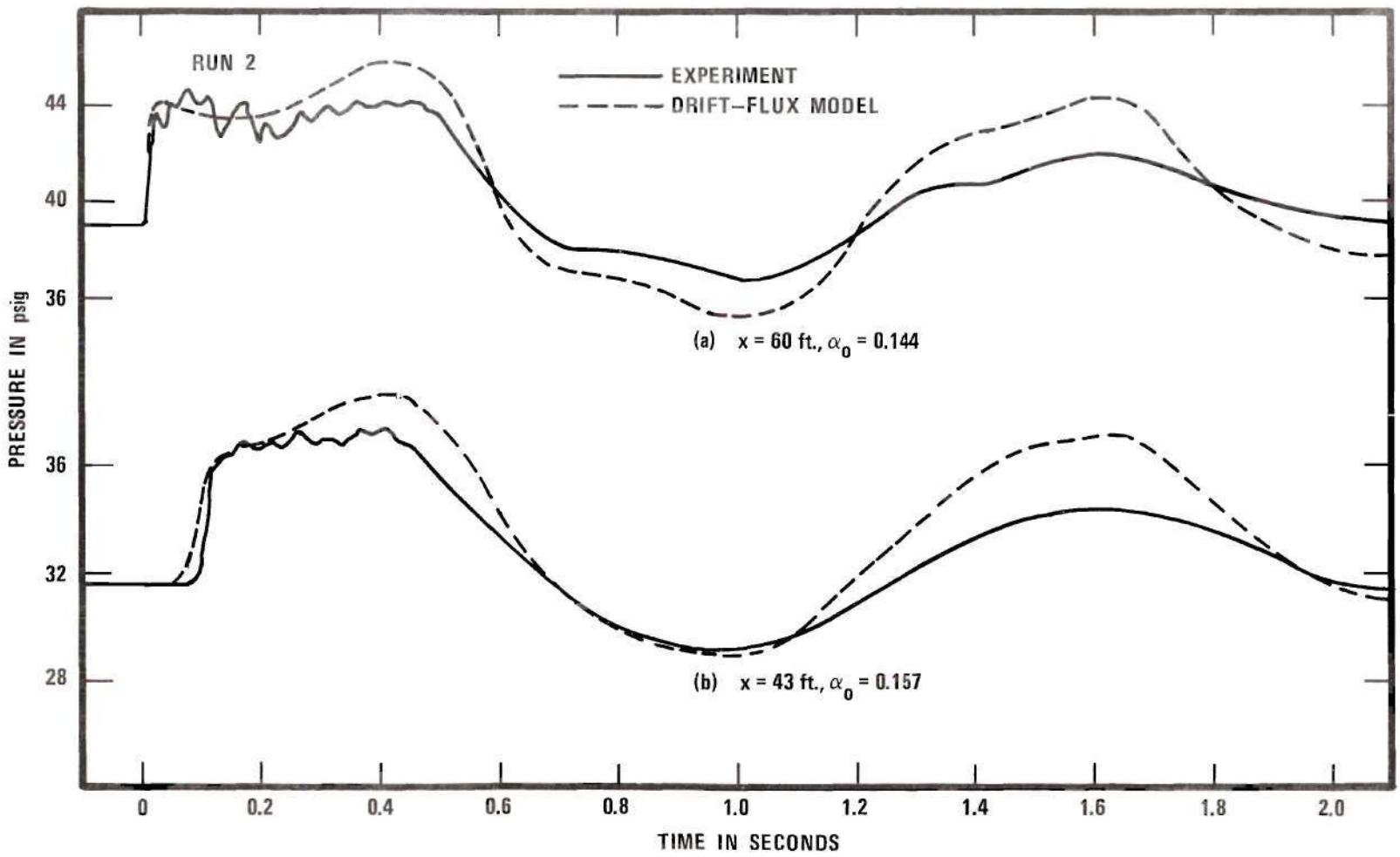

Figure 42. Comparison of Measured Transient Pressures in Slug Flow with Drift-Flux Model. Rapid Valve Closure with u_o = 1.98 ft/sec in Plexiglass Pipe.

2 to 4 inches and 12 to 20 inches, respectively. These irregularities are not accounted for in the simulation with the drift-flux model, as it does not consider the shape and spacing of slugs. The experimental record shows a higher damping than that predicted by the drift-flux model. The predicted system period is seen to agree well with the actual one, however.

Copper-Tubing Apparatus

Slug flow was observed in the copper tube for void fractions as low as $\beta = 0.005$. The pipe was horizontal and air was injected from the top of the cross section. The liquid flow was in the turbulent regime with the water velocity maintained at 4 to 5 ft/sec. Two typical runs are considered, the details of which are also included in Table 3 as Runs 3 and 4. Numerically computed pressure transients for these runs have been obtained using the drift-flux model, for which the value of the distribution parameter C_o has been assumed to be 1.2. One hundred Δx divisions were used for computations. The details regarding the computational procedure are identical to those described for Runs 1 and 2.

The experimental and analytical pressure-trace records for Runs 3 and 4 are shown in Figs. 43 and 44. The amplitudes and the periods predicted by the numerical model agree very well with the experimental values. The experimental records show a reflection of the waves near the reservoir end, which may be attributed to a regulating valve located near that end of the pipe.

As the 334-ft long copper tube has been wound as a coil, as shown in Fig. 2, it is inclined at approximately 0.4° with the horizontal. Wallis [20], and Maneri and Zuber [54] have discussed the effect of in-

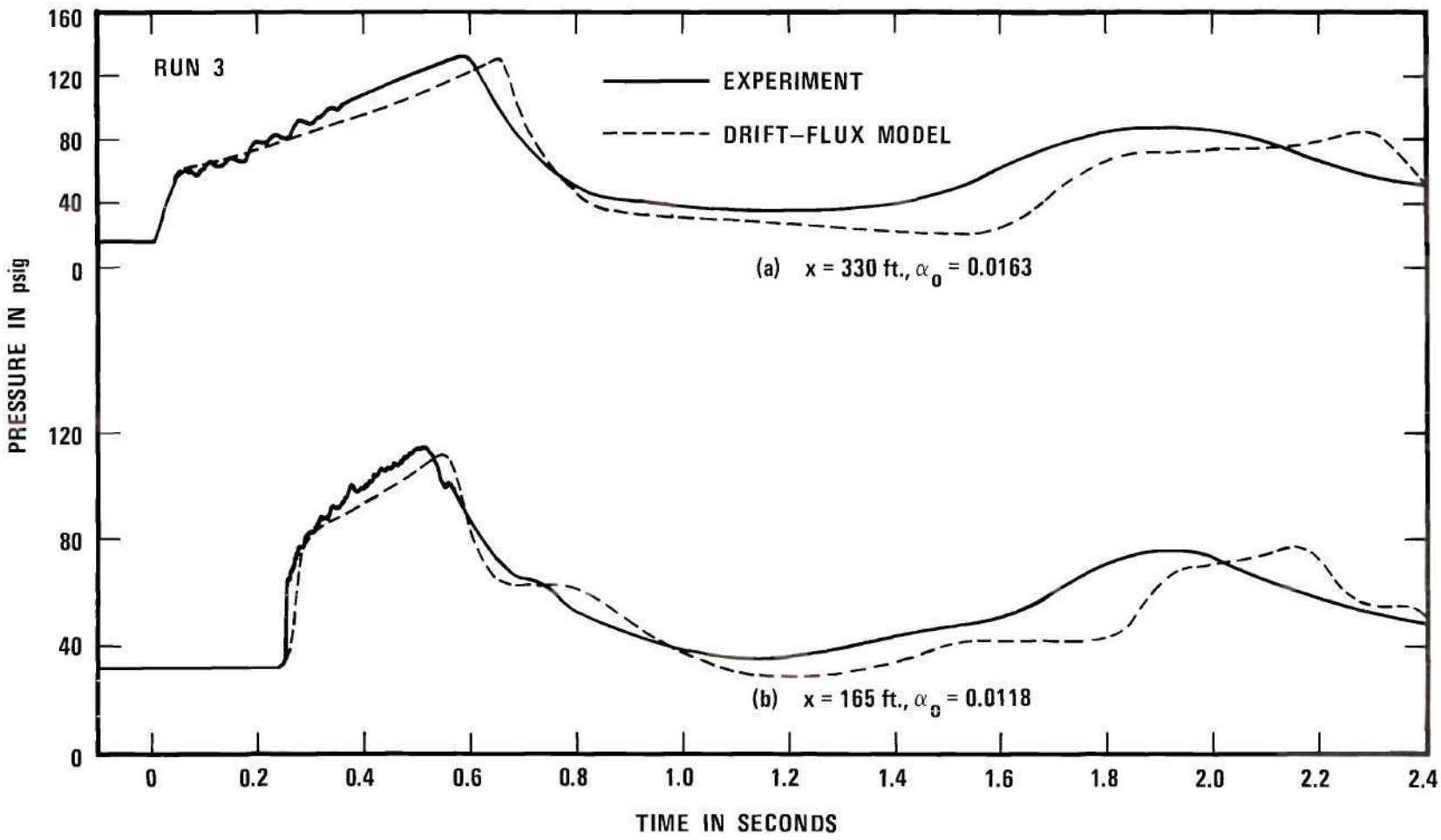

Figure 43. Comparison of Measured Transient Pressures in Slug Flow with Drift-Flux Model. Rapid Valve Closure with u_o = 4.91 ft/sec. in Copper Tubing.

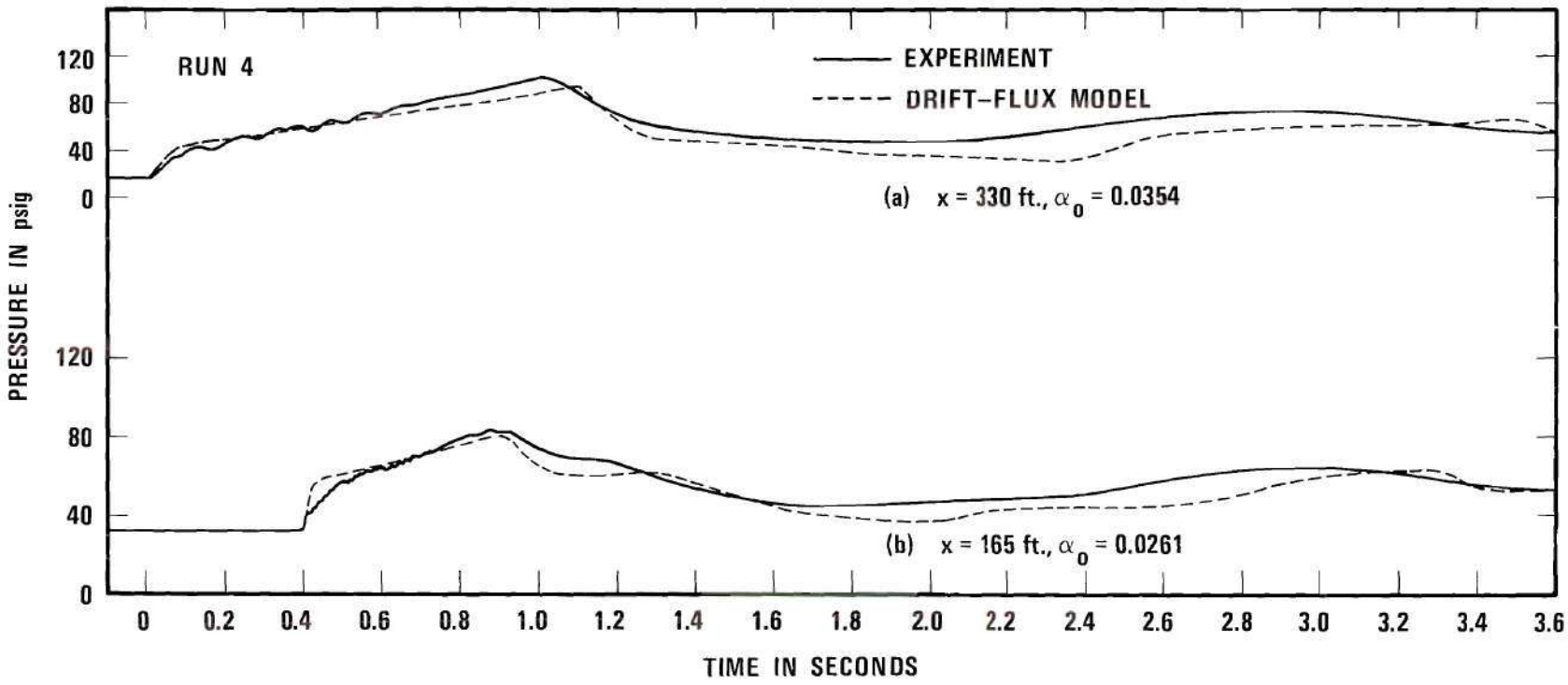

Figure 44. Comparison of Measured Transient Pressures in Slug Flow with Drift-Flux Model. Rapid Valve Closure with u_o = 4.83 ft/sec. in Copper Tubing.

clination on steady slug flow, reporting that, in an inviscid liquid, bubbles can rise faster than in a vertical pipe if the axis of the pipe is as low as 2° from the horizontal. Although no information is available on slug flows at inclination as small as 0.4°, it is very clear from the curves of rise velocities reported by Wallis [20], and by Maneri and Zuber [54], that the rise velocity is not definitely zero at some angles. Instead, the rise velocity may have as high a value as that for a vertical flow. This means that, for the present setup, which has a very small downward inclination, the weighted mean drift velocity may not be zero as used in the computations. However, it appears that the effect of this on the transients may be very small.

Considering the good agreement between experiment and theory for the transient results using both of the apparatuses the drift-flux model also appears to be a useful tool for the analysis of unsteady slug flow.

CHAPTER XI

CONCLUSIONS

The essential conclusions of this investigation are itemized as follows:

1. Two models have been proposed for the transient analysis of bubbly gas-liquid mixtures flowing through pipes: a bubble-dynamics model and a drift-flux model. Both models are capable of handling shock formation and shock propagation, and are relatively simple compared to the conventional method of characteristics, which requires inclusion of complex shock-wave theory as an internal boundary condition.

2. Both of the proposed models compare reasonably well with experimental results in bubbly air-water mixtures for the simple case of transients resulting from the rapid closure of a downstream valve. The agreement between measured and calculated amplitude and phase of the transient pressures is acceptable.

3. The bubble-dynamics model is valid for bubbly flow if the bubbles are uniformly distributed and of uniform size and shape However, even for nonuniform bubbles, the use of an average bubble size has been found to give satisfactory results.

4. The bubble-dynamics model is capable of predicting transient bubble motion relative to the liquid motion.

5. The drift-flux model can be employed to incorporate the effect of velocity and concentration profiles on the transients. The model is very simple and can also be used for analysis of transients in

slug flow.

6. With the bubble-dynamics model the effect of pipe-wall elasticity and water compressibility can be included. The model is also well suited for very low void fractions if the bubbles are very small and uniformly sized.

7. The bubble-size distribution across the pipe cross section influences the propagation speed of pressure disturbances.

8. For the range of bubble sizes involved in this investigation (0.5 to 4 mm) the adiabatic theory gives an adequate representation of the bubble behavior, as well as an adequate prediction of the wave celerity.

9. The formation of shock waves by the steepening of compression waves is demonstrated experimentally and numerically.

10. Based upon the shock-wave classification proposed by Noordzij and van Wijngaarden [28], only B and C-type shock waves were observed in this study. C-type shock structure was only observed for very weak shock waves.

11. The structure of the shock waves formed by steepening of compression waves is influenced by the structure of the compression waves themselves, limiting the application of the shock-tube theory of Noordzij and van Wijngaarden to shock waves in long conduits. The thickness of the steep portion and the period of oscillations behind the shock are much higher than values predicted by theory.

12. Thermal relaxation may be of importance as shock waves of C-type were observed for shocks with strength as high as 1.6.

13. Oscillations existing behind a shock wave are damped out

very quickly. The amplitudes of the oscillations are much smaller than the pressure rise associated with the shock itself, perhaps suggesting that no appreciable error is involved in neglecting dispersion effects in transient analysis of gas-liquid mixtures.

CHAPTER XII

RECOMMENDATIONS

From the experience gained in performing this investigation the following recommendations are made:

1. For the system of governing partial differential equations associated with the proposed bubble-dynamics and drift-flux models, it would be worthwhile to obtain the characteristic roots and the compatibility equations. These equations are useful in representing the boundary conditions in both models.

2. If the characteristic equations could be derived, it should be possible to obtain a method of transient analysis with a grid of characteristics by incorporating the Hugoniot shock relationships as an internal boundary condition from the point of shock inception.

3. Additional experimental investigations are recommended to study the influence of bubble distribution on wave celerity.

4. A detailed study on the structure of shock waves in a long vertical conduit containing nearly spherical bubbles uniformly distributed is recommended.

5. The suitability of other available explicit methods, implicit methods, and explicit-implicit methods for the numerical integration of the system of equations in the conservation form should be ascertained and compared with the Lax-Wendroff two-step scheme.

6. Development of a method of transient analysis in slug flow that incorporates the length and spacing of slugs is recommended.

7. The usefulness of the proposed models for such practical transient problems as pump power failure, turbine shutdown, etc., should be examined.

8. The two-step Lax-Wendroff numerical scheme should be applied to situations for which the gas production term in the conservation of mass equations is not zero.

APPENDIX A

METERING OF AIR FLOW

The air flow into the test pipes was measured using a micrometering valve with a 0.055 inch diameter orifice. The stem of the valve could be accurately rotated and set to any desired number of turns by a built-in vernier scale. Calibration of the meter was conducted for three settings of the meter, covering the desired range of air flow with water as the test fluid. The water discharge Q_ℓ was measured volumetrically by using a graduated cylinder and a stop watch. The pressure drop Δp across the meter was measured using a manometer. For each setting a representative orifice diameter D_o was obtained to correspond to the fraction of full opening. The coefficient of discharge C_d of the meter and the Reynolds number Re of the flow were obtained from

$$C_d = \frac{4Q_\ell}{\pi D_o^2 (2\Delta p/\rho_\ell)^{\frac{1}{2}}} \tag{A.1}$$

and

$$Re = \frac{4Q_\ell}{\pi D_o \nu_\ell} \tag{A.2}$$

The calibration curves are essentially plots of C_d against Re for each of the settings. A typical calibration curve is shown in Fig. 45 for a setting 2 turns open.

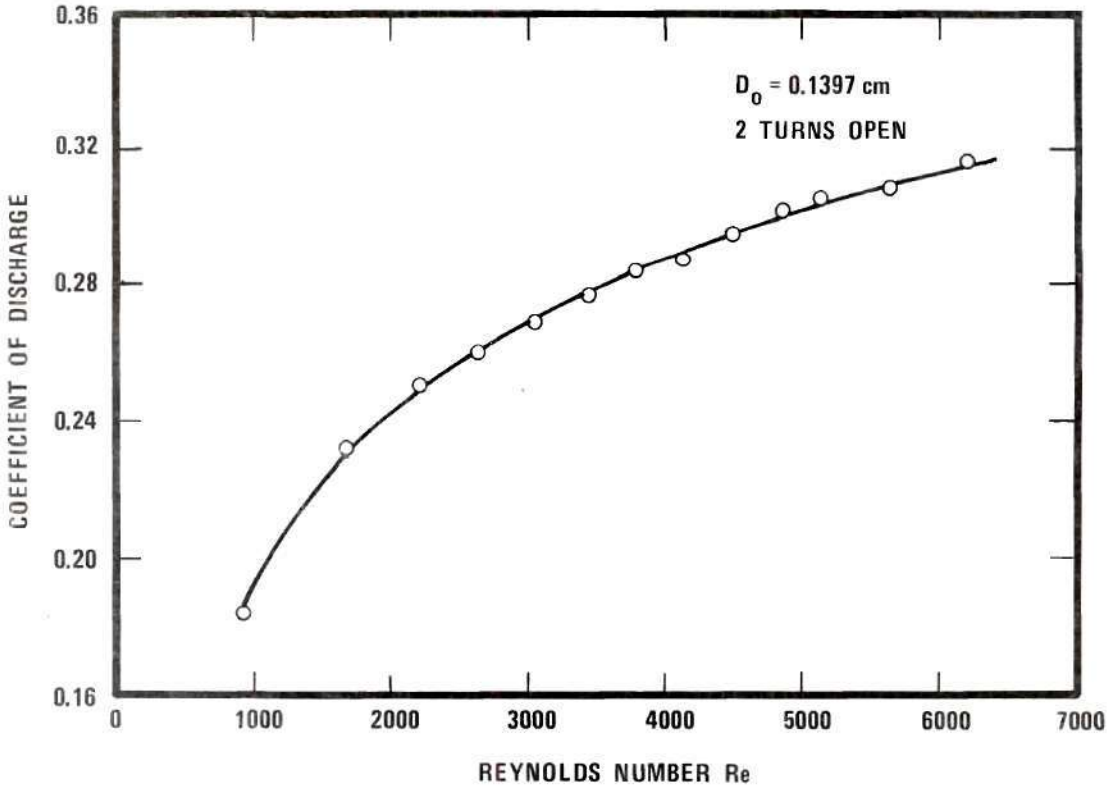

Figure 45. A Typical Flow-Calibration Curve for Air Mic metering Valve.

To calculate the air flow a value for Re/C_d is initially estimated from the known pressure drop Δp across the meter by

$$Re/C_d = \frac{D_o(2\Delta p/\rho_g)^{1/2}}{\nu_g} \tag{A.3}$$

with ρ_g and ν_g being known at the particular pressure. Using the calibration curve a value of Re is then obtained by trial to satisfy the calculated value of Re/C_d. From the final value of Re the mass rate of air flow M_a is determined from

$$M_a = \frac{\pi}{4} D_o \mu_g Re \tag{A.4}$$

Knowing the mass flow rate of air, the pressure distribution along the pipe, and the water discharge, the distribution of the initial volumetric quality β along the pipe can then be computed.

APPENDIX B

STEADY-STATE FRICTION

The steady-state friction factors for both water flow and bubbly mixtures were based upon piezometric pressure-gradient measurements. The piezometric-head gradients for water velocities ranging from 2 to 10 ft/sec, corresponding to Reynolds number ranging from 15000 to 70000, were obtained for bubbly flow, for which β was varied from approximately 0.004 to 0.018. As the use of a constant friction factor for transient two-phase flow is somewhat arbitrary, extensive measurements and evaluations of the steady-state friction factor for a wide range of air concentrations were not attempted.

Measured values of the Darcy-Weisbach resistance coefficient f are listed in Table 4 for the case of single-phase water flow. The theoretical values based upon Blasius smooth pipe relationship agree closely with experiment values.

For the bubbly-flow regime, Table 5 shows the values of the calculated friction factors based on the mixture density and volumetric flux of the liquid. For a majority of the runs the friction factors for the downward flow are seen to be slightly less than those for upward flow. The ratios of the two-phase flow friction factor to the smooth-pipe friction factor for liquid flow are also calculated and listed in Table 5.

To avoid complexities, the two-phase flow friction factor is assumed to be a constant for the transient flow computations. For the plexiglass pipe the two-phase flow f is based upon the average value of

Table 4. Calculation of Steady-State Friction Factor in the Plexiglass Pipe for Water Flow

Run number	Discharge cfs	Velocity ft/sec	Re x 10^{-4}	$\Delta h_f/L$	Friction Factor f_ℓ	
					Measured	Blasius
1	0.0110	1.923	1.506	0.021	0.0310	0.0285
2	0.0196	3.427	2.683	0.052	0.0243	0.0246
3	0.0244	4.266	3.309	0.077	0.0232	0.0234
4	0.0274	4.790	3.750	0.095	0.0227	0.0227
5	0.0351	6.136	4.804	0.155	0.0226	0.0214
6	0.0437	7.640	5.638	0.223	0.0210	0.0205
7	0.0469	8.199	6.051	0.262	0.0214	0.0202
8	0.0523	9.143	7.159	0.304	0.0199	0.0194
9	0.0561	9.808	7.680	0.349	0.0198	0.0191
10	0.0481	8.409	5.799	0.268	0.0208	0.0204
11	0.0384	6.713	4.954	0.176	0.0215	0.0212
12	0.0292	5.105	3.997	0.113	0.0221	0.0224
13	0.0231	4.039	3.162	0.076	0.0256	0.0237
14	0.0158	2.762	2.038	0.039	0.0273	0.0266

Table 5. Calculation of Friction Factor in the Plexiglass Pipe for Bubbly Air-Water Mixtures

Run No.	j_ℓ ft/sec	β %	Reservoir Pressure p_o psig	Re $\times 10^{-4}$	Horizontal Leg			Riser			Downcomer		
					$\frac{\Delta h_f}{L}$	f	f/f_ℓ	$\frac{\Delta h_f}{L}$	f	f/f_ℓ	$\frac{\Delta h_f}{L}$	f	f/f_ℓ
1	6.678	1.319	50	5.231	0.180	0.0221	1.057	0.187	0.0219	1.047	0.191	0.0223	1.066
2	5.052	1.686	50	3.956	0.117	0.0255	1.138	0.126	0.0274	1.223	0.118	0.0256	1.142
3	4.091	1.857	53	3.205	0.077	0.0257	1.089	0.085	0.0282	1.195	0.081	0.0268	1.135
4	4.091	1.151	52	3.205	0.078	0.0258	1.089	0.082	0.0272	1.148	0.078	0.0258	1.089
5	4.091	0.409	49	3.205	0.072	0.0236	1.000	0.077	0.0253	1.072	0.072	0.0236	1.000
6	8.409	1.020	39	6.586	0.260	0.0213	1.081	0.278	0.0218	1.106	0.279	0.0218	1.106
7	8.217	1.032	42	6.435	0.260	0.0213	1.070	0.267	0.0219	1.100	0.266	0.0218	1.095
8	9.108	0.962	35	7.134	0.295	0.0196	1.015	0.317	0.0211	1.092	0.322	0.0214	1.108
9	7.587	0.993	40	5.943	0.212	0.0202	1.010	0.236	0.0227	1.135	0.213	0.0205	1.025
10	6.227	1.460	40	4.875	0.160	0.0229	1.075	0.170	0.0243	1.141	0.168	0.0240	1.126

f in Table 6, or 1.09 f_{ℓ}, the friction factor for water flow. It may be noted that the frictional loss for the transient two-phase flow is a function of the mixture velocity and the mixture density, both of which vary with time and distance. Hence, a true representation of the friction offered by the pipe wall can become very complicated.

APPENDIX C

LAX-WENDROFF TWO-STEP SCHEME

The Lax-Wendroff two-step scheme is an explicit finite-difference method of second-order accuracy. The first step uses the first-order scheme of Lax [54], which is considered as an intermediate step. The details on the Lax-Wendroff two-step scheme and their stability criteria are discussed in detail by Ames [38], and by Richtmyer and Morton [39].

Consider a set of conservation equations of the form

$$\frac{\partial Q_{i1}}{\partial t} + \frac{\partial Q_{i2}}{\partial x} = Q_{i3} \tag{C.1}$$

in which $i = 1,2,3$. Integrating (C.1) from x to $x + 2\Delta x$ and t to $t + \Delta t$, and using the finite-difference approximations proposed by Lax [54]

$$Q_{i1}(x + \Delta x,\ t + \Delta t) = 0.5\,[Q_{i1}(x + 2\Delta x,\ t) + Q_{i1}(x,t)\,]$$
$$-0.5\,\Delta t/\Delta x\,[Q_{i2}(x + 2\Delta x,\ t) - Q_{i2}(x,t)\,]$$
$$+0.5\,\Delta t\,[Q_{i3}(x + 2\Delta x,t) + Q_{i3}(x,t)\,] + 0(\Delta x^2,\ \Delta t) \tag{C.2}$$

Equation (C.2) represents the first step and is illustrated in Fig. 46.

Integrating (C.1) from $x - \Delta x$ to $x + \Delta x$ and t to $t + 2\,\Delta t$, and using the finite-difference approximations of Lax and Wendroff [40]

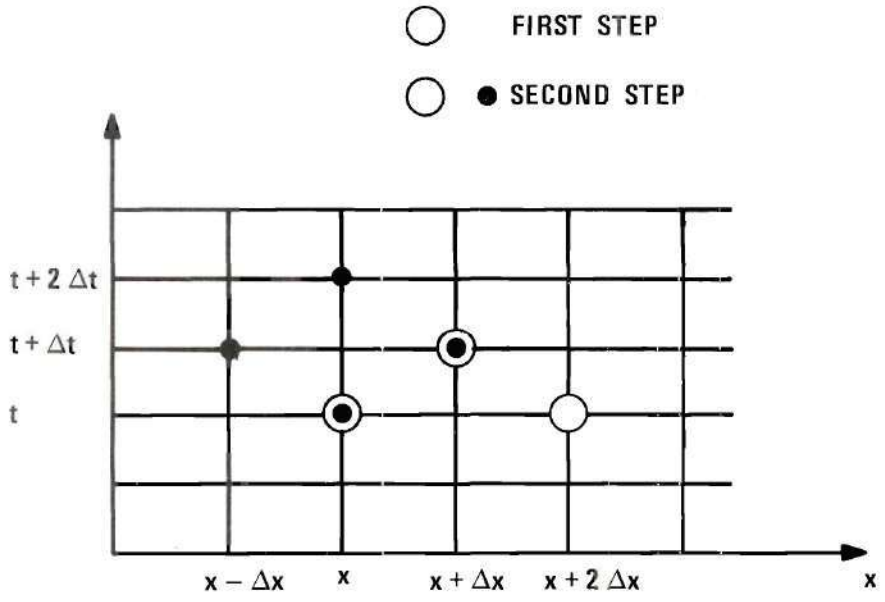

Figure 46. Definition Sketch for Lax-Wendroff Two-Step Scheme.

$$Q_{i1}(x, t + 2\Delta t) = Q_{i1}(x, t) - \Delta t/\Delta x\,[Q_{i2}(x + \Delta x, t + \Delta t) - Q_{i2}(x - \Delta x, t + \Delta t)] + \Delta t\,[Q_{i3}(x + \Delta x, t + \Delta t) + Q_{i3}(x - \Delta x, t + \Delta t)] + 0(\Delta x^2, \Delta t^2) \quad (C.3)$$

Equation (C.3) represents the second step illustrated in Fig. 46.

The stability requirement of the Lax-Wendroff scheme is that

$$\frac{\Delta t}{\Delta x} \leq \frac{1}{|\lambda|} \quad (C.4)$$

in which λ is the maximum eigenvalue of the coefficient matrix of the linearized version of the system represented by Eq. (C.1). This condition is known as Courant-Friedrichs-Lewy Convergence condition.

For the system of conservation equations representing the bubble-dynamics model described in Chapter VI, the value of λ is very difficult to evaluate because of the complex nature of the equations. However, based on an isothermal bubble behavior for a similar system of equations, Prosperetti and van Wijngaarden [22] determined the eigenvalue $|\lambda|$ to be given by $0.5\,(|u| + |v|) + a_{mp}$. For adiabatic bubble behavior this value may be different, of course. An upperbound of $|u| + |v| + a_{mp}$ was found to produce stable numerical computations, and was therefore used. For the drift-flux model, which differs from a homogeneous model only by a drift-flux term in the momentum equation, a value of $\lambda = |v_m| + a_{mp}$ from the homogenous model was employed because it yielded stable computations. When $\Delta t/\Delta x = 1/|\lambda|$ at each and every mode, the Lax-Wendroff scheme gives the most accurate results. For air-water mixtures a_{mp} is a function of pressure and void fraction, and hence differs from node to

node. Thus, $\Delta t/\Delta x$ can not be chosen to be equal to $1/|\lambda|$ at all nodes. The possibility of the existence of a discontinuity in the form of a shock wave also exists. When shock waves form, a numerical computations, using the Lax-Wendroff scheme produces an over shooting of the shock front followed by damped oscillations. The elimination of these effects may be effected by introducing additional numerical viscosity, as described in the following.

Smoothing Procedure

Kranenburg [5, 43] has used a smoothing procedure which was found well suitable for the present case and was hence adopted. Referring to Fig. 47, a smoothing parameter θ_i is defined as

$$\theta_i\ (x,\ t) = \frac{0.5\ Q_{il}\ (x + 2\Delta x,\ t)\ - Q_{il}\ (x,\ t) + 0.5\ Q_{il}\ (x - 2\Delta x,\ t)}{\Delta Q_{ir}} \qquad (C.5)$$

in which ΔQ_{ir} is a reference interval variable of $Q_{il}\ (x, t)$. If θ_i exceeds a reference value θ_r, numerical viscosity is added to those particular mesh points, as follows.

If $|\theta_i| > \theta_r$

$$Q'_{il}\ (x, t) = Q_{il}\ (x, t) + 0.5\ \Delta Q_{ir}\ \theta_i\ (x, t) \qquad (C.6)$$

If $|\theta_i| \leq \theta_r$

$$Q'_{il}\ (x, t) = Q_{il}\ (x, t) \qquad (C.7)$$

where $Q'_{il}\ (x, t)$ represents the smoothed variable.

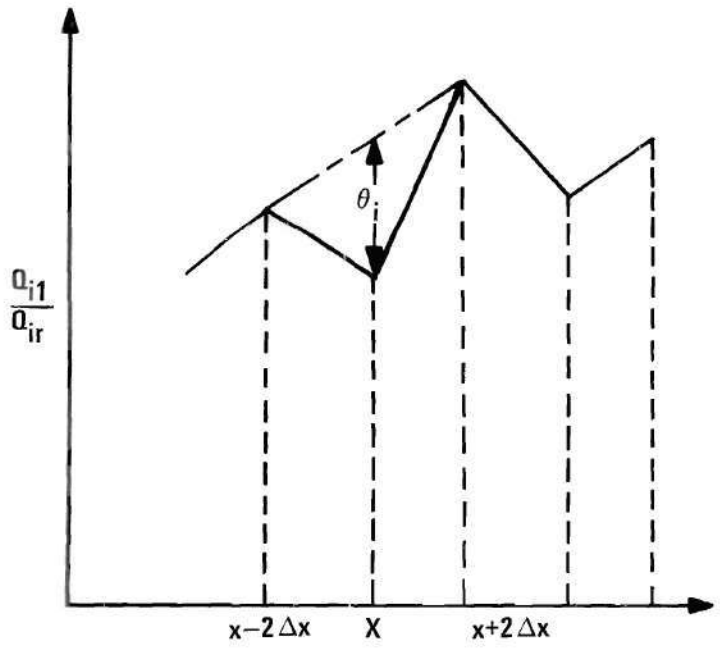

Figure 47. Definition Sketch for Smoothing Operator θ_i.

The parameter ΔQ_{ir} can be approximated by the maximum change of the variable Q_{il} over a distance of 4 meshes. This can be achieved from an initial computation without any smoothing. Of course, the value of ΔQ_{ir} does not influence the magnitude of corrected values of Q_{il} as ΔQ_{ir} is cancelled out by taking the product $\Delta Q_{ir}\ \theta_i\ (x, t)$ in Eq. (C.6).

Fig. 48 shows the effect of smoothing for various values of the reference parameter θ_r. Maximum smoothing is obtained for $\theta_r = 0$. It is necessary, however, to select a value of θ_r that yields just enough smoothing. Otherwise, low frequency waves associated with the transient phenomenon may be affected. A value of $\theta_r = 0.03$ has been found to give a satisfactory result, as seen in Fig. 48. Very little smoothing is induced as θ_r approaches a value of 0.5. Kranenburg [43] has shown that if

$$\theta_r > \frac{8\pi^2}{(L/\Delta x)^2} \tag{C.8}$$

the smoothing procedure does not influence to any considerable extent the low-frequency waves associated with the transients. For $L/\Delta x = 60$, θ_r must be greater than 0.02.

Lax-Wendroff Scheme and The Method of Characteristics

In order to obtain a comparison between the numerical results based upon the Laxendroff two-step scheme with those based upon a fixed grid of characteristics, two cases of transients produced by a rapid closure of a valve at the downstream end of the plexiglass pipe were considered. Using a homogeneous model with a fixed grid, for

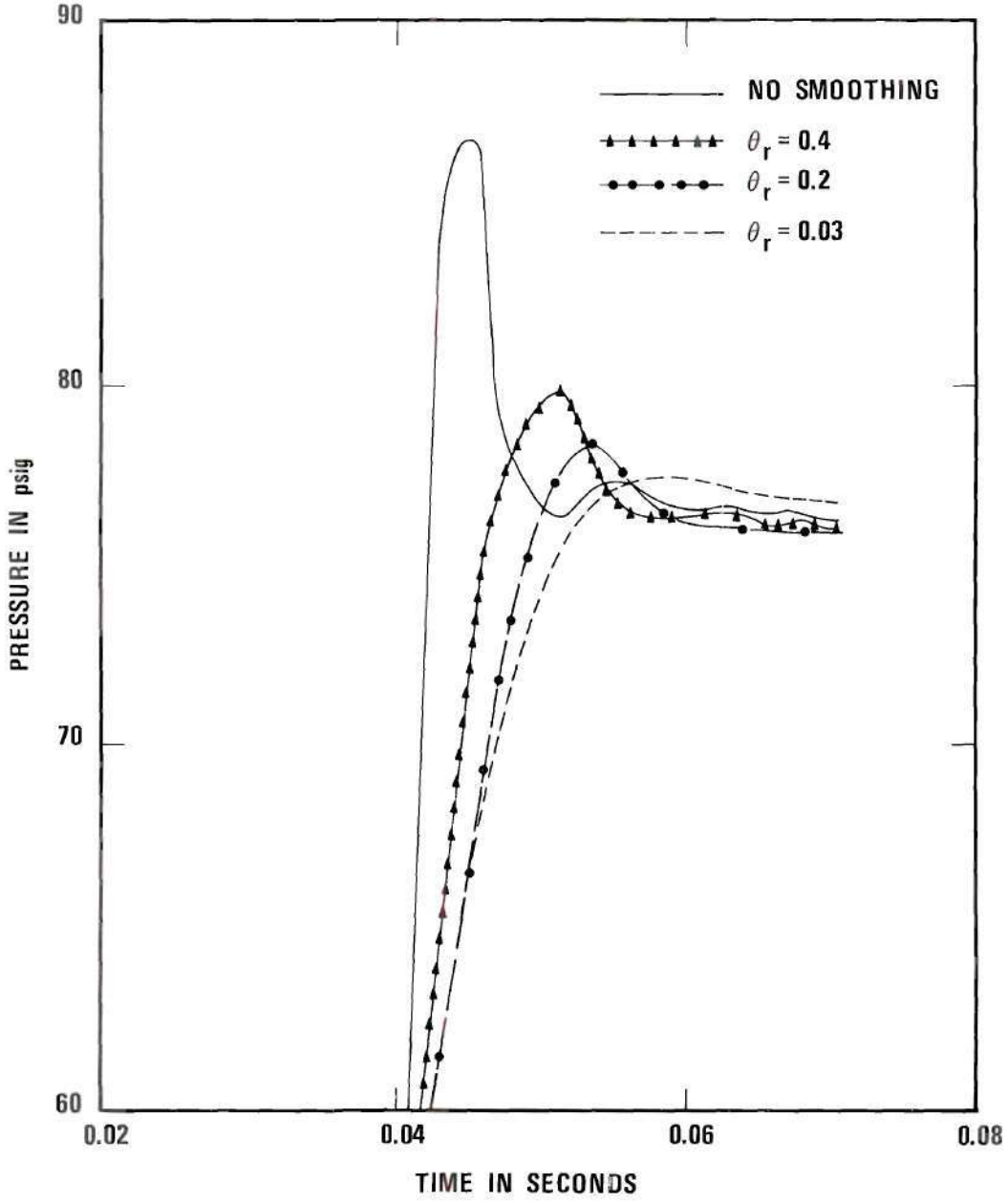

Figure 48. Effect of Smoothing on Lax-Wendroff Scheme.

which $L/\Delta x = 60$, Δt is evaluated at each time step to satisfy the CFL condition. In the case of the Lax-Wendroff scheme, the boundary conditions were simulated with the method of characteristics. First, the case of pure waterhammer with no air present is considered. In this case $\Delta x/\Delta t$ is equal to $a_{\ell p}$, the wave speed in the liquid, at all nodes at all times. The numerical results for this linear problem with steady-state friction are shown in Fig. 49. It can be seen that the methods agree perfectly, which is not surprising as the Lax-Wendroff method is known to be exact when $\Delta x/\Delta t = |\lambda|$ for all nodal points.

Secondly, a case of transients in bubbly air-water mixture is considered. The closure time of the downstream valve is chosen so that no shock wave formed. The absence of a shock wave was confirmed by proving that characteristics did not intersect when employing an irregular grid of characteristics solution. The problem is nonlinear as the propagation speed of a disturbance depends upon the pressure and the void fraction, both of which are variables in space and time. The boundary conditions corresponded to the rapid closure of a valve at one end and a constant pressure reservoir at the other end. Smoothing was effected as described earlier, with the parameter $\theta_r = 0.03$. The results obtained from both methods are shown in Fig. 50. The Lax-Wendroff scheme imposes a numerical damping which causes some amplitude attenuation. However, as evident from Fig. 50, this attenuation is extremely small and in general the agreement is quite good between the two methods, establishing the suitability of the Lax-Wendroff scheme for the present study.

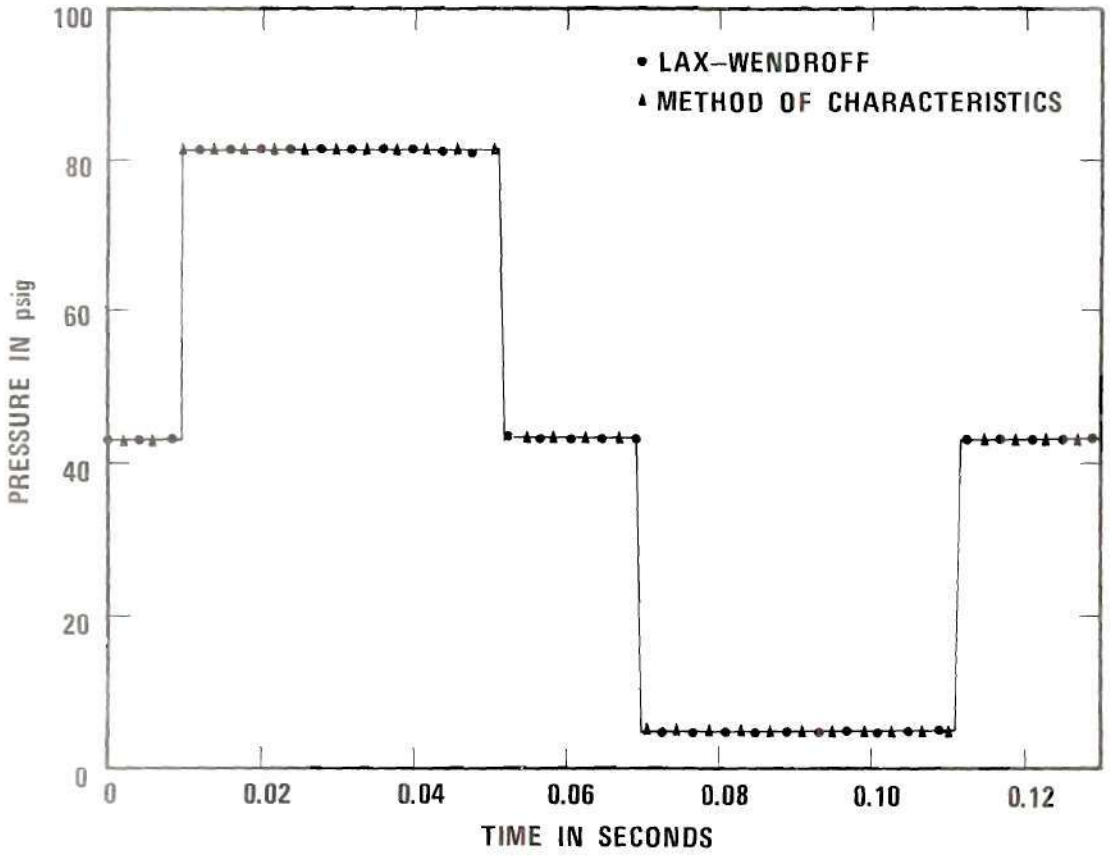

Figure 49. Comparison of Transient Pressures at x = 43 ft from Lax-Wendroff Solution with Fixed Grid of Characteristics Solution for Pure Waterhammer. Rapid Valve Closure with u_o = 1.4 ft/sec and t_c = 0 in Plexiglass Pipe.

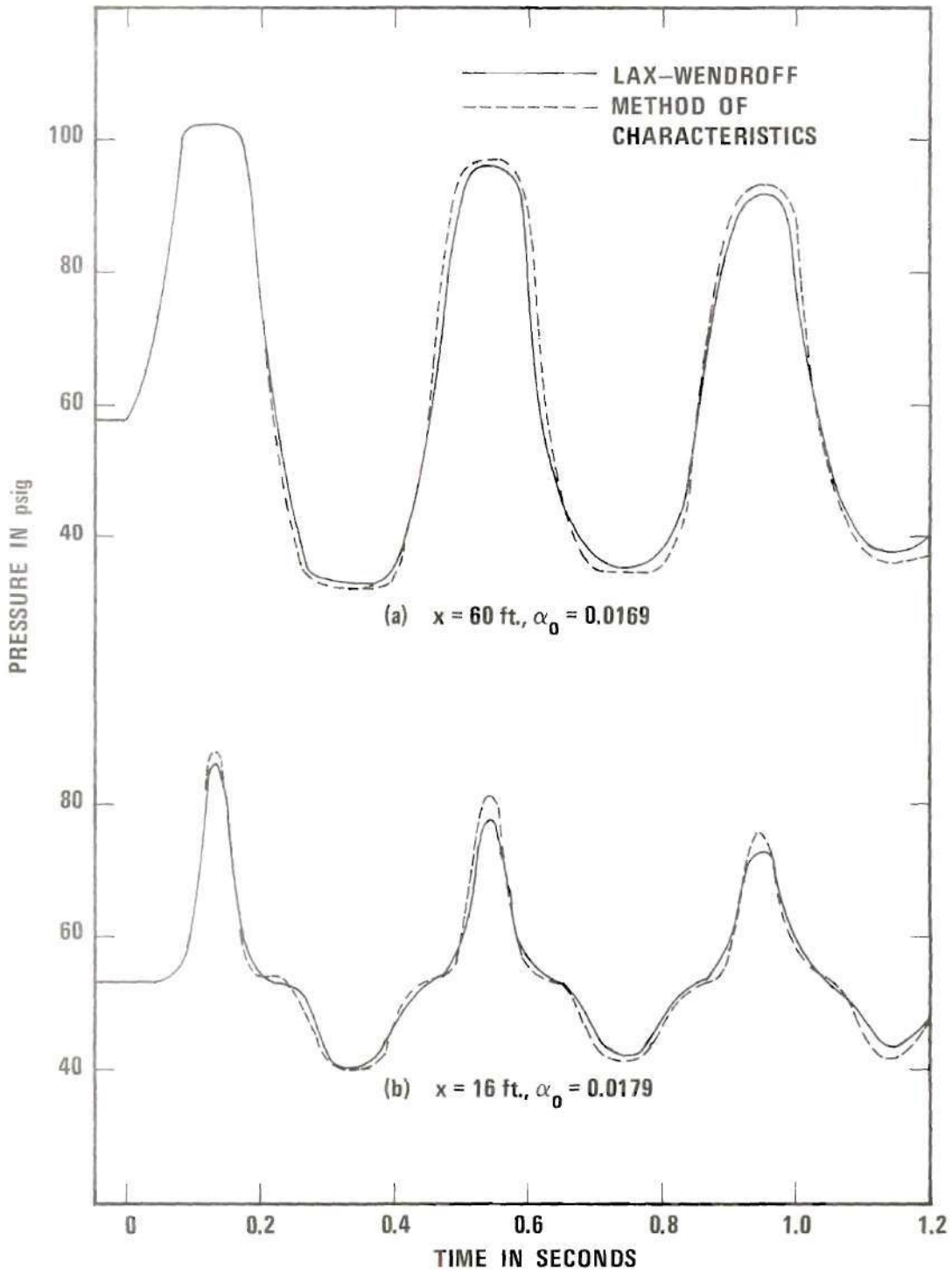

Figure 50. Comparison of Results of Lax-Wendroff Scheme with Fixed Grid of Characteristics. Rapid Valve Closure with u_o = 4.33 ft/sec and t_c = 0.08 sec in Plexiglass Pipe.

APPENDIX D

TIME AND AREA AVERAGING

The field equations and the constitutive equations associated with the drift-flux model discussed in Chapter VII are obtained by means of an averaging procedure. In a two-phase flow problem it is possible to formulate the equations in terms of the local instant variables. Such a formulation would result in a multiboundary problem causing considerable and perhaps insurmountable mathematical difficulties in solving the problem. To avoid these difficulties it is necessary to derive the equations in terms of macroscopic properties by using an appropriate averaging procedure. The importance of averaging and the various averaging techniques have been discussed by Ishii [48,49]. Eulerian averaging procedure to obtain time and area averaged equations expressed in terms of time and area averaged variables has been used in the present study and the averaging technique is the same as that described by Ishii [48, 49]. The method is very extensive involving averaging of variables, averaging of functions and averaging of derivatives of functions. A very brief discussion of the averaging procedure follows.

Time Averaging

The occupant of a particular point in the cross section of the pipe carrying a two-phase mixture varies randomly from liquid to gas to an interface. Our purpose is to time average the fluid properties and the field equations so that they can be treated as composed of smooth

continuous variables or functions.

Let Δt be a small interval of time over which the random variables at a particular point are averaged. Let $[\Delta t]_T$ represent the part of Δt when the point is occupied by gas or liquid and $[\Delta t]_S$ represent the part of Δt when the point is occuppied by an interface. We assume $[\Delta t]_S$ to be composed of arbitrarily small intervals ζ. The fraction of time occupied by gas and liquid are defined by taking the limit $\zeta \to o$. The Eulerian time average of a function $F(x_o, t_o)$ is given by

$$\overline{F}(x_o, t_o) = \lim_{\zeta \to o} \frac{1}{\Delta t} \int_{[\Delta t]_T} F(x_o, t)dt \tag{D.1}$$

The time averaged probability that a point is occupied by gas is assumed to be the local void fraction α and hence, the probability that a point is occupied by liquid is $(1-\alpha)$. We can obtain a relation for the average of a function F for the two-phase flow as

$$\overline{F}_m = \overline{F}_g + \overline{F}_\ell \tag{D.2}$$

with suffixes g, ℓ and m denoting the gas, liquid and mixture respectively.

Pressure, temperature, desnity, etc. are grouped as intensive properties, Ishii [48]. Let G by an intensive property. Then the weighted time averaged value of G_k is given by

$$\overline{\overline{G}}_k = \frac{\overline{G_k}}{\alpha_k} \tag{D.3}$$

with $k = g, \ell$ and $\alpha_g = \alpha$ and $\alpha_\ell = 1-\alpha$. For the mixture

$$\overline{G_m} = \alpha \overline{\overline{G_g}} + (1-\alpha) \overline{\overline{G_\ell}} \tag{D.4}$$

Hence, the average density of the mixture is

$$\overline{\rho_m} = \alpha \overline{\overline{\rho}_g} + (1-\alpha) \overline{\overline{\rho}_\ell} \tag{D.5}$$

A function associated with volumes per unit time such as velocity, energy, momentum etc. may be defined as an extensive charactered function, Ishii [48]. Let ψ be such a function. The weighted mean value of ψ_k is given by

$$\overline{\overline{\psi}_k} = \overline{\rho_k \psi_k} / \overline{\rho_k}, \quad k = g, \ell \tag{D.6}$$

and

$$\overline{\overline{\psi}_m} = [\alpha \overline{\overline{\rho}_g} \overline{\overline{\psi}_g} + (1-\alpha) \overline{\overline{\rho}_\ell} \overline{\overline{\psi}_\ell}] / \overline{\rho_m} \tag{D.7}$$

Hence, the average mixture velocity is

$$\overline{\overline{v}_m} = [\alpha \overline{\overline{\rho}_g} \overline{\overline{v}_g} + (1-\alpha) \overline{\overline{\rho}_\ell} \overline{\overline{v}_\ell}] / \overline{\rho_m} \tag{D.8}$$

The time averaging of the derivative of a function is very complicated as the interfacial transport has to be considered Ishii [48] uses the Leibniz rule to express the time average of the derivative as a derivative of the time average. If the surface transport at the interface is zero the problem becomes very simple because in that case the time average of a derivative is simply the derivative of the time average. In the present study there is no mass and heat transfer between the phases and the surface tension effects are neglected. Hence, as an example

$$\overline{\frac{\partial}{\partial x}(\rho_m \psi_m v_m)} = \frac{\partial}{\partial x}\overline{(\rho_m \psi_m v_m)} \tag{D.9}$$

Time Average of Convective Term

We can express the time average of the convective term in terms of time averaged weighted quantities.

$$\overline{\rho_m \psi_m v_m} = \overline{\rho_g \psi_g v_g} + \overline{\rho_\ell \psi_\ell v_\ell} \tag{D.10}$$

If the turbulent fluctuations of the variables can be neglected in the present one-dimensional formulation of the problem we can write Eq. (D.10) using Eq. (D.6) as

$$\overline{\rho_m \psi_m v_m} = \alpha \bar{\bar{\rho}}_g \bar{\bar{\psi}}_g \bar{\bar{v}}_g + (1-\alpha)\, \bar{\bar{\rho}}_\ell \bar{\bar{\psi}}_\ell \bar{\bar{v}}_\ell \tag{D.11}$$

Define a diffusion velocity

$$V_{km} = \bar{\bar{v}}_k - \bar{\bar{v}}_m \tag{D.12}$$

Using Eqs. (D.12) and (D.7)

$$\overline{\rho_m \psi_m v_m} = \bar{\rho}_m \bar{\bar{\psi}}_m \bar{\bar{v}}_m + J^D \tag{D.13}$$

where

$$J^D = \sum_{k\,=\,g,\,\ell} \alpha_k \bar{\bar{\rho}}_k \bar{\bar{\psi}}_k V_{km} \tag{D.14}$$

and is often referred to as a diffusion flux.

Area Averaging

The area average of a function G is defined as

$$\langle G \rangle = \frac{1}{A} \int_A G dA \tag{D.15}$$

The area average of the void fraction is

$$\langle \alpha \rangle = \frac{1}{A} \int_A \alpha dA \tag{D.16}$$

If G is an intensive variable and $\overline{\overline{G}}$ is its weighted time average value then the time and area averaged weighted value of G is

$$\langle\langle G_k \rangle\rangle = \frac{\langle \alpha_k \overline{\overline{G}}_k \rangle}{\langle \alpha_k \rangle}, \quad k = \ell, g \tag{D.17}$$

where $\langle \alpha_g \rangle = \langle \alpha \rangle$ and $\langle \alpha_\ell \rangle = 1 - \langle \alpha \rangle$. For the intensive property of the mixture

$$\langle \overline{G}_m \rangle = \langle \alpha \rangle \langle\langle G_g \rangle\rangle + (1-\langle \alpha \rangle) \langle\langle G_\ell \rangle\rangle \tag{D.18}$$

If ψ is an extensive charactered function

$$\langle\langle \psi_k \rangle\rangle = \frac{\langle \alpha_k \overline{\overline{\rho}}_k \overline{\overline{\psi}}_k \rangle}{\langle \alpha_k \overline{\overline{\rho}}_k \rangle}, \quad k = \ell, g \tag{D.19}$$

For the mixture

$$\langle\langle\psi_m\rangle\rangle = \langle\bar{\rho}_m\bar{\bar{\psi}}_m\rangle/\langle\bar{\rho}_m\rangle = [\langle\alpha\rangle\ \langle\langle\rho_g\rangle\rangle\ \langle\langle\psi_g\rangle\rangle + (1-\langle\alpha\rangle)\ \langle\langle\rho_\ell\rangle\rangle\ \langle\langle\psi_\ell\rangle\rangle]/\langle\bar{\rho}_m\rangle \tag{D.20}$$

Also, we have

$$\langle\bar{\rho}_m\rangle = \langle\alpha\rangle\ \langle\langle\rho_g\rangle\rangle + (1-\langle\alpha\rangle)\ \langle\langle\rho_\ell\rangle\rangle \tag{D.21}$$

$$\langle\langle v_m\rangle\rangle = [\langle\alpha\rangle\ \langle\langle\rho_g\rangle\rangle\ \langle\langle v_g\rangle\rangle + (1-\langle\alpha\rangle)\ \langle\langle\rho_\ell\rangle\rangle\ \langle\langle v_\ell\rangle\rangle]/\langle\bar{\rho}_m\rangle \tag{D.22}$$

For a pipe of uniform cross-sectional area the area average of the derivative of a function is simply the derivative of the area average of the function. If pipe wall elasticity is neglected this is true for all derivatives with respect to x and t.

Area Average of the Convective Term

Consider the time averaged convective term $\rho_m\psi_m v_m$ as given by Eq. (D.13).

$$\langle\overline{\rho_m\psi_m v_m}\rangle = \langle\bar{\rho}_m\bar{\bar{\psi}}_m\bar{\bar{v}}_m\rangle + \left\langle\sum_{k\,=\,g,\,\ell}\alpha_k\bar{\bar{\rho}}_k\bar{\bar{\psi}}_k V_{km}\right\rangle \tag{D.23}$$

A new diffusion velocity $\tilde{V}_{km}$ may be defined as

$$\tilde{V}_{km} = \bar{\bar{v}}_k - \langle\langle v_m\rangle\rangle \tag{D.24}$$

Obviously $\tilde{V}_{km}$ is different from V_{km} and Ishii [48] expresses the difference between them as a covariant of $\tilde{V}_{km}$. This gives

using Eq. (D.19) and D.20)

$$\langle \overline{\rho_m \psi_m v_m} \rangle = \langle \bar{\rho}_m \rangle \langle\langle \psi_m \rangle\rangle \langle\langle v_m \rangle\rangle$$

$$+ \sum_{k = g,\ \ell} \langle \alpha_k \rangle \langle\langle \rho_k \rangle\rangle \langle\langle \psi_k \rangle\rangle \tilde{V}_{km}$$

$$+ \sum_{k = g,\ \ell} \mathrm{Cov}\ (\langle \alpha_k \rangle \langle\langle \rho_k \rangle\rangle \langle\langle \psi_k \rangle\rangle \tilde{V}_{km}) \qquad \text{(D.25)}$$

For the derivative of the convective term we have

$$\langle \frac{\partial}{\partial x} (\overline{\rho_m \psi_m v_m}) \rangle = \frac{\partial}{\partial x} \langle \overline{\rho_m \psi_m v_m} \rangle \qquad \text{(D.26)}$$

or

$$\langle \frac{\partial}{\partial x} (\overline{\rho_m \psi_m v_m}) \rangle = \frac{\partial}{\partial x} (\langle \bar{\rho}_m \rangle \langle\langle \psi_m \rangle\rangle \langle\langle v_m \rangle\rangle)$$

$$+ \frac{\partial}{\partial x} \sum_{k = g,\ \ell} \langle \alpha_k \rangle \langle\langle \rho_k \rangle\rangle \langle\langle \psi_k \rangle\rangle \tilde{V}_{km}$$

$$+ \frac{\partial}{\partial x} \sum_{k = g,\ \ell} \mathrm{Cov}\ (\langle \alpha_k \rangle \langle\langle \rho_k \rangle\rangle \langle\langle \psi_k \rangle\rangle \tilde{V}_{km}) \qquad \text{(D.27)}$$

Ishii [48] has proved that the last term is extremely small compared to the other term of Eq. (D.27) and hence may be neglected. So, we have

$$\langle \frac{\partial}{\partial x} (\overline{\rho_m \psi_m v_m}) \rangle = \frac{\partial}{\partial x} (\langle \bar{\rho}_m \rangle \langle\langle \psi_m \rangle\rangle$$

$$\langle\langle v_m \rangle\rangle) + \frac{\partial}{\partial x} \sum_{k = g,\ \ell} \langle \alpha_k \rangle \langle\langle \rho_k \rangle\rangle \langle\langle \psi_k \rangle\rangle \tilde{V}_{km} \qquad \text{(D.28)}$$

For the mass balance equation $\psi = 1$ and

$$< \frac{\partial}{\partial x} \; (\overline{\rho_m v_m})> = \frac{\partial}{\partial x} \; (<\overline{\rho}_m> \; <<v_m>>)$$

$$+ \frac{\partial}{\partial x} \sum_{k \,=\, g,\; \ell} <\alpha_k> \; <<\rho_k>> \; \tilde{V}_{km} \qquad \text{(D.29)}$$

Zuber and Findlay [50] have given the following expressions for $\tilde{V}_{km}$, $k = g, \ell$

$$\tilde{V}_{gm} = (1 - <\alpha>) \; \frac{<<\rho_\ell>> \; <<v_r>>}{<\overline{\rho}_m>} \qquad \text{(D.30)}$$

and

$$\tilde{V}_{\ell m} = - <\alpha> \; \frac{<<\rho_g>> \; <<v_r>>}{<\overline{\rho}_m>} \qquad \text{(D.31)}$$

where

$$<<v_r>> = <<v_g>> - <<v_\ell>> \qquad \text{(D.32)}$$

Using Eqs. (D.30), (D.31) and (D.32) we can show that

$$\frac{\partial}{\partial x} \sum_{k \,=\, g,\; \ell} <\alpha_k> \; <<\rho_k>> \; \tilde{V}_{km} = 0 \qquad \text{(D.33)}$$

Hence,

$$<\frac{\partial}{\partial x} \; (\overline{\rho_m v_m})> = \frac{\partial}{\partial x} \; (<\overline{\rho}_m> \; <<v_m>>) \qquad \text{(D.34)}$$

For the momentum balance equation $\psi_m = v_m$ and

$$\left\langle \frac{\partial}{\partial x} \left(\overline{\rho_m v_m v_m} \right) \right\rangle = \frac{\partial}{\partial x} \left(\langle \overline{\rho}_m \rangle \langle\langle v_m \rangle\rangle \langle\langle v_m \rangle\rangle \right)$$

$$+ \frac{\partial}{\partial x} \sum_{k = g,\ \ell} \langle \alpha_k \rangle \langle\langle \rho_k \rangle\rangle \langle\langle v_k \rangle\rangle \tilde{V}_{km} \qquad \text{(D.35)}$$

Using Eqs. (D.30) to (D.32) we can prove that

$$\sum_{k = g,\ \ell} \langle \alpha_k \rangle \langle\langle \rho_k \rangle\rangle \langle\langle v_k \rangle\rangle \tilde{V}_{km} = - \langle \alpha \rangle \langle\langle \rho_g \rangle\rangle$$

$$\langle\langle \rho_\ell \rangle\rangle \langle\langle v_r \rangle\rangle \langle\langle v_r \rangle\rangle (1-\langle \alpha \rangle)/\langle \overline{\rho}_m \rangle \qquad \text{(D.36)}$$

Again by definition of a drift velocity V_{gj}, Zuber and Findlay [50],

$$V_{gj} = (1-\langle \alpha \rangle) \langle\langle v_r \rangle\rangle \qquad \text{(D.37)}$$

Hence,

$$\sum_{k = g,\ \ell} \langle \alpha_k \rangle \langle\langle \rho_k \rangle\rangle \langle\langle v_k \rangle\rangle \tilde{V}_{km}$$

$$= - \frac{\langle \alpha \rangle \langle\langle \rho_g \rangle\rangle \langle\langle \rho_\ell \rangle\rangle}{(1-\langle \alpha \rangle) \langle \overline{\rho}_m \rangle} V_{gj}^2$$

Eq. (D.35) becomes

$$\left\langle \frac{\partial}{\partial x} \left(\overline{\rho_m v_m v_m} \right) \right\rangle = \frac{\partial}{\partial x} \left(\langle \overline{\rho}_m \rangle \langle\langle v_m \rangle\rangle \langle\langle v_m \rangle\rangle \right)$$

$$- \frac{\partial}{\partial x} \left[\frac{\langle \alpha \rangle \langle\langle \rho_g \rangle\rangle \langle\langle \rho_\ell \rangle\rangle V_{gj}^2}{(1-\langle \alpha \rangle) \langle \overline{\rho}_m \rangle} \right] \qquad \text{(D.39)}$$

Eqs. (D.34) and (D.39) have been used in obtaining the field equations

in Chapter VII. For the sake of simplicity all the notations used in this Appendix to denote the time and area averaged weighted variables have been dropped in Chapter VII.

APPENDIX E

OBSERVATIONS ON SHOCK STRUCTURE

From the photographs of the shock waves at different locations along the plexiglass pipe, it is noted that only B and C-type of shocks are seen to occur in this study. Based on the classification used by Noordzij and van Wijngaarden [28] B and C-type of shocks are defined. Only weak shocks with $p_1/p_o < 1.6$ were observed to be of the C-type. In general, a weak B-type shock changes its structure to C-type during its travel along the pipe. The thickness d_B of the steep portion of B-type shocks, and the wave length Λ_B of the oscillations behind it, were measured for a number of runs and tabulated in Tables 6 to 8. In this investigation shock waves were formed by steepening of compression waves as a result of rapid downstream valve closure. For all of the experiments listed in Tables 6 to 8 the time of closure was maintained at approximately 10 ms, meaning that the compression wave has a very thick front initially.

Noordzij [32] and Noordzij and van Wijngaarden [28] have both shown that both the thickness of a shock wave and the oscillations behind it depend on the strength of the shock, the initial void fraction, and the size of the bubbles. As in the present investigation the bubbles are not of uniform size and are not distributed uniformly in the vertically downward flow and horizontal flow portions of the pipe, the measurements of Λ_B and d_B show a good scatter. Furthermore, the measurements of Λ_B are of limited use as no definite uniform peroidicity has been observed in most of the cases. The period Λ_B was based upon the first two crests of the oscillations behind the shock.

Noordzij [32] has proposed theoretical expressions for the thickness d_B and the wave length Λ_B. Using the theoretical expressions of Noordzij [32] given in Chapter IV as Eqs. (4.36) and (4.39), the parameters d_B and Λ_B are calculated and presented in Table 9, along with the corresponding experimental values. The theoretical values are an order of magnitude smaller than the experimental values. This is not very surprising as Eq. (4.36) and (4.39) are only strictly valid for shock waves propagating in a shock tube, for which the shock has a very steep front initially. In fact, the initial shock form has been reported by Noordzij [32] to be of the A-type. The parameters p_o, p^*, p_1 etc., used in Tables 6 to 8 have been defined in Fig. 5 earlier. The accuracy of the measured experimental values of R_o, d_B and Λ_B is somewhat limited by the accuracy of resolution from the photographs.

Table 6. Experimental Results on the Structure of B-type Shock Waves in Downcomer

Experiment Number	P_o psia	β_o %	P_1/P_o	U ft/sec	$R_o(10^3)$ ft	p^*/p_o	d_B ft	Λ_B ft
7-21-2	32.7	3.05	1.80	395	5.45	1.31	0.42	1.32
7-21-4	32.7	2.44	1.89	457	5.61	1.46	0.66	1.19
7-21-7	32.7	1.46	2.11	627	5.35	1.64	0.90	1.41
7-21-8	32.7	1.36	2.16	681	4.95	1.67	1.09	2.67
7-21-9	32.7	1.25	2.22	721	4.95	1.63	0.83	1.65
7-21-11	32.7	1.06	2.44	800	5.61	1.92	1.50	1.87
7-21-14	32.7	0.80	2.68	1000	4.95	1.98	1.34	2.68
7-21-18	32.7	0.98	2.53	765	4.62	1.61	1.22	2.30
7-23-1	45.5	3.10	1.70	457	5.14	1.40	0.83	1.07
7-23-2	45.5	2.81	1.75	500	4.92	1.40	1.00	1.63
7-23-3	45.5	2.62	1.81	552	5.31	1.44	0.80	1.85
7-23-6	45.5	1.86	2.01	681	4.73	1.57	0.81	1.79
7-23-7	45.5	1.60	2.08	762	4.80	1.66	1.06	2.31
7-23-8	45.5	1.38	2.09	780	4.97	1.84	1.53	1.91
7-23-12	45.5	0.74	2.54	1143	4.97	1.97	1.58	2.63
7-23-14	45.5	0.91	2.45	947	4.63	1.68	0.95	1.14
7-23-15	45.5	1.13	2.23	797	4.28	1.75	0.96	2.71
7-23-17	45.5	0.82	2.45	1000	4.28	2.09	1.60	2.30
7-23-18	45.5	0.94	2.50	892	4.11	1.84	1.25	2.41
7-23-20	45.5	0.53	2.84	1250	4.46	2.08	1.75	3.13

Table 7. Experimental Results on the Structure of B-type Shock Waves in Horizontal Leg

Experiment Number	p_o psia	β_o %	p_1/p_o	U ft/sec	$R_o(10^3)$ ft	p^*/p_o	d_B ft	Λ_B ft
7-10-3	29.9	2.87	1.76	392	5.7	1.33	2.20	3.14
7-10-5	29.9	2.29	1.96	500	5.1	1.55	1.80	2.00
7-10-6	29.9	1.92	2.08	512	4.9	1.52	1.54	2.56
7-10-7	29.9	1.70	2.17	512	4.9	1.77	1.02	1.54
7-10-9	29.9	1.26	2.33	727	4.9	1.77	0.68	1.45
7-10-10	29.9	1.07	2.49	762	4.9	2.02	0.76	1.52
7-10-13	29.9	0.54	3.47	1333	4.9	1.73	1.53	2.67

Table 8. Experimental Results on the Structure of B-Type Shock Waves in Riser

Experiment Number	p_o psia	β_o %	p_1 / p_o	U ft/sec	$R_o (10^3)$ ft	p^* / p_o	d_B ft	Λ_B ft
8-14-3	47.7	2.51	1.63	500	4.45	1.34	0.88	1.63
8-14-4	47.7	2.24	1.68	506	4.45	1.42	1.14	1.52
8-14-5	47.7	2.02	1.73	516	4.45	1.31	0.65	0.77
8-14-6	47.7	1.68	1.84	571	4.14	1.42	0.71	1.04
8-14-7	47.7	1.54	1.92	667	4.14	1.27	0.67	1.00
8-14-8	47.7	1.30	2.01	696	4.14	1.63	0.70	1.56
8-14-9	47.7	1.07	2.09	727	4.14	1.65	1.09	1.27
8-14-11	47.7	0.90	2.24	825	3.35	1.63	1.16	1.16
8-14-15	47.7	0.86	2.34	909	3.35	1.92	1.36	1.59
7-31-1	44.3	3.00	1.72	444	4.28	1.27	0.88	1.67
7-31-2	44.3	2.78	1.75	471	4.28	1.34	1.18	2.35
7-31-3	44.3	2.46	1.81	485	4.28	1.36	1.33	1.46
7-31-5	44.3	2.15	1.90	542	4.28	1.38	0.95	1.22
7-31-6	44.3	1.64	2.09	640	3.98	1.59	1.22	1.44
7-31-8	44.3	1.23	2.22	744	3.98	1.45	0.94	1.67
7-31-11	44.3	0.94	2.63	936	3.78	1.52	0.94	1.17
7-31-20	44.3	0.80	2.63	909	3.78	1.61	0.91	1.09
7-31-15	44.3	0.58	3.03	1185	3.39	1.45	0.89	1.48
7-31-13	44.3	0.72	2.90	1067	3.39	1.45	0.96	1.86

Table 9. Comparison of Experimental and Theoretical Results on the Structure of B-type Shock Waves

Experiment Number	p_1/p_o	β_o %	d_B in ft		Λ_B in ft	
			Measured	Theoretical	Measured	Theoretical
7-21-2	1.80	3.05	0.42	0.08	1.32	0.12
7-21-8	2.16	1.36	1.09	0.10	2.67	0.14
7-21-18	2.53	0.98	1.22	0.11	2.30	0.14
7-23-1	1.70	3.10	0.83	0.08	1.07	0.12
7-23-6	2.01	1.86	0.81	0.09	1.79	0.13
7-23-12	2.54	0.74	1.58	0.13	2.63	0.17
7-10-3	1.76	2.87	2.20	0.09	3.14	0.14
7-10-10	2.49	1.07	0.76	0.11	1.52	0.14
8-14-2	1.59	2.72	0.68	0.08	1.14	0.12
8-14-6	1.84	1.68	0.71	0.09	1.04	0.13
8-14-8	2.01	1.30	0.70	0.09	1.56	0.13
7-31-1	1.72	3.00	0.88	0.07	1.67	0.10
7-31-3	1.81	2.46	1.33	0.07	1.46	0.11
7-31-8	2.22	1.23	0.94	0.08	1.67	0.12
7-31-20	2.63	0.80	0.91	0.09	1.09	0.11
7-31-15	3.03	0.58	0.89	0.10	1.48	0.11

The thickness of C-type shocks are based upon the distance between the beginning of the rising front to the point where the profile becomes more or less flat. The latter point could be only very approximately located. C-type shocks are observed only for a very few experiments where a weak shock existed, and are mainly found in the vertically downward propagation of the shock in the riser. Table 10 shows the experimental results on C-type shocks. The thickness d_c obtained theoretically from Eq. (4.40) are compared with the experimental values in Table 11. In this case the theoretical values are seen to be consistently higher than the experimental ones.

Table 10. Experimental Results on the Structure of C-Type Shock Waves in the Riser

Experiment Number	P_o psia	β_o %	P_1/P_o	U ft/sec	$R_o(10^3)$	d_C ft
3-18-13	32.2	4.38	1.40	294	5.48	5.88
3-18-14	32.2	4.36	1.48	288	5.48	6.34
3-18-16	32.2	3.82	1.50	333	5.48	7.98
7-29-1	32.7	3.74	1.60	308	5.45	6.16
7-17-1	32.0	3.55	1.58	314	5.50	5.50
8-14-1	47.7	2.80	1.60	432	4.45	4.54
8-14-2	47.7	2.72	1.57	457	4.45	4.57

Table 11. Comparison of Experimental and Theoretical Results on C-type Shock Waves

Experiment Number	P_1/P_o	β_o %	d_C in ft	
			Measured	Theoretical
3-18-13	1.40	4.38	5.88	15.31
3-18-14	1.48	4.36	6.34	14.48
3-18-16	1.50	3.82	7.98	13.29
7-29-1	1.60	3.74	6.16	12.37
7-17-1	1.58	3.55	5.50	12.25
8-14-1	1.60	2.80	4.54	8.67
8-14-2	1.57	2.72	4.57	8.45

REFERENCES

1. Pearsall, I. S., "The Velocity of Water Hammer Waves," Symposium on Surges in Pipelines, London, November 2-3, 1965, Proceedings, Institution of Mechanical Engineers, Vol, 180, Part 3E, 1965-66, Paper 2.

2. Hulsemann, J., "Sound Velocity Related to Dissolved Gas in Sea Water," Journal of Geophysical Research, Vol. 77, No. 12, 1972, pp. 2204-2206.

3. Swaffield, J. A., "A Study of the Influence of Air Release on Column Separation in an Aviation Kerosene Pipeline," Proceedings, Institution of Mechanical Engineers, Vol. 186, 56/72, 1972, pp. 693-703.

4. Driels, M. R., "An Investigation of Pressure Transients in a System Containing a Liquid Capable of Air Absorption," Journal of Fluids Engineering, Transactions, American Society of Mechanical Engineers, Vol. 95, December, 1973, pp. 408-414.

5. Kranenburg, C., "Gas Release During Transient Cavitation in Pipes," Paper 10892, Journal of the Hydraulics Division, Proceedings, American Society of Civil Engineers, Vol. 100, N., HY10, October, 1974, pp. 1383-1398.

6. Sheer, T. J., "Computer Analysis of Water Hammer in Power Station Cooling Water Systems," International Conference on Pressure Surges, Canterbury, England, September 6-8, 1972, Paper D1.

7. Moody, F. J., "Maximum Two-Phase Vessel Blowdown from Pipes," Journal of Heat Transfer, Transactions, American Society of Mechanical Engineers, Vol. 88, August, 1966, pp. 285-293.

8. Henry, R. E., and Fauske, H. K., "The Two-Phase Critical Flow of One-Component Mixtures in Nozzles, Orifices, and Short Tubes," Journal of Heat Transfer, Transactions, American Society of Mechanical Engineers, Vol. 93, May, 1971, pp. 179-187.

9. Moody, F. J., "Time-Dependent Pipe Forces Caused by Blowdown and Flow Stoppage," Journal of Fluids Engineering, Transactions, American Society of Mechanical Engineers, Vol. 95, December, 1973, pp. 422-428.

10. D'Arcy, D. F., "On Acoustic Propagation and Critical Mass Flux in Two-Phase Flow," Journal of Heat Transfer, Transactions, American Society of Mechanical Engineers, Vol. 93, November, 1971, pp. 413-421.

11. Silberman, E., "Sound Velocity and Attenuation in Bubbly Mixtures Measured in Standing Wave Tubes," Journal of the Acoustical Society of America, Vol. 29, No. 8, August, 1957, pp. 925-933.

12. Hsieh, D.-Y., and Plesset, M. S., "On the Propagation of Sound in a Liquid Containing Gas Bubbles," The Physics of Fluids, Vol. 4, No. 8, August, 1961, pp. 970-975.

13. Henry, R. E., "Pressure Wave Propagation in Two-Phase Mixtures," Chemical Engineering Progress Symposium Series, Heat Transfer Conference, Minneapolis, August 3-6, 1969, Vol. 66, No. 102, pp. 1-10.

14. van Wijngaarden, L., "On the Equations of Motion for Mixtures of Liquid and Gas Bubbles," Journal of Fluid Mechanics, Vol. 33, Part 3, 1968, pp. 465-474.

15. van Wijngaarden, L., "One-Dimensional Flow of Liquids Containing Small Gas Bubbles," Annual Review of Fluid Mechanics, Vol. 4, 1972, pp. 369-396.

16. Campbell, I. J., and Pitcher, A. S., "Shock Waves in a Liquid Containing Gas Bubbles," Proceedings, Royal Society of London, Series A, Vol. 243, 1958, pp. 534-545.

17. Crespo, A., "Sound and Shock Waves in Liquids Containing Bubbles," The Physics of Fluids, Vol. 12, No. 1, November, 1969, pp. 2274-2282.

18. Noordzij, L., "Shock Waves in Bubble-Liquid Mixtures," Proceedings of the IUTAM Symposium on Nonsteady Flow of Water at High Speeds, Leningrad, 1971, pp. 369.

19. Henry, R. E., Grolmes, M. A., and Fauske, H. K., "Pressure-Pulse Propagation in Two-Phase One- and Two-Component Mixtures," Reactor Analysis and Safety Division, Argonne National Laboratory, Report ANL-7792, March, 1971.

20. Wallis, G. B., One-Dimensional Two-Phase Flow, McGraw-Hill, New York, 1969.

21. Carstens, M. R., and Hagler, T. W., "Water Hammer Resulting from Cavitating Pumps," Proceedings, Journal of the Hydraulics Division, American Society of Civil Engineers, Vol. 90, No. HY6, November, 1964, pp. 161-184.

22. Prosperetti, A., and van Wijngaarden, L., "On the Characteristics of the Equation of Motion for Bubbly Flow and the Related Problem of Critical Flow," Journal of Engineering Mathematics, Vol. 10, April, 1976.

23. Mori, Y., Hijikata, K., and Komine, A., "Propagation of Pressure Waves in Two-Phase Flow," International Journal of Multiphase Flow, Vol. 2, 1975, pp. 139-152.

24. Fanelli, M., and Reali, M., "A Theoretical Determination of the Celerity of Waterhammer Waves in a Two-Phase Fluid Mixture," L'Energia Elettrica, Vol. 52, No. 5, April, 1975, pp. 186-194.

25. Plesset, M. S., on Bubble Dynamics in Cavitation in Real Liquids, edited by Davies, R., Elsvier, Amsterdam - New York, 1964.

26. van Wijngaarden, L., "Propagation of Shock Waves in Bubble-Liquid Mixtures," Journal of Heat Mass Transfer, Vol. 6, 1972, pp. 637-648.

27. Gregor, W., and Rumpf, H., "Velocity of Sound in Two-Phase Media," International Journal of Multiphase Flow, Vol I, 1975, pp. 753-769.

28. Noordzij, L., and van Wijngaarden, L., "Relaxation Effects, Caused by Relative Motion, on Shock Waves in Gas-Bubble/Liquid Mixtures," Journal of Fluid Mechanics, Vol. 66, Part 1, 1974, pp. 115-143.

29. Lighthill, M. J., Surveys in Mechanics, edited by Batchelor, G. K., and Davies, R. M., Cambridge University Press, 1956.

30. van Wijngaarden, L., "On the Structure of Shock Waves in Liquid-Bubble Mixtures," Applied Science Research, Vol. 22, July 1972, pp. 366-381.

31. Levich, V. G., Physico-Chemical Hydrodynamics, Prentice Hall, 1962.

32. Noordzij, L., "Shock Waves in Mixtures of Liquids and Air-Bubbles," Ph.D. dissertation, Twente Institute of Technology, The Netherlands, 1973.

33. Whitham, G. B., Linear and Nonlinear Waves, John Wiley & Sons, New York, 1974.

34. Streeter, V. L., and Wylie, E. B., Hydraulic Transients, McGraw-Hill Book Co., New York, 1967.

35. Lamb, H., Hydrodynamics, Cambridge University Press, 1932.

36. Lyczokowski, R. W., Gidaspow, D., Solbrig, C. W., and Hughes, E. D., "Characteristics and Stability Analyses of Transient One-Dimensional Two-Phase Flow Equations, ASME Paper No. 75-WA/HT-23, 1975.

37. Dronkers, J. J., Tidal Computations in Rivers and Coastal Waters, North-Holland Publications Co., Amsterdam, 1964.

38. Ames, W. F., Nonlinear Partial Differential Equations in Engineering, Academic Press, New York, 1965.

39. Richtmyer, R. D., and Morton, K. W., Difference Methods for Initial Value Problems, Interscience Publications, New York, 1967.

40. Lax, P. D., and Wendroff, B., "Systems of Conservation Laws," Communications on Pure and Applied Mathematics, Vol. XIII, 1960, pp. 217-237.

41. Richtmyer, R. D., "A Survey of Difference Methods for Nonsteady Fluid Dynamics," NCAR Technical Notes, 63-2, 1962.

42. Gourlay, A. R., and Morris, J. L., "Hopscotch Difference Methods for Nonlinear Hyperbolic Systems," IBM Journal of Research and Development, Vol. 16, 1972, pp. 349-353.

43. Kranenburg, C., "Transient Cavitation in Pipelines," Report Number 73-2, Laboratory of Fluid Mechanics, Department of Civil Engineering Delft University of Technology, The Netherlands, 1973.

44. Gary, J., "On Certain Finite Difference Schemes for Hyperbolic Systems," Mathematics of Computations, Vol. 18, 1964, pp. 1-18.

45. Gourlay, A. R., and Morris, J. L., "Finite Difference Methods for Nonlinear Hyperbolic Systems," Mathematics of Computations, Vol. 22, 1968, pp. 28-39.

46. McGuire, G. R., and Morris, J. L., "Explicit-Implicit Schemes for the Numerical Solution of Nonlinear Hyperbolic Systems," Mathematics of Computations, Vol. 29, 1975, pp. 407-424.

47. Vliegenthart, A. C., "The Shumann Filtering Operator and the Numerical Computation of Shock Waves," Journal of Engineering Mathematics, Vol. 4, 1970, pp. 341-348.

48. Ishii, M., "Thermally Induced Flow Instabilities in Two-Phase Mixtures in Thermal Equilibrium," Ph.D. Thesis, Georgia Institute of Technology, Atlanta, Ga., June, 1971.

49. Ishii, M., Thermo-Fluid Dynamics Theory of Two-Phase Flow, Eyrolles, Paris, 1975.

50. Zuber, N., and Findlay, J. A., "Average Volumetric Concentration in Two-Phase Flow Systems," Journal of Heat Transfer, Transactions, American Society of Mechanical Engineers, November, 1965, pp. 453-468.

51. Zuber, N., "Flow Excursions and Oscillations in Boiling Two-Phase Flow Systems with Heat Addition", Symposium on Two-Phase Flow Dynamics, Eindhoven, Vol. 1, September, 1967, pp. 1071.

52. Zielke, W., "Frequency-Dependent Friction in Transient Pipe Flow", Journal of Basic Engineering, Transactions, American Society of Mechanical Engineers, Vol. 90, March, 1968, pp. 109-124.

53. Martin, C. S., "Vertically Downward Two-Phase Slug Flow", Accepted for Publication in Journal of Fluids Engineering, Transactions, American Society of Mechanical Engineers.

54. Maneri, C. C., and Zuber, N., "An Experimental Study on Plane Bubbles Rising at Inclination", International Journal of Multiphase Flow, Vol. 1, Number 5, 1974, pp. 623-645.

55. Lax, P. D., "Weak Solutions of Nonlinear Hyperbolic Equations and Their Numerical Computations", Communications on Pure and Applied Mathematics, Vol. VII, 1954, pp. 159-193.

VITA

Mahadevan Padmanabhan was born in Trivandrum, India, on August 14, 1943. He attended local schools and graduated from the College of Engineering, Trivandrum, in January 1964. He obtained his Master's degree from Indian Institute of Technology, Madras, India, in August 1966, after two years of graduate study, specializing in Hydraulic Engineering. From March 1967 to February 1968 he was employed as a construction engineer by M/S Fertilizers and Chemicals Ltd, Alwaye, India. In February 1968 he joined the Faculty of Civil Engineering of the College of Engineering, Trivandrum, India, as a Lecturer and worked till March 1970. He was awarded a fellowship for advanced research in West Germany under a German Academic Exchange Service Program in March 1970. Under this program he was engaged in research on "Flow Induced Vibrations in Hydraulic Structures" at the Institute of Hydromechanics of the University of Karlsruhe, Germany, till October, 1972.

In March 1973, Mr. Padmanabhan joined the School of Civil Engineering of the Georgia Institute of Technology, Atlanta. He obtained a Master's degree in March 1975, and continued towards his Ph. D. degree. Throughout the period of graduate study he was supported by a Graduate Research Assistantship and was working with Dr. C. S. Martin, Professor.

Mr. Padmanabhan is a member of the Institution of Engineers (India) and has a number of publications to his credit. He was married to Ranjana, H. in November, 1972 and has no children.